Cranfield University

Rebecca Y N Wong

Advanced fibre optic long period grating sensors; design, fabrication and sensing

Engineering Photonics
School of Engineering

PhD Thesis

Supervisors: Dr. Stephen W James and Prof. Ralph P Tatam
May 2014

Cranfield University

Engineering Photonics
School of Engineering
PhD Thesis
2014

Rebecca Y N Wong

Advanced fibre optic long period grating sensors; design, fabrication and sensing

Supervisors: Dr. Stephen W James and Prof. Ralph P Tatam

May 2014

This thesis is submitted in partial fulfillment of the requirements for the degree of Doctor of Philosophy

Abstract

This thesis describes the process and technique used to fabricate reproducible optical fibre long period gratings (LPG) of various types. It explores how they can be exploited for use as highly selective and sensitive sensors. A versatile method for fabricating LPG sensors has been demonstrated. The single system has the capability of fabricating LPGs of different configurations, such as uniform period, those operating at the phase matching turning point (PMTP), as well as phase shifted and chirped. LPGs were characterised for their sensitivities to temperature, axial strain and surrounding refractive index. The gratings at the PMTP were found to show higher sensitivities to external influences.

Novel sensing configurations that exploit the properties of LPGs were also constructed. An LPG coated with a molecularly imprinted ceramic coating was demonstrated to offer a selective method for porphyrin detection. A composite nanoscale of a titanium oxide (TiO_2) matrix and 5, 10, 15, 20 Tetrakis-(N-methyl-piridinium-4-yl)-21H, 23H-porphine tertakis (p-toluenesulfonate) [TMPyP] porphyrin template film was deposited on the LPG via liquid phase deposition. Attempts to rebind porphyrins to the matrix were carried out. The LPGs transmission spectrum exhibited a higher sensitivity to the target TMPyP template than it did to other, structurally similar porphyrins, showing high selectivity.

A continuously chirped long period grating (CCLPG) sensor for monitoring directional flow and cure of an epoxy resin is also presented. The asymmetric properties of the CCLPG were exploited to facilitate the measurement of the direction of the flow. The CCLPG was also used to monitor changes in the refractive index of the resin during its cure, showing close agreement with a fibre optic Fresnel refractometer.

Acknowledgements

First and foremost, I would like to thank my supervisor, Dr. Stephen James for his invaluable help, patience and encouragement for the duration of the PhD. He always made himself available to answer any questions and offer me guidance when it was needed. Thank you to Prof. Ralph Tatam, the many meetings we had and for his constructive recommendations which helped me think of ways to improve my work.

Thank you to all the people in the laboratory who have helped me, taught me new skills and allowed me to distract them with numerous conversations. I would like to express my very great appreciation to Dr. Edmond Chehura who never hesitated to offer his assistance and for providing his knowledge with experiments. I am also grateful to Stephen Staines for his expertise and how he was able to decipher my descriptions to design and craft items that were used in many of my experiments.

Finally, I would like to thank my friends and family for their unwavering support.

Contents

List of Figures

List of Tables

Chapter 1

Introduction to optical fibre grating sensors

1.1 Introduction

Optical fibres, as we know them today, were introduced around the 1950s [1]. Since their inception, the technology and applications have developed significantly into fields such as sensing and telecommunications. The first commercial use of the optical fibre was in the medical field as an endoscope for carrying out minimally invasive diagnoses on patients. However, the light loss from the optical fibre was high and information could only be transferred successfully over a relatively short distance.

During the early 1970's, scientists at Corning Glass Works were eventually able to create a low loss (less than 20 dB/km) optical fibre system capable of carrying information over a long distance [2] and in 1977, the first optical telephone communications system was installed [2].

Nowadays, optical fibres are also known for their state of the art in losses (around 0.20 dB/km at 1.55 μm [3]) and high communication data rates of more than 10 Gbit/s [4]. The properties of the light propagating in the fibre can be influenced by the surrounding environment; this allows the use of an optical fibre as a sensor.

1.2 Optical fibres

An optical fibre is a thin and flexible cylindrical dielectric waveguide that transports optical information from one place to another. They typically consist of a core, surrounded by cladding which has a lower refractive index. Outside the cladding,

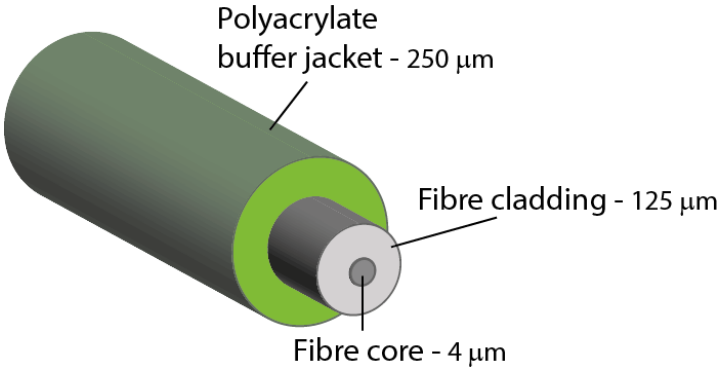

Figure 1.1: An illustration of a single mode optical fibre showing the core, cladding, outer buffer jacket and typical dimensions.

there is a buffer jacket which protects the fibre and enhances its mechanical strength (see figure 1.1). A fibre's waveguiding properties are governed by its geometry, (e.g. its shape and dimensions) and its refractive index profile (the change in refractive index between the core and cladding). Optical fibres can be fabricated using plastics, or using silica, either pure or doped with another material (to vary the refractive index).

1.3 Optical fibre grating sensors

An optical fibre sensor can be classed as either extrinsic or intrinsic, [5] depending on how it is operated/used. An intrinsic sensor uses the fibre as the sensing element; the measurand interacts directly with the light propagating through the fibre and causes changes in the characteristics of the transmitted or reflected light. In an extrinsic sensor, the interaction between the measurand and the light takes place in a region outside the optical fibre. The modulated light is carried to a detector via the same or different optical fibre and is processed by an external device [5]. Many different types of fibre optic sensors have been configured. Some of these sensors include optical fibre interferometers, evanescent field sensors e.g. fibre tapers and polished devices, polarimetric sensors, and grating sensors [6]. Interferometric sensors have generally exhibited greater sensitivity, especially when they are configured such that the measurand is measured as a function of optical phase. Grating based fibre sensors are perhaps currently the most widely researched and applied to real life situations. They are easy to configure, offer high signal to noise ratio, and exhibit stable signals immune to degradation because they are wavelength encoded. Their wavelength multiplexing capabilities allow multiple gratings to be inscribed in a single fibre, allowing a greater network of information to be carried and detected

over extended space.

An optical fibre grating can be defined as 'an optical fibre with a localised periodic refractive index perturbation pattern inscribed in the core such that it diffracts the optical signal in the guided mode at specific wavelengths into other core-bounded modes, cladding modes, or radiation modes' [7].

The phenomena that occurs with in-fibre gratings were first observed by Hill et al. in 1978 [8]. The first permanent Bragg gratings within an optical fibre were created when a single mode argon laser beam was pumped through the core of a photosensitive fibre, which had a high germanium dopant concentration. A standing wave was created in the fibre, causing a permanent change in refractive index in parts of the core of the fibre. Since then, the research and development in in-fibre gratings have had a great impact not only in telecommunications but also in optical fibre sensing applications. They have been used in a wide range of fields such as medicine, the oil and gas industry and for structural monitoring in civil, automotive and aerospace structures [9, 10, 11] .

Optical fibre gratings work as intrinsic devices and are therefore able to control the propagation of light inside the fibre. Fibre gratings consist of a periodic perturbation of the properties of the fibre which is usually a change in refractive index in the core of the fibre. There are two general classes of in-fibre gratings, which are known by their broad names; fibre Bragg grating (FBG) and long period grating (LPG).

The period of an FBG is typically sub-micron and promote coupling between the propagating core mode and the counter-propagating core mode at a wavelength that satisfies the phase matching Bragg conditions [11, 12], as illustrated in figure 1.2. This means that the light is only guided within the core of the fibre. An optical property of this is that the light will not be readily affected by the refractive index of the external surroundings the fibre could potentially come into contact with. However, this aspect also holds the FBG at a disadvantage as it limits its capabilities as a sensor, primarily to the measurement of temperature and strain.

LPGs have periods which typically range from less than 100 μm to 1 mm [11] and promotes coupling between the propagating core mode and one or more of the co-propagating cladding modes (see figure 1.3). As coupling of light involves cladding modes, the response of the attenuation bands of the transmission spectrum will be

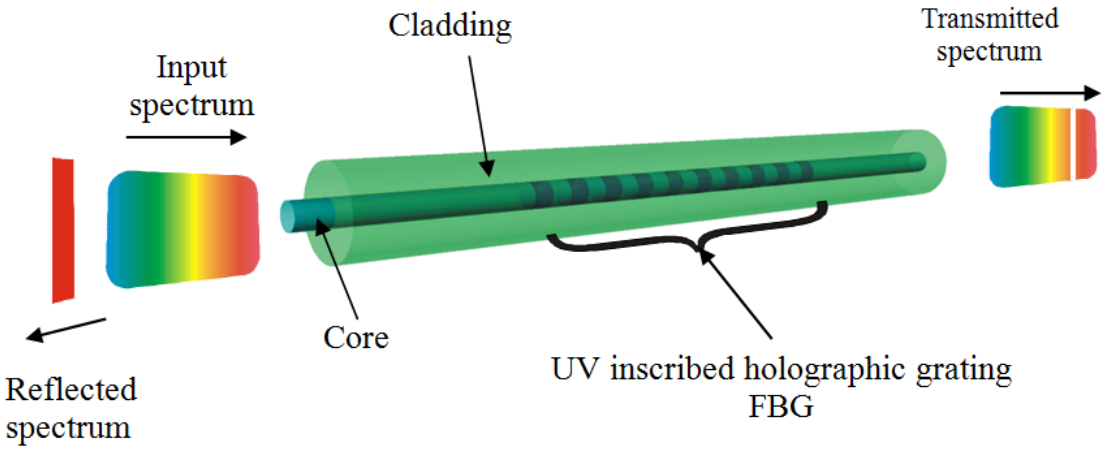

(a)

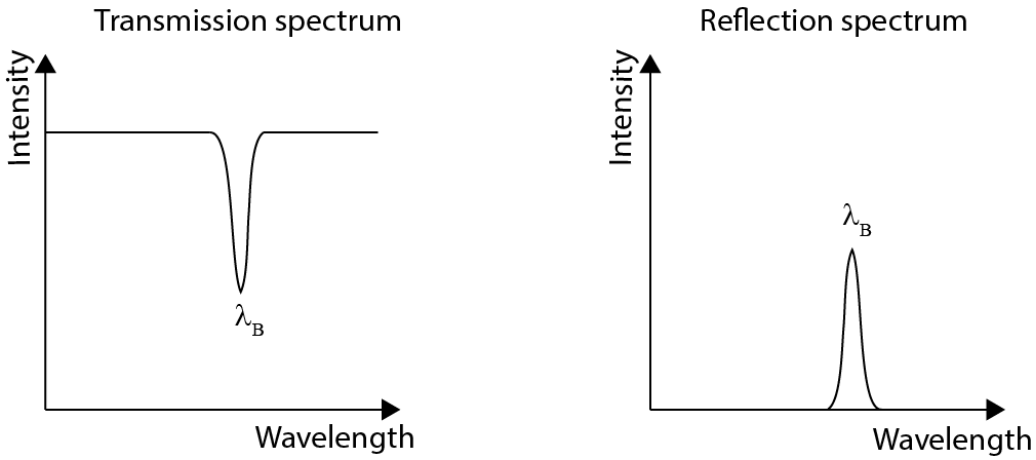

(b)

Figure 1.2: (a) Schematic diagram of an FBG. (b) shows a typical transmission and reflection spectrum and only the wavelength of light, λ_B, that satisfies the Bragg condition, is reflected.

greatly influenced by their external surroundings and local environment [13]. LPGs have been used as sensors for certain measurands which include, but are not limited to, temperature, strain, pressure, bending and refractive index changes of fluids and liquids [14]. It is possible to bias the sensitivity of the LPG, making LPGs attractive as sensor elements to measure one or multiple measurands at the same time [11]. One way of doing this is to coat the LPG with a functional coating to make chemical sensors [15, 16].

Some other advantages that optical fibre sensors offer over conventional sensors are their small dimensions (diameters are typically 40 μm 125 μm), and their suitability for use in harsh environments. Optical fibres have the ability to transmit a large bandwidth of light, and transmission through the fibre is relatively straightforward [6]. Other advantages of optical fibres include their ability to transmit light over large distances, usually 100's of metres or even kilometres [9, 10], their flexibility and small size (cross-sectional area) allow them to access areas that may otherwise be awkward to reach by other equipment and they can carry much more information than an electrical wire; many sensors can be multiplexed on a single length of fibre which allows quasi-distributed sensing. Fibre optic sensors have been used for fully distributed sensing, and as this utilises the entire fibre there are no sensing dead zones [17, 18]. The properties of light propagating through an optical fibre that can be influenced by the surrounding environment include intensity, wavelength (and frequency), phase, modal distribution and polarisation. These properties can be influenced directly by the measurand of interest, or the fibre can be packaged such that these characteristics can be modified by the environmental parameters of interest. The ability to measure these characteristics of the propagating light facilitates the development of sensors. Gratings allow these changes in fibre properties to be interpreted by something that is relatively easily measured - a simple change in wavelength. This implies that by using a variety of approaches, the information concerning the interaction between the surrounding environment and the fibre can be successfully extracted so the same fibre sensor can be used to monitor different properties.

However, optical fibres do not make perfect sensors. For instance, a sensor is likely to exhibit cross sensitivity to more than one measurand. This could lead to undesired errors in the results [10]. A possible way to overcome this issue would be to use an additional sensor which is shielded from one measurand but still monitors other parameters. Other methods include using two sensor elements with a different

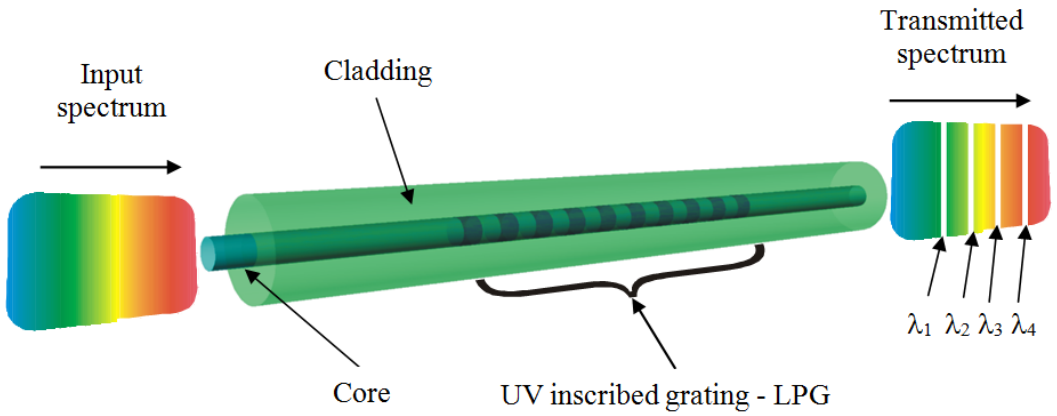

(a)

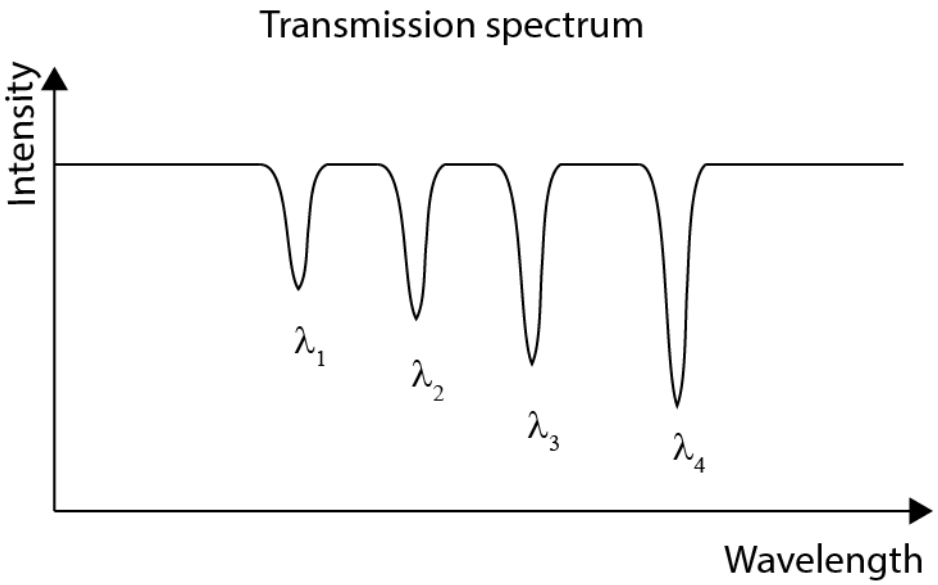

(b)

Figure 1.3: (a) Schematic diagram of an LPG where (b) illustrates the attenuation bands in the transmission spectrum at wavelengths λ_1 - λ_4 which satisfy the phase matching condition.

sensitivities by virtue of the fibre composition of geometry [19] or using a single sensor element that interacts with more than one mode of the fibre, where these modes have different environmental responses (e.g. core and cladding) [20].

A number of LPG configurations have been reported that exhibit different sensing attributes for a variety of applications. Examples of these include the uniform period LPG [21], phase shifted LPG [22], tilted LPG [23] and chirped LPG [24]. This is discussed in more detail in chapter 2. All of these types can be tailored to extend their applications to other measurands as well as to enhance their response to specific stimuli. Methods to tailor the properties of LPGs and other sensors such as tapered fibres and tilted fibre Bragg gratings, have used nano-molecular deposition as a means of coating the sensors with functional materials. Deposition techniques that are in use include Langmuir-Blodgett film deposition, electrostatic self assembly and molecular imprinting.

The developments in optical fibre sensors centred on the deposition of functional nano-scale coatings have recently become of great interest because of the envisaged potential applications, particularly in chemical and bio-sensing. These coatings improve the fibre's sensing capabilities by making them respond differently to different stimuli, be it to temperature or refractive index and concentrations of chemicals in the surrounding environment such as liquids or vapours [15]. The sensors have the capability to be deployed in the biochemical industry to measure chemical concentrations and can also be applied to environmental sensing of gaseous species.

1.4 Thesis aims

This thesis concentrates on the fabrication and application of different types of optical fibre long period gratings. It explores the capabilities of LPGs as sensing devices and shows ways in which they can be applied.

A point-by-point method for fabricating fibre optic long period gratings was developed. This allowed high precision, versatile and repeatable fabrication of LPGs.The versatility of the system is demonstrated by fabricating chirped phase shifted LPGs. The system is used to explore some of the stringent properties required to write gratings as, for example, those at the phase matching turning point (PMTP) where the transmission spectrum is very sensitive.

Experiments have been carried out to evaluate the practical characteristics of particular long period gratings; uniform period, phase matching turning point and continuously chirped. These configurations are chosen as their sensitivities to certain measurands are later utilised for sensing purposes.

There is considerable interest in the development of optical fibre based chemical sensors [15, 25, 26, 27, 28]. The current trends in this area involve the deposition of a functional nano-scale coating onto the surface of the optical fibre. Chemically induced changes in the optical characteristics of the coating can influence the properties of modes propagating in the optical fibre, which can be observed by monitoring the transmission spectrum of the fibre device. An LPG operating at the PMTP, modified with a molecularly imprinted ceramic coating is demonstrated to offer a selective method for porphyrin detection. A composite nanoscale film is deposited to show a sensor that is selective and sensitive to a particular species.

Composite materials are being used as structural components in many applications, for example aerospace, as they offer a better strength to weight ratio when compared to traditional materials used for the same purpose [29]. Methods of monitoring the development process (resin infusion and cure monitoring) and damage assessment are always of interest, particularly those offering in-situ and real time measurement capabilities. In many cases it is not possible to visually observe the resin flow front during infusion and therefore alternative methods have to be used. An attractive avenue is the use of optical fibre sensors [29, 30, 31, 32]. A continuously chirped long period grating (CCLPG) was used to perform directional flow sensing of a UV-cured epoxy resin and to subsequently monitor the resin cure via the measurement of the change in refractive index. Directionality of flow along the fibre can be determined due to the asymmetric nature of the attenuation bands of the transmission spectrum. The change in the refractive index of the resin during cure is determined in the same experiment using a fibre optic Fresnel based refractometer.

1.5 Thesis chapter summary

Chapter one: This chapter contained a brief introduction to fibre optics and outlines the aims of the thesis.

Chapter two: Chapter two covers the theory and physics of optical fibre LPGs. A brief overview of a selection of different types of long period gratings is also given.

Chapter three: This chapter covers the methods used for fabricating long period gratings. The chapter also covers the set up used during fabrication and the different types of LPGs that the technique is capable of.

Chapter four: The characterisation of different LPG configurations is described. These configurations include uniform period, phase matching turning point and continuously chirped. The sensitivities of the attenuation bands to temperature, strain, refractive index were characterised.

Chapter five: Chapter five exploits the sensing capabilities of LPGs operating near the phase matching turning point coated with a functional material. The LPGs are modified with a molecularly imprinted ceramic coating to demonstrate a selective method for porphyrin detection.

Chapter six: Chapter six explores the use of chirped long period gratings (CLPG) for use as a directional flow sensor and as a resin cure monitor by means of measuring refractive index. The CLPG's capabilities were assessed using refractive index oils and confirmed by monitoring a UV cured epoxy resin.

Chapter seven: Chapter seven summarises the results and conclusions from the previous experimental chapters. The possibilities for future improvements and for developing the work further are also presented.

1.6 Summary

This chapter gave an overview of optical fibres, highlighting optical fibre gratings and discussing their advantages for use as sensors. The different classifications of fibre gratings and their different features; the fibre Bragg grating and long period grating were introduced. The aims of the thesis and a brief summary of each chapter were also presented.

References

[1] J Hecht. *City of Light: The Story of Fiber Optics*. Oxford University Press, 1999.

[2] A H Cherin. *An Introduction to Optical Fibers*. McGraw-Hill, 1983.

[3] T Miya, Y Terunuma, T Hosaka, and T Miyashita. Ultimate low-loss single-mode fibre at 1.55 μm. *Electronics Letters*, 15(4):106–108, 1979.

[4] H Gahfouri-Shiraz. *The Principles of Semiconductor Laser Diodes and Amplifiers: Analysis and Transmission Line Laser Modelling*. Imperial College Press, 2003.

[5] E Udd. Overview of fiber optic sensors. In S Yin, Ruffin P B, and F T S Yu, editors, *Fiber Optic Sensors: Second Edition*, pages 2–34. 2008.

[6] B Lee. Review of the present status of optical fiber sensors. *Optical Fibre Technology*, 9(2):57–79, 2003.

[7] R Kashyap and J M López-Higuera. Fibre grating technology: Theory, photosensitivity, fabrication and characterization. In J M López-Higuera, editor, *Handbook of Optical Fibre Sensing Technology*, pages 349–377. 2001.

[8] K O Hill, Y Fujii, D C Johnson, and B S Kawasaki. Photosensitivity in optical fiber waveguides: Application to reflection filter fabrication. *Applied Physics Letters*, 32(10):647–649, 1978.

[9] M Campbell. *Sensor Systems for Environmental Monitoring: Sensor Technologies*. Chapman and Hall, 1997.

[10] J M López-Higuera. Introduction to fibre optic sensing technology. In J M López-Higuera, editor, *Handbook of Optical Fibre Sensing Technology*, pages 1–30. 2001.

[11] S W James and R P Tatam. Optical fibre long-period grating sensors: characteristics and application. *Measurement Science and Technology*, 14(5):R49–R61, 2003.

[12] K O Hill. Fiber Bragg gratings. In M Bass and E W Van Stryland, editors, *Fiber Optics Handbook: Fiber, Devices and Systems for Optical Communications*, pages 9.1–9.11. 2002.

[13] L Zhang, W Zhang, and I Bennion. In-fiber grating optic sensors. In S Yin, P B Ruffin, and F T S Yu, editors, *Fiber Optic Sensors, Second Edition*, pages 109–162. 2008.

[14] O Frazão, L A Ferreira, and F M Araújo. Applications of fiber optic grating technology to multi-parameter measurement. *Fiber and Integrated Optics*, 24(3):227–244, 2005.

[15] S M Topliss, S W James, F Davis, S P J Higson, and R P Tatam. Optical fibre long period grating based selective vapour sensing of volatile organic compounds. *Sensors and Actuators B: Chemical*, 143(2):629–634, 2010.

[16] Y Zhao, F Pang, Y Dong, J Wen, S Chen, and T Wang. Refractive index sensitivity enhancement of optical fiber cladding mode by depositing nanofilm via ALD technology. *Optics Express*, 21(22):26136–26143, 2013.

[17] S Huang, M M Ohn, and R M Measures. Phase-based Bragg intragrating distributed strain sensor. *Applied Optics*, 35(7):1135–1142, 1996.

[18] D Y Wang, Y Wag, J Gong, and A Wang. Fully distributed fiber-optic hydrogen sensing using acoustically induced long-period grating. *Photonics Technology Letters*, 23(11):733–735, 2011.

[19] S W James, M L Dockney, and R P Tatam. Simultaneous independent temperature and strain measurement using in-fibre Bragg grating sensors. *Electronics Letters*, 32(12):1133–1134, 1996.

[20] E Chehura, S W James, and R P Tatam. Temperature and strain discrimination using a single tilted fibre Bragg grating. *Optics Communications*, 275(2):344–347, 2007.

[21] C C Ye, S W James, and R P Tatam. Simultaneous temperature and bend sensing with long-period fiber gratings. *Optics Letters*, 25(14):1007–1009, 2000.

[22] S W James, S M Topliss, and R P Tatam. Properties of length-apodized phase-shifted lpgs operating at the phase matching turning point. *Journal of Lightwave Technology*, 30(13):2203–2209, 2012.

[23] T Mizunami and T Fukuda. Fem calculation and the effects of hydrogen diffusion in fabrication processes of long-period fiber gratings. *Optical Communications*, 259(2):581–586, 2006.

[24] M Yan, S Luo, L Zhan, Y Wang, Y Xia, and Z Zhang. Step-changed period chirped long-period fiber gratings fabricated by CO_2 laser. *Optics Communications*, 281(10):2784–2788, 2008.

[25] X Chen, Zhou K, Zhang L, and Bennion I. Optical chemsensor based on etched tilted Bragg grating structures in multimode fiber. *IEEE Photonics Technology Letters*, 17(4):864–866, 2005.

[26] C S Cheung, S M Topliss, S W James, and R P Tatam. Response of fibre optic long period gratings operating near the phase matching turning point to the deposition of nanostructured coatings. *Journal of the Optical Society of America B Optical Physics*, 25(6):897–902, 2008.

[27] P S Grant and M J McShane. Development of multilayer fluorescent thin film chemical sensors using electrostatic self-assembly. *IEEE Sensors Journal*, 3(2):139–146, 2003.

[28] S W James and R P Tatam. Fibre optic sensors with nano-structured coatings. *Journal of Optics A: Pure and Applied Optics*, 8(7):S430–S444, 2006.

[29] C Keulen, B Rocha, M Yildiz, and A Suleman. Embedded fiber optic sensors for monitoring processing, quality and structural health of resin transfer molded components. *Journal of Physics: Conference Series*, 305(1):1–9, 2011.

[30] S J Buggy, E Chehura, S W James, and R P Tatam. Optical fibre grating refractometers for resin cure monitoring. *Journal of Optics A: Pure and Applied Optics*, 9(6):S60–S71, 2007.

[31] C Keulen, M Yildiz, and A Suleman. Multiplexed FBG and etched fiber sensors for process and health monitoring of 2-&-3-D RTM components. *Journal of Reinforced Plastics and Composites*, 30(12):1055–1064, 2011.

[32] S Triollet, L Robert, E Marin, and Y Ouerdane. Liquid resin infusion process monitoring with embedded superimposed long period and short period Bragg grating sensor. *EPJ Web of Conferences*, 6(34003):1–9, 2010.

Chapter 2

Long Period Grating Theory

2.1 Optical fibre principle of operation

2.1.1 Guided and radiation modes

In a cylindrical dielectric waveguide, a mode is a set of electromagnetic waves that propagate energy in the waveguide [1]. In an unperturbed loss-less system, at a particular angular frequency, ω, a finite number of modes can be supported by an optical fibre. These modes are guided within the core of the fibre and travel with propagation constants, β which are functions of the wavelength of the optical source and of the properties of the fibre. To obtain a more detailed understanding of the fibre's propagation constants, Maxwell's equations and the boundary conditions associated with the electromagnetic field are used [1, 2].

From Maxwell's equations, the important result is the wave equation for the electromagnetic waves that may propagate along an optical fibre. The wave equation in cylindrical co-ordinates for the z- components of E, H, E_z and H_z [3] can be written as:

$$\frac{\partial^2\psi}{\partial r^2} + \frac{1}{r}\frac{\partial\psi}{\partial r} + \left(k^2 - \beta^2 - \frac{1}{r^2}\right)\psi = 0 \tag{2.1}$$

where $\psi = E_z, H_z$, r is the radial coordinate, β is the propagation constant, $k = \omega^2 n^2/c$, ω is the angular frequency $= 2\pi f$.

The propagation constant is represented by:

$$\beta = \frac{\omega n_{eff}}{c} = 2\pi n_{eff}\lambda \tag{2.2}$$

where n_{eff} is the effective refractive index and c is the speed of light in a vacuum. For modes propagating within the core, the discrete set of propagation constants are confined to [4]

$$n_2 k <\mid \beta \mid < n_1 k \tag{2.3}$$

where n_2 and n_1 are the refractive indices of the cladding and core, respectively, and k is the free space propagation constant; $k = 2\pi/\lambda$.

The forward ($\beta > 0$) and backward ($\beta < 0$) propagating constants of the guided modes and their relative positions are represented in figure 2.1 [4, 5].

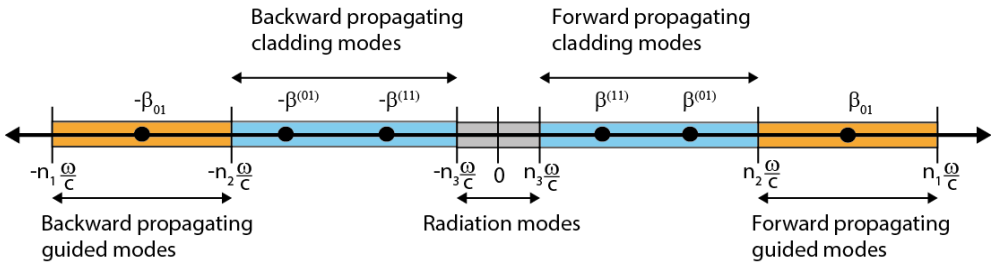

Figure 2.1: Propagation constants of the guided modes and modal distribution in an optical fibre. The yellow sections represent the propagating guided modes, the blue sections represent the propagating cladding modes and the grey the radiation modes. (-)β^{01} and (-)β^{11} are the propagating constants of the lowest order cladding modes and (-)β_{01} is the propagating constant of the core mode. ω is the angular frequency, n_x is the refractive index and c is the speed of light. Adapted from [4] and [5].

Radiation modes also satisfy Maxwell's equations and the boundary conditions, though unlike guided modes there are an infinite number of these non-propagating modes which cause a continuous loss of power from the guided modes. Some of the radiation is trapped within the fibre by reflections from the cladding/air boundary, these modes are termed cladding modes. In a long period grating, which couples propagating core and cladding modes, the discrete propagation constants of the cladding modes are confined to (if the cladding is surrounded by a lower refractive index, n_3) [3]:

$$n_3 k <\mid \beta \mid < n_2 k \tag{2.4}$$

2.1.2 Long period gratings

LPGs consists of a periodic modulation of the propagation constants of the modes of an optical fibre, with periods ranging typically from less than 100 μm to 1 mm [6] with lengths of 10s of millimetres. Figure 2.2 shows a schematic of an LPG with a uniform period, Λ and figure 2.3 shows the refractive index profile of an LPG; there is a sinusoidal change in the refractive index of the core. LPGs facilitate the coupling of light from the propagating core mode to one or more co-propagating cladding modes at discrete wavelengths. Some of the light coupled into the cladding is lost through scattering at the cladding/air interface and by absorption. This results in a transmission spectrum (figure 2.4) that contains a number of attenuation bands centred around a set of discrete wavelengths. As the characteristics of the coupling are dependent on the properties of the cladding modes, the attenuation bands of the transmission spectrum will be influenced by the fibre's external environment, such as changes in the surrounding refractive index.

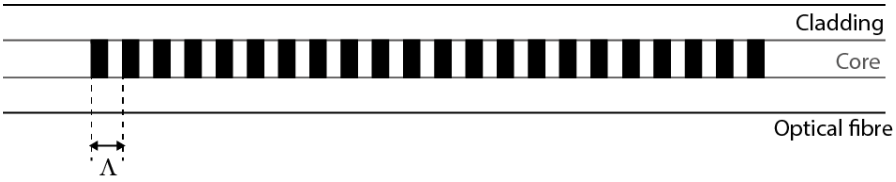

Figure 2.2: Long period grating with a uniform period, Λ, where the dark sections indicate irradiation.

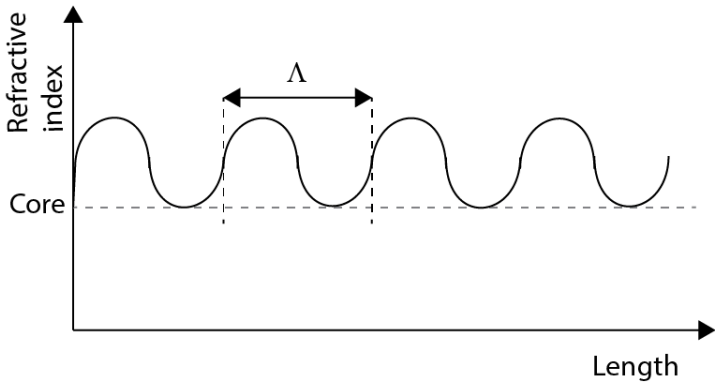

Figure 2.3: Refractive index profile of an LPG with a uniform period, Λ, where the peaks indicate the irradiated sections. The horizontal grey dotted line represents the refractive index of the core of the fibre.

The coupling of light between the co-propagating core and cladding modes occurs at discrete wavelengths and is dependent upon the phase matching condition being satisfied [7]:

$$\lambda = [n_{eff}(\lambda) - n^i_{clad}(\lambda)]\Lambda \tag{2.5}$$

where n_{eff} is the effective refractive index of the propagating core mode and n^i_{clad} is the refractive index of the ith cladding mode and Λ is the period of the LPG.

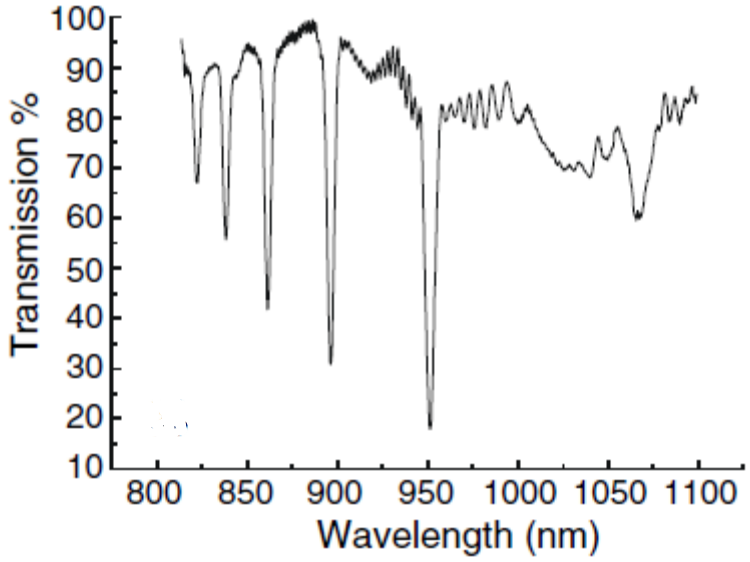

Figure 2.4: Transmission spectrum of a 400 μm LPG written in B-Ge co-doped photosensitive fibre [6].

The important factors that affect the depth of the attenuation bands are the depth of the index modulation, the overlap integral of the core and cladding mode that couple at the resonance wavelength and the length of the grating. This minimum transmission depth, T_i, is given by [6]:

$$T_i = 1 - sin^2(\kappa_i L) \tag{2.6}$$

where κ_i is the coupling coefficient for the ith cladding mode and L is the length of the LPG.

For a given modulation in refractive index induced in the fibre via exposure to, for example, UV irradiation, the guided core mode will only fully couple to one particular cladding mode; all other cladding modes will be either under or over coupled. As the coupling coefficient is dependent on the overlap of the electric field profiles of the core and cladding modes to which the light is coupled, it is different for each cladding mode so, for a given length, the attenuation bands of the transmission spectrum will then have different minimum transmission depths.

2.2 Modelling long period gratings

To predict the resonance wavelengths of an LPG, the effective indices of the core and cladding modes must first be calculated. By modelling features of an LPG, it helps determine the decision for choosing a particular period of an LPG sensor for any application.

The process can be broken down in a number of steps as follows:

1. Calculate the effective refractive indices of the core and cladding modes.
2. Calculate the electric field profiles of the core and cladding.
3. Determine the phase matching dispersion curves.

MATLAB has been used to apply the Transfer Matrix Method (TMM) to model and simulate a three-layer (core, cladding, ambient) cylindrical waveguide as shown in figure 2.5. TMM was used as it is fast and accurate and can be loosely based on coupled-mode theory, which is accurate but slow. Coupled-mode theory is used to describe configurations in which a slight perturbation or modification of the waveguide causes two or more modes to couple with each other. These modes travel through the fibre with discrete propagation constants, β, which are dependent on the wavelength of the light source as well as the structure of the fibre. The code was developed based on the theoretical formulation from the following papers by Erdogan (1997), Othonos (1997) and Anemogiannis et al. (2003) [8, 9, 10, 11].

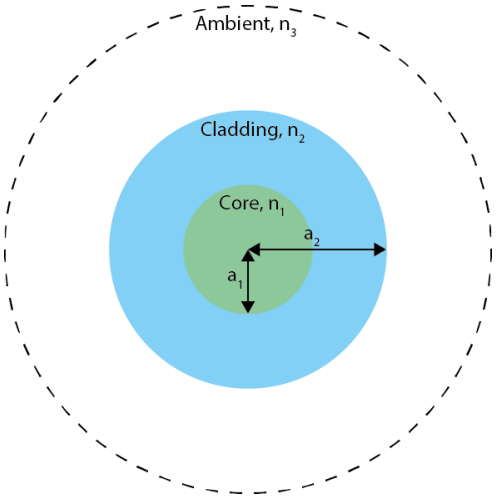

Figure 2.5: Three layer model of an optical fibre with the core refractive index, n_1, cladding refractive index, n_2, the ambient refractive index, n_3 and the core and cladding radii, a_1 and a_2 respectively.

As an optical fibre has two waveguide structures within it, one is a high refractive index core surrounded by a lower refractive index cladding and the other is the cladding surrounded by air [6], they are approached separately; the code models interactions between the core and the cladding modes at the core-cladding boundary and also the interactions between cladding modes with the air at the cladding-air boundary.

The propagation modes of the fibre were simplified by treating them as linearly polarised (LP). This is due to the fact that the refractive indices of the core and the cladding are similar in magnitude and so are regarded as weakly guiding [12]. The LP modes are almost transversely polarised, being dominated by one transverse electric field component and one transverse magnetic field component [12]. The transverse electric field component propagating along the z-axis is given by

$$\begin{aligned} U_{vj,i}(r,\phi,z) &= exp(-j\beta_{vj}z)\Psi_{vj,i}(r,\phi) \\ &= exp(-j\beta_{vj}z)\Phi_v(\phi)R_{vj,i}(r) \\ &= exp(-j\beta_{vj}z)\begin{Bmatrix} cos(v\phi) \\ sin(v\phi) \end{Bmatrix} \times \begin{Bmatrix} A_{vj,i}J_v(r\gamma_{vj,i}) + B_{vj,i}Y_v(r\gamma_{vj,i}) \\ A_{vj,i}I_v(r\gamma_{vj,i}) + B_{vj,i}K_v(r\gamma_{vj,i}) \end{Bmatrix} \end{aligned} \tag{2.7}$$

$$\text{when} \begin{matrix} \beta_{vj,i} < k_0 n_i \\ \beta_{vj,i} > k_0 n_i \end{matrix}$$

where $\beta_{vj,i}$ is the propagation constant of the LP_{vj} mode, $\gamma_{vj,i} = \sqrt{|k_0^2 n_i^2 - \beta_2^{vj}|}$ is the magnitude of the transverse wavenumber, ϕ is the azimuthal angle and $A_{vj,i}$ and $B_{vj,i}$ are non-normalised field expansion coefficients determined by the boundary conditions within the cylindrical layer i. $J_v(r\gamma_{vj,i})$ and $Y_v(r\gamma_{vj,i})$ are the Bessel functions of the first and second order v, and $I_v(r\gamma_{vj,i})$ and $K_v(r\gamma_{vj,i})$ are the modified Bessel functions of the first and second order v. v is a non-negative integer number.

The TMM was used in order to determine the propagation constants of the 3 layer optical fibre waveguide. The continuity condition of the radial variation of the field (see equation 2.7) along the interface between two cylindrical layers (core/cladding and cladding/environment) was applied. This condition required that the electric fields in the two adjacent layers to be equal at their interface. The derivative of the two fields with respect to the radius also had to be equal at the same interface. The continuity condition therefore provided two equations whose solution could be

represented as a matrix:

$$\begin{bmatrix} A_{vj,i} \\ B_{vj,i} \end{bmatrix} = \begin{bmatrix} \frac{m_{11}^{i,j+1}(\beta_{vj})}{Q_i} & \frac{m_{12}^{i,j+1}(\beta_{vj})}{Q_i} \\ \frac{m_{21}^{i,j+1}(\beta_{vj})}{Q_i} & \frac{m_{22}^{i,j+1}(\beta_{vj})}{Q_i} \end{bmatrix} \begin{bmatrix} A_{vj,i+1} \\ B_{vj,i+1} \end{bmatrix} \tag{2.8}$$

where

$$\begin{aligned} m_{11}^{i,j+1}(\beta_{vj}) &= \gamma_{vj,i} D_v'(r_i\gamma_{vj,i}) C_v(r_i\gamma_{vj,i+1}) - \gamma_{vj,i} D_v(r_i\gamma_{vj,i}) C_v'(r_i\gamma_{vj,i+1}) \\ m_{12}^{i,j+1}(\beta_{vj}) &= \gamma_{vj,i} D_v'(r_i\gamma_{vj,i}) D_v(r_i\gamma_{vj,i+1}) - \gamma_{vj,i} D_v(r_i\gamma_{vj,i}) D_v'(r_i\gamma_{vj,i+1}) \\ m_{21}^{i,j+1}(\beta_{vj}) &= -\gamma_{vj,i} C_v'(r_i\gamma_{vj,i}) C_v(r_i\gamma_{vj,i+1}) + \gamma_{vj,i} C_v(r_i\gamma_{vj,i}) C_v'(r_i\gamma_{vj,i+1}) \\ m_{22}^{i,j+1}(\beta_{vj}) &= -\gamma_{vj,i} C_v'(r_i\gamma_{vj,i}) D_v(r_i\gamma_{vj,i+1}) + \gamma_{vj,i} C_v(r_i\gamma_{vj,i}) D_v'(r_i\gamma_{vj,i+1}) \\ Q_i &= \frac{2}{\pi r_i} \text{ when } \beta_{vj} < K_0 n_i \\ &= \frac{-1}{r_i} \text{ when } \beta_{vj} > K_0 n_i \end{aligned} \tag{2.9}$$

In the TMM; the electric field in one layer was related to the field in the next layer by a matrix. Thus, for a two layer waveguide equation 2.7 could be re-written as

$$\begin{bmatrix} A_{vj,1} \\ B_{vj,1} \end{bmatrix} = M_{1,2} \begin{bmatrix} A_{vj,2} \\ B_{vj,2} \end{bmatrix} \tag{2.10}$$

where 1 represents the core, 2 represents the cladding and $M_{1,2}$ is the first matrix on the right hand side of equation 2.8.

The electric field in the innermost and outermost layers had to be finite, which required the condition that coefficients $B_{vj,1}$ and $A_{vj,N}$ be zero, with N being the number of layers in the waveguide. This meant that the matrix had to be $M_{1,2} = 0$, i.e. $M_{2,2}^{1,2}(B_{i,j}) = 0$ (see equation 2.9).

The propagation constants of the modes of the fibre waveguide were obtained by solving the equation for zero crossing using a MATLAB subroutine. These solutions were then used to calculate the effective refractive index of the core.

For a three layer waveguide, to incorporate the cladding and air interface, the transfer matrix (equation 2.10) was adapted and written as

$$\begin{bmatrix} A_{vj,1} \\ B_{vj,1} \end{bmatrix} = M_{1,2} M_{2,3} \begin{bmatrix} A_{vj,3} \\ B_{vj,3} \end{bmatrix} = M \begin{bmatrix} A_{vj,3} \\ B_{vj,3} \end{bmatrix} \tag{2.11}$$

where

$$M = M_{1,2} \cdot M_{2,3} \tag{2.12}$$

The matrix M for the three layer waveguide was the equivalent of the matrix $M_{1,2}$ for the two layer waveguide (equation 2.10). The solution for the propagation constants of the cladding modes and hence the effective refractive indices could therefore follow a similar algorithm. In this case, for the electric field to be finite in the innermost and outermost layers, $M_{2,2} = 0$.

The radius of the cladding is greater than that of the core and is therefore able to guide many different light modes. Figure 2.6 shows that the effective refractive indices of the modes decreases with increasing wavelength. For the higher cladding modes, the gradient of the curve becomes steeper, indicating that this effect becomes more prominent and the dispersion of the cladding modes becomes greater as the wavelength increases. The parameters used for modelling the fibre are detailed in table 2.1, which represent the photosensitive Fibercore PS750 fibre used for experiments in this thesis [13].

Table 2.1: Parameters used for modelling optical fibre, based on values of the Fibercore PS750 fibre [13].

Core radius (a_1)	62.6 μm
Cladding radius (a_2)	2.2 μm
Core refractive index (n_1)	1.4583
Cladding refractive index (n_2)	1.4533
Ambient refractive index (n_3)	1.0

Using the calculated dispersion of the modes of the core and cladding, a group of phase matching curves can be produced. In figures 2.7 and 2.8 the phase matching curves for the first 7 (LP_{02} - LP_{08}) then LP_{013} - LP_{022} cladding modes, respectively, are plotted. These figures show how the wavelengths that facilitate coupling between the core and cladding modes are dependent on the period of the LPG. The graphs from both graphs indicate that coupling to lower-order modes can be achieved using gratings with longer periods and those with shorter periods will promote coupling to the higher-order modes. By modelling the phase matching dispersion curves, it is possible to relate the attenuation bands in experimentally obtained transmission spectra to the cladding modes to which light is coupled.

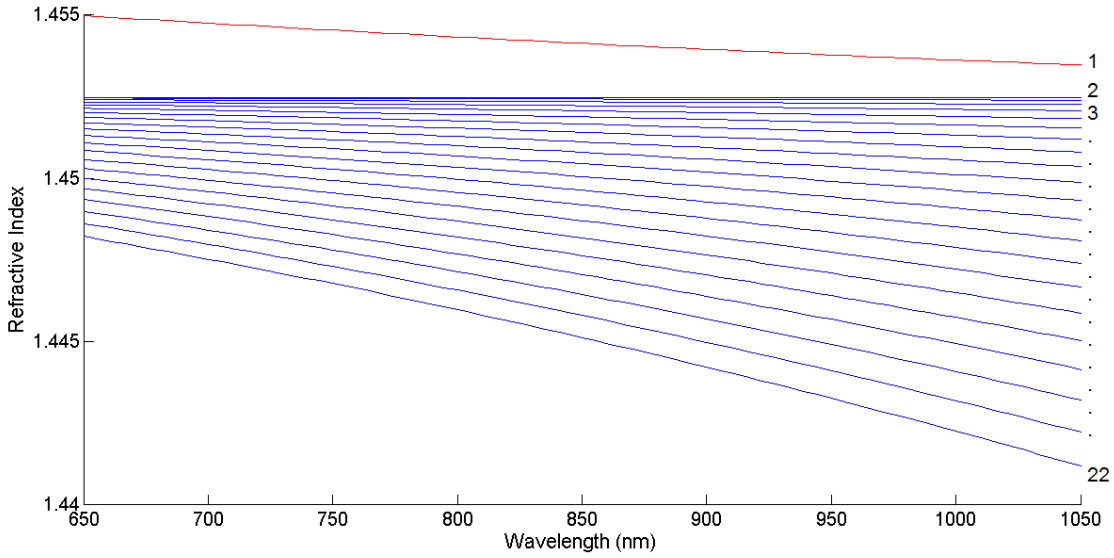

Figure 2.6: Effective refractive indices of the core (red) and first 21 cladding modes (blue) against wavelength. The numbers refer to the cladding modes LP_{0x}.

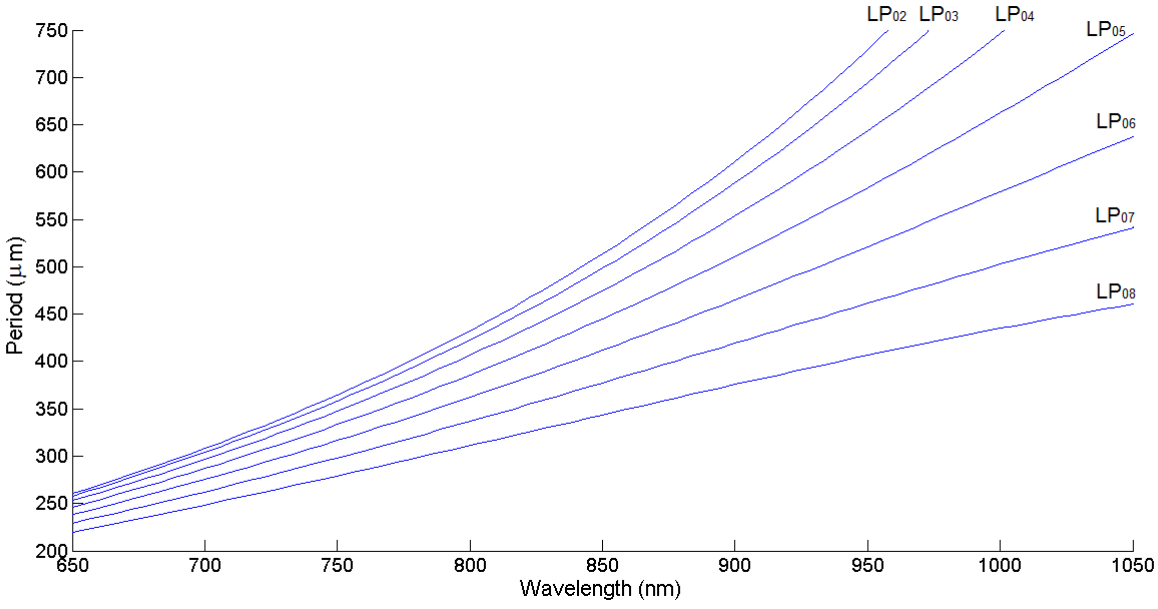

Figure 2.7: LPG phase matching curves, where the period is plotted against wavelength for the coupling to the LP_{02} - LP_{08} cladding modes.

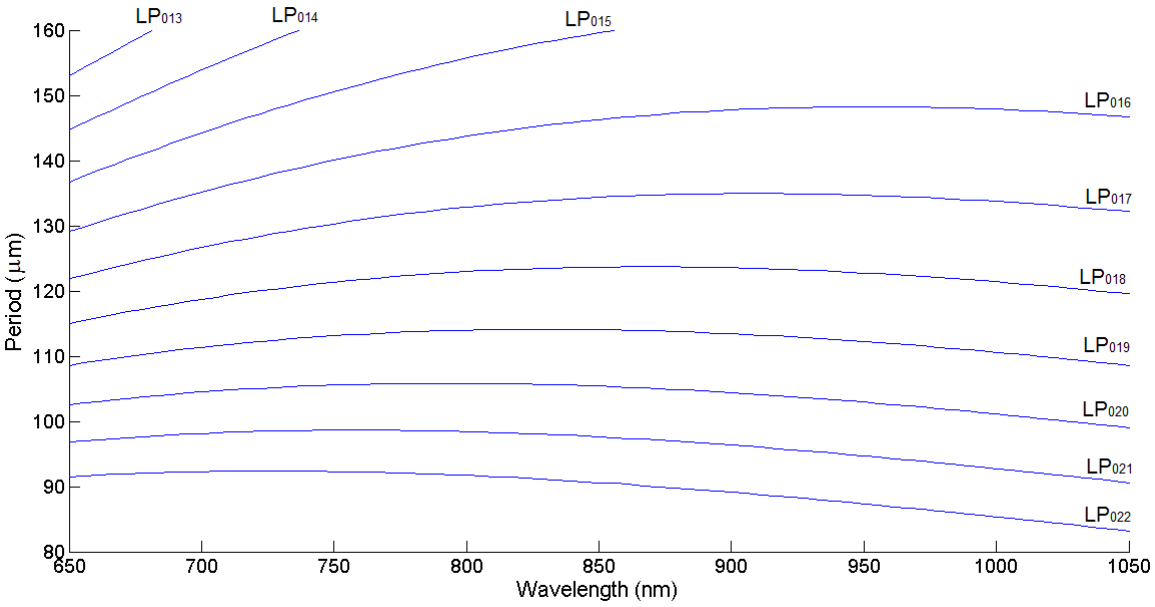

Figure 2.8: LPG phase matching curves, where the period is plotted against wavelength for the coupling to the LP_{013} - LP_{022} cladding modes.

2.3 Long period grating sensitivities

2.3.1 Origin of temperature sensitivity

The temperature sensitivity of an optical fibre LPG is dependent on the period of the grating, the composition of the fibre, and the order of the cladding mode to which coupling occurs. By using the chain rule and differentiating equation (from equation 2.5), the LPG sensitivity can be understood [7]:

$$\frac{d\lambda}{dT} = \frac{d\lambda}{d(\delta n_{eff})}\left[\frac{dn_{eff}}{dT} - \frac{dn_{clad}}{dT}\right] + \Lambda\frac{d\lambda}{d\Lambda}\frac{1}{L}\frac{dL}{dT} \tag{2.13}$$

where λ is the central wavelength of the attenuation band, T is the temperature, n_{eff} is the effective refractive index of the propagating core mode and n_{clad} is the effective refractive index of the propagating cladding mode, $d(\delta n_{eff}) = n_{eff} - n_{clad}$, Λ is the period of the LPG and L is the length of the LPG.

The first term on the right hand side (RHS) of equation 2.13 is attributed to the thermo-optic effect and is thus a material contribution. As the temperature changes, the differential refractive index between the core and the cladding changes. This contribution is dependent on the order of the different cladding modes, and the material composition of the fibre. The second term is the waveguide contribution

and depends on the LPG period. For LPGs with periods greater than 100 μm, the dominating effects are from the material contribution, while for periods less than 100 μm, this effect is negligible [7].

By taking into account the contributions from this combination of influences, LPGs have been fabricated with the ability to respond with a positive sensitivity, negative sensitivity or even insensitivity to temperature. For LPGs used as temperature sensors, a high sensitivity would be required. Shu et al. [14] reported a temperature sensitivity of 2.75 nm(^{o}C)$^{-1}$ in LPGs fabricated in photosensitive B-Ge co-doped fibre. However, the LPG's sensitivity to temperature can also pose problems if it is intended to measure other measurands. The ability to fabricate LPGs with at least one insensitive attenuation band is attractive, for instance for producing temperature insensitive sensors [7, 15]. Other means of suppressing the temperature sensitivity have included changing the composition of the fibre by doping the core [16] and by coating fibre with materials with positive thermo-optic coefficient [17]. The former showed a change in temperature sensitivity of -0.142 nm(^{o}C)$^{-1}$ to 0.002 nm(^{o}C)$^{-1}$ and the latter from -0.049 nm(^{o}C)$^{-1}$ to 0.0007 nm(^{o}C)$^{-1}$.

2.3.2 Origin of axial strain sensitivity

An LPG's axial strain sensitivity is also dependant on material and waveguide contributions. By differentiating equation 2.5 with respect to axial strain, ϵ, the wavelength shift can be obtained.

$$\frac{d\lambda}{d\epsilon} = \frac{d\lambda}{d(\delta n_{eff})}\left[\frac{dn_{eff}}{d\epsilon} - \frac{dn_{clad}}{d\epsilon}\right] + \Lambda\frac{d\lambda}{d\Lambda} \tag{2.14}$$

The material effects stem from the strain-optic effect as well as the change in the fibre's transverse dimensions, while the waveguide contribution comes from the slope of the phase matching curve $\frac{d\lambda}{d\Lambda}$. For periods greater than 100 μm, the material contribution is negative and the waveguide contribution is positive [7], offering the opportunity, by appropriate choice of parameters, to design a sensor with a resonance band that is insensitive to strain.

Bhatia and Vengsarkar [18] showed that the strain sensitivity of an LPG varied greatly depending on the type of fibre that was used. By using a dispersion shifted fibre, a negative strain sensitivity of -7.27 nm(%ϵ)$^{-1}$ was measured, yet with a 980 nm single mode fibre a 15.21 nm(%ϵ)$^{-1}$ positive sensitivity for the fifth-order

attenuation band was reported. It was shown that it was possible to fabricate a temperature- and strain-insensitive torsion sensor using a phase shifted LPG. The wavelength separation between the peaks of the attenuation band only changed with applied twists [19] and did not experience cross sensitivity from the other measurands.

2.3.3 Surrounding refractive index sensitivity

The LPG's sensitivity to changing surrounding refractive index (RI) derives from the phase matching condition's dependence on the effective refractive index of the fibre's cladding modes. The effective refractive indices of the cladding modes are determined by the difference between the refractive index of the cladding and the refractive index of the surrounding environment. The greatest sensitivity occurs when the surrounding refractive index approaches that of the fibre cladding. Higher cladding modes experience a greater sensitivity than lower cladding modes [20].

By exploiting the sensitivity of LPGs to surrounding RI, sensors have been developed for liquid level measurements [21], for determining concentrations of chemicals [22], and as biosensors and chemical sensors [23, 24, 25]. When the RI of the surrounding medium approaches that of the fibre cladding, the attenuation bands experience large wavelength shifts, with shifts of 100 nm having been reported [15]. Methods of adjusting the RI sensitivity include coating an LPG with a functional material (see section 2.4.6), whereby the LPG can be made more or less sensitive to refractive index and other measurands [26]. Introducing a bend radius of 20 mm allowed an LPG to discern water and a 5 wt% saline solution [27].

2.4 Types of long period gratings

Due to the increasing use of LPGs in a variety of applications in sensing and communications, many variations of LPGs have been configured and employed. Some of these configurations are mentioned below.

2.4.1 Long period gratings at the phase matching turning point

The phase matching curves (2.9) show that each cladding mode of an optical fibre has a turning point. However, the phase matching turning point (PMTP) for a

low order mode occurs at a higher wavelength an period than that of a high order cladding mode [28]. For shorter periods near the PMTP, coupling occurs to a cladding mode at two wavelengths 2.10. The transmission spectrum of LPGs fabricated with a period that matches the PMTP have been reported to have high sensitivity to external surroundings [29, 14]. For this thesis, the turning points at lower order cladding modes are at wavelengths which are outside the range of interest (600 nm -1100 nm) or outside the wavelength range of the available spectrometers (also see chapter 3). To be able to write LPGs within this range, optical fibre with a short cut-off wavelength of 627 nm was used.

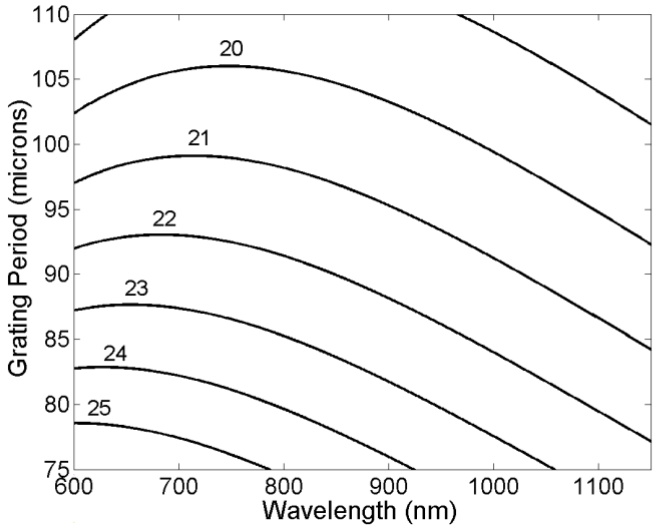

Figure 2.9: Phase matching curves of the LP_{020} - LP_{025} modes showing the relationship between grating period and wavelength [29].

The uses for LPGs at the PMTP include refractive index sensing, strain and temperature sensing [14, 30]. Such gratings, when coated with an appropriate functional film also have the potential to be used as highly sensitive chemical sensors [29]. When an external parameter influences the LPG, the effective indices of the cladding modes shift. This will cause the two attenuation bands of the mode at the PMTP to move further apart, or move towards each other.

2.4.2 Chirped long period gratings

There are two ways in which a long period grating can be chirped; continuously (figure 2.11(a)) or stepped (figure 2.11(b)). A step chirped long period grating (SCLPG) is one where the periods are varied in large discrete steps and consists of a number of sections where the period in each section is constant [31]. When an LPG

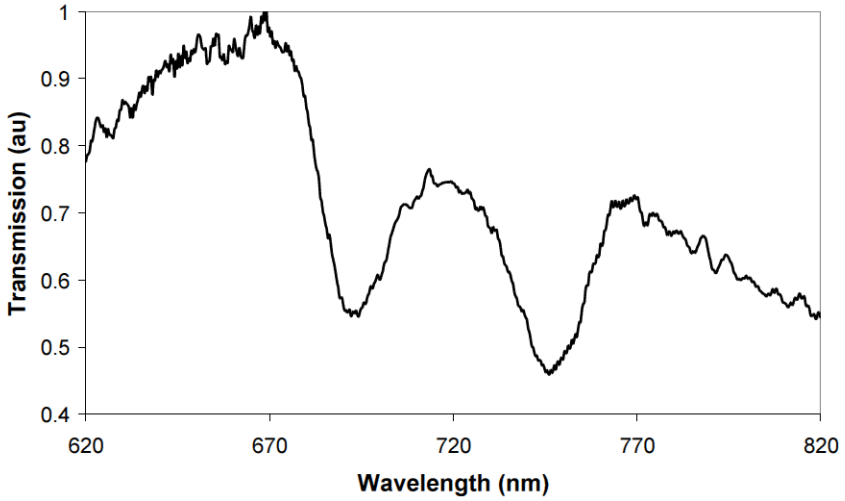

Figure 2.10: Transmission spectrum of a long period grating with a period selected that it lay just below the PMTP (LP_{024} mode) with a period of 80 μm fabricated in Fibrecore SM750 single mode fibre [29].

is designed to have a period that varies continually from one end of the grating to the other according to some prescribed function which, for example, could be linear it is referred to as a continuously chirped long grating (CCLPG) [32].

For a chirped grating, the grating period, Λ, can be expressed as a function of the position along the grating, z [31]

$$\Lambda(z) = \Lambda_o + Cz \tag{2.15}$$

where Λ_o is the starting period and C is the chirp constant.

The attenuation bands of chirped gratings have a larger bandwidth and show a decrease in their attenuation (see figure 2.12), as the variation of the period along the axis of the grating means the coupled wavelengths vary as a function of the position along the LPG [33]. The central wavelengths of the attenuation bands can be derived by combining equations 2.15 and 2.5. The attenuation of the bands are shallow as the length of the LPGs contributing to the coupling at each wavelength is small.

Chirped long period gratings (CLPG) have been proposed for use as directional flow sensors [33] where the broadened attenuation band changes shape depending on the position of the material along the grating. They have also been used as tunable multi-wavelength filters [31]. Das *et al* proposed a wavelength division multiplex-

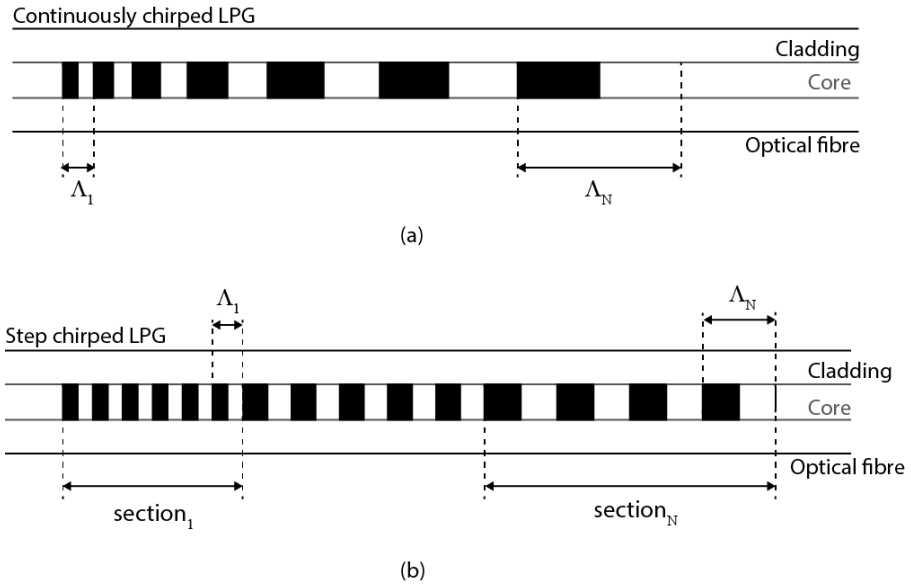

Figure 2.11: (a) Continuously chirped and (b) step chirped LPGs where Λ_1 denotes the first period and Λ_N the final period. In the step chirped configuration, the period remains the same for each section. The black sections denote the irradiated sections of the core.

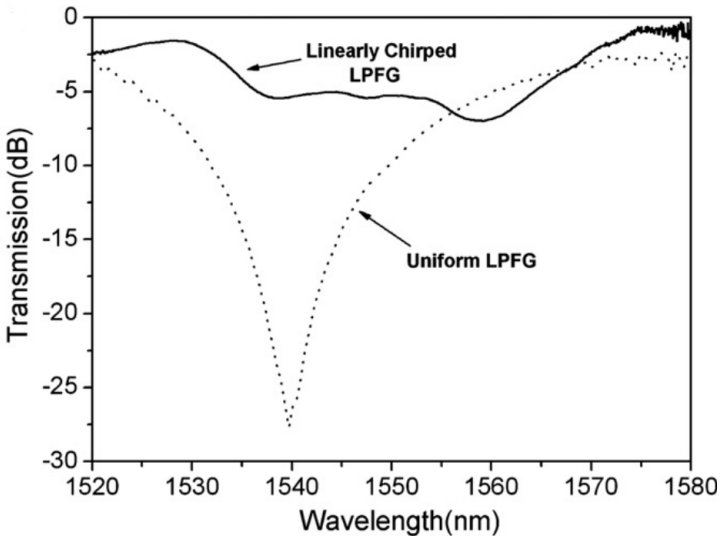

Figure 2.12: Transmission spectra of a linearly chirped LPG represented by the solid line (605 - 655 μm period) and a uniform period LPG (625 μm period) represented by the dotted line [31]. The fibre used was Corning SMF28. LPFG is defined as long period fibre grating.

ing isolator by fabricating two concatenated CLPGs. A channelled spectrum with almost equally spaced bands is produced [34].

2.4.3 Cascaded long period gratings

A cascaded LPG consists of two or more LPGs written along the same section of fibre in series. When two identical LPGs are written in a single length of fibre, the interaction of the coupled core and cladding modes creates a channelled spectrum with each attenuation band. The first LPG works as normal and couples some of the light from the core to the cladding. The light then propagates in the grating free region towards the second grating via the core and the cladding. At the second LPG, the cladding mode couples back into the core to form a Mach-Zehnder interferometer (figure 2.13) [35]. Due to the difference between the effective refractive indices of the core and cladding modes, the light coupled from the cladding back into the core at the second LPG experiences a different optical path length compared with the light that propagated through the cladding. As with any path length imbalanced interferometer, when viewed in the wavelength domain, the interference generates a channelled spectrum, as shown in figure 2.14. The distance between the gratings determines the period of the channelled spectrum pattern within the attenuation bands of the LPG [36]. The fringe pattern is fine enough (due to narrow bandwidth) to offer a higher sensitivity and resolution for sensing purposes. The smaller the separation, the longer the period of the channelled spectrum. Other parameters which affect the characteristics of the transmission on the cascaded long period grating are the number of gratings written, and the length of each grating.

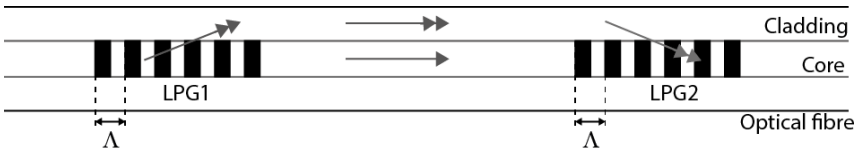

Figure 2.13: Illustration showing the operation of a cascaded LPG with the light from LPG1 coupling back into LPG2. Reproduced from [35].

Cascaded long period gratings have been used for applications such as bend sensing where it is shown that when bends are induced in the fibre the attenuation of the attenuation bands increases and the channelled spectrum degrades [37]. Other uses include refractive index measurement, transverse load measurement and the multiplexing of LPG based sensors [35]. If both the gratings are covered with a material that changes the surrounding refractive index, the fringe pattern will be reduced and the attenuation bands shift [38]. However, if only the gap between the gratings is covered with a high RI material, the attenuation bands can be much more sensitive than that of a single uniform period LPG and the channelled spectrum changes whilst the envelope of the band remains unchanged [39]. By adding a transverse

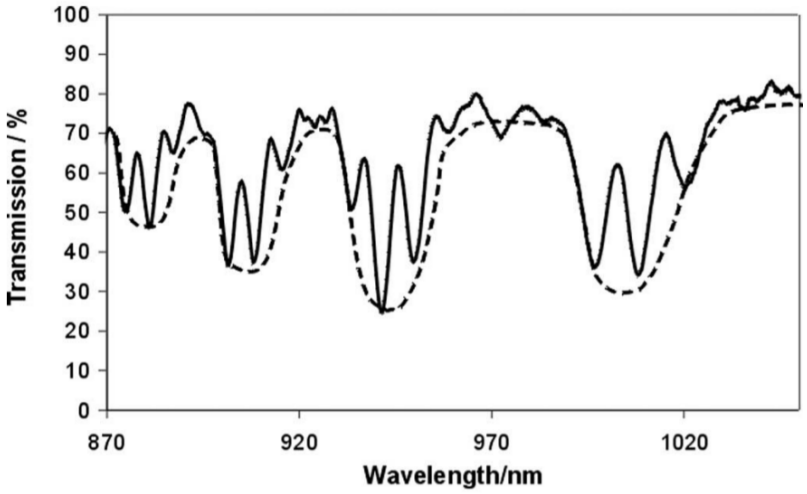

Figure 2.14: Transmission spectrum of a cascaded LPG with two LPGs; interference fringes are created in the attenuation bands [35].

load, the fringes of the channelled spectrum reduce until they disappear at a given load. The pattern reappears with a π phase shift as there is a further increase in load, due to the changes in the phase of the modes [38]. Murphy et al. demonstrated the effect of multiplexing two LPG sensors in series. By using Fourier techniques, the phase of the channelled spectrum of each LPG could be discerned and therefore discriminate between different measurands acting on each LPG [35].

2.4.4 Tilted long period gratings

An LPG can be written such that there is a periodic modulation of the refractive index of the fibre created at an angle with respect to the optical axis of the fibre (see figure 2.15). The angle between the normal of the tilted fringes and the axial direction of the optical fibre is known as the tilt angle, θ. This angle causes the light to couple to different cladding modes than those of a uniform (non-tilted) LPG [40] and also make it possible to choose any desired resonant wavelengths by adjusting the tilt angle in fibre amplifiers [41]. In non-tilted LPGs, the fundamental LP_{01} core more couples to cladding modes with the same azimuthal order number $l = 1$ (LP_{lm}). However, with tilted LPGs, this core mode can couple to modes with higher azimuthal order numbers [42, 43].

As shown in figure 2.15, tilted LPGs can be fabricated using an amplitude mask. Due to the tilt angle of the amplitude mask θ, the period of the grating, Λ_t, becomes

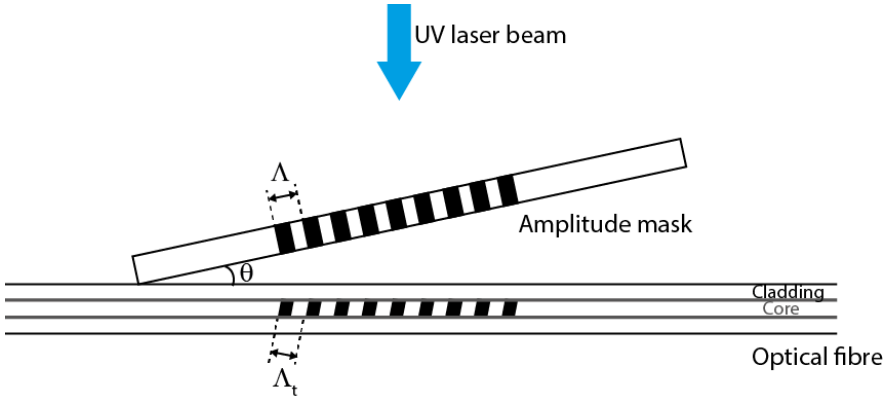

Figure 2.15: Schematic showing how tilted LPGs can be fabricated with an amplitude mask (period, Λ) positioned at angle, θ, to the axis of the fibre. The period of the grating, Λ_t changes according to the tilt of the angle. Adapted from [41].

[41]

$$\Lambda_t = \Lambda cos\theta \tag{2.16}$$

where Λ is the period of the grating if no tilt was introduced. The period of the grating increases when a tilt is introduced.

The phase matching condition is thus modified and the resonant wavelengths, λ_t, are represented by

$$\lambda_t = [n_{eff}(\lambda_t) - n^i_{clad}(\lambda_t)]\Lambda cos\theta \tag{2.17}$$

where n_{eff} is the effective refractive index of the propagating core mode and n^i_{clad} is the refractive index of the ith cladding mode.

Figure 2.16 shows a comparison of the transmission spectrum of LPG fabricated with at a tilt of 0^o and at a tilt angle of 35^o. When there is no tilt, three attenuation bands are evident but with the addition of a tilt, a fourth band becomes visible indicating the modes coupled to can change by imposing a tilt on the LPG.

Tilted LPGs (TLPG) have been used as pressure sensors where Zhang *et al.* [44] showed that a larger tilt angle lead to a higher pressure sensitivity. TLPGs have also been demonstrated as a means of controlling the resonant wavelengths for gain equalisation in amplifiers [41].

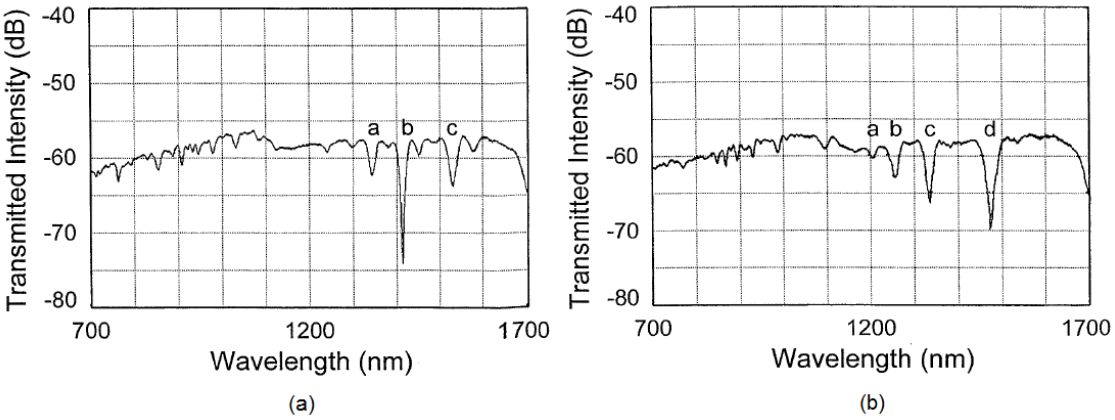

Figure 2.16: Transmission spectra of a 460 μm LPG fabricated in a single mode fibre (Sumitomo Electric Industries) with an amplitude mask with (a) no tilt (0^o) and (b) 35^o tilt angle [41]. The attenuation bands are labelled with a - c with an extra band produced, d, in (b) due to the tilt angle.

2.4.5 Phase shifted long period gratings

Disrupting the periodicity in one or more places in the grating structure (as shown in figure 2.17) creates phase steps, which can be used to create extra features with the LPG attenuation bands as shown in figure 2.18.

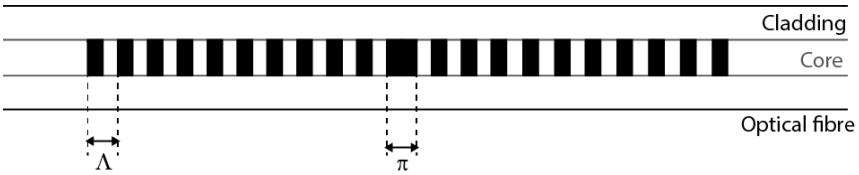

Figure 2.17: A phase shifted LPG of period Λ with a single phase shift, π, in the centre of the grating.

The period of a long period grating with a uniform structure can be described by re-occurring 2π phase shifts. When a single π phase shift is created in the middle of the grating (as shown in section 3.3.4.2) two attenuation bands are generated either side of the resonance wavelength due to the constructive interference at phase matching wavelengths of the light coupled into the cladding from the section of grating on either side of wave step [45]. The resulting LPG spectrum will consist of narrower attenuation bands which can lead to high resolution measurements.

It is possible to create more than one phase shift in a single grating. When LPGs with multiple phase shifts are written, the difference in wavelength between the split attenuation band increases. However, when they are equally spaced, extra bands

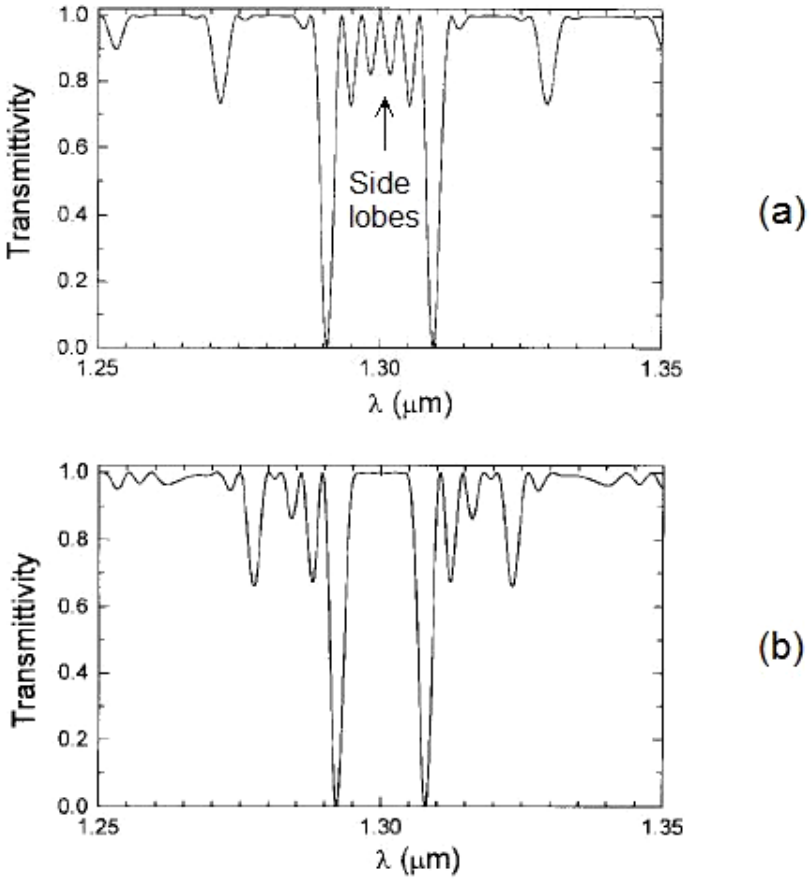

Figure 2.18: Transmission spectrum of (a) a LPG with 5 π phase shifts that are equally spaced and (b) a LPG with π phase shifts and length apodisation [46].

appear in between them and are known as side lobes. To suppress these lobes it is possible to distribute the phase shifts along the length of the grating in the form of, for example, a Gaussian distribution; this is known as length apodisation [28, 45]. Figure 2.18 shows the transmission spectrum of a phase shifted LPGs with 5 π phase shifts with and without length apodisation [46].

Phase shifted LPGs have been used as an optical bandpass filter [47] and as they have narrower attenuation bands means it is possible to resolve smaller wavelength shifts for a greater sensitivity and higher resolution measurements in sensor systems.

2.4.6 Coating deposition on long period gratings

By applying appropriate coatings to the surface of the cladding it is possible to influence the coupling of modes to modify the sensitivity of an optical fibre sensor (section 5 discusses a chemical sensor where an LPG is coated with nanoscale thin film). The deposition of a coating can make a sensor insensitive or reduce its sen-

sitivity to a measurand; by coating an LPG for example, the thermal response of the attenuation bands can be reduced with a material with a negative thermo-optic coefficient [6]. Smietana *et al.* [26] demonstrated a plasma deposited silicon nitride thin film coated LPG, which allowed them to tune the LPG's sensitivity to refractive index such that changes induced by other measurands could be detected with reduced cross sensitivity. Other examples to show the use of coated LPGs include relative humidity sensors, by coating with a hydrogel sensitive to humidity changes [48]. Coated LPGs have been exploited as gas and chemical sensors. For instance, silica based porous films infused with an ammonia sensitive material have been used as a highly sensitive detector of ammonia in water with fast response times of less than 100 seconds [23, 49].

2.5 Summary

This chapter covers the basic theory of LPGs and gives and types of LPGs. A simple Matlab model was introduced to provide a qualitative analysis of the phase matching dispersion curves of an LPG. This facilitated the decision when choosing LPG periods and it gave an indication as to which modes were being coupled to. The chapter includes the origins of LPG's sensitivities to certain measurands, underlining why they are useful and versatile as sensors. An overview of different types of LPGs that have been fabricated, how they work and what they have been used for was also discussed. Table 2.2 summarises the the different configurations of LPGs and highlights some of the applications they have been used for.

Table 2.2: Summary of different types of LPGs, highlighting the main attributes and applications they have been used for.

Type of LPG	**Characteristics**	**Application**
Phase matching turning point	Sensitive dual resonance bands	RI sensing [30], strain sensing [14], temperature sensing [14], chemical sensing [29]
Chirped	Broad attenuation bands	Directional flow [33], tuneable multi-wavelength filters [31]
Cascaded	Chanelled spectrum pattern	Bend sensing [37],RI sensing [38, 39], strain sensing [38]
Tilted	Resonance dependent on tilt angle	Pressure sensing [44], gain amplification [41]
Phase shifted	Two attenuation bands generated around the resonance wavelength	Optical bandpass filter [47]

References

[1] C C Davis. *Lasers and Electro-Optics*. Cambridge University Press, 1996.

[2] P Yeh. *Optical Waves in Layered Material*. John Wiley & Sons Inc., 1998.

[3] S J Buggy. *Composite material process monitoring using optical fibre gratings sensors*. PhD thesis, Cranfield University, 2008.

[4] V Bhatia. *Properties and Sensing Applications of Long-Period Gratings*. PhD thesis, Virginia Polytechnic Institute and State University, 1996.

[5] A M Vengsarkar, P J Lemaire, J B Judkins, Bhatia V, T Erdogan, and Sipe J E. Long-period fiber gratings as band-rejection filters. *Journal of Lightwave Technology*, 14(1):58–65, 1996.

[6] S W James and R P Tatam. Optical fibre long-period grating sensors: characteristics and application. *Measurement Science and Technology*, 14(5):R49–R61, 2003.

[7] V Bhatia, D K Campbell, D Sherr, T G D'Alberto, N A Zabaronick, G A Ten Eyck, K A Murphy, and R O Claus. Temperature-insensitive and strain-insensitive long-period grating sensors for smart structures. *Optical Engineering*, 36(7):1872–1878, 1997.

[8] T Erdogan. Cladding-mode resonances in short- and long- period fiber grating filters. *Journal of the Optical Society of America A*, 14(8):1760–1773, 1997.

[9] T Erdogan. Fibre grating spectra. *Journal of Lightwave Technology*, 15(8):1277–1294, 1997.

[10] A Othonos. Fiber Bragg gratings. *Review of Scientific Instruments*, 68(12):4309–4341, 1997.

[11] E Anemogiannis, E N Glytsis, and T K Gaylord. Transmission characteristics of long-period fiber gratings having arbitrary azimuthal/radial refractive index variations. *Journal of Lightwave Technology*, 21(1):218–227, 2003.

[12] D Gloge. Weakly guiding fibers. *Applied Optics*, 10(10):2252–2258, 1971.

[13] Fibercore Ltd. PS750 fibre parameters. *Personal communication*, 2014.

[14] X Shu, T Allsop, B Gwandu, and Bennion I Zhang, L. High-temperature sensitivity of long-period gratings in B-Ge co-doped fiber. *IEEE Photonics Technology Letters*, 13(8):818–820, 2001.

[15] V Bhatia, D K Campbell, T G D'Alberto, G A Ten Eyck, , D Sherr, K A Murphy, and R O Claus. Standard optical fiber long-period gratings with reduced temperature sensitivity for strain and refractive-index sensing. *Proceedings of OFC, Optical Fiber Communicaiton Conference*, FB:346–347, 1997.

[16] Y G Han, C S Kim, U C Paek, and Y Chung. Performance enhancement of long period fiber gratings for strain and temperature sensing. *IEICE Transactions of Electronics*, E83-C(3):282–286, 2000.

[17] J N Jang, S Y Kim, S W Kin, and M S Kim. Temperature insensitive long-period fibre gratings. *Electronics Letters*, 35(24):2134–2136, 1999.

[18] V Bhatia and A M Vengsarkar. Optical fiber long-period grating sensors. *Optics Letters*, 21(9):692–694, 1996.

[19] X L Li, W G Zhang, J Ruan, and S S Zhang. Temperature- and strain-insensitive torsion sensor based on phase shifted ultra-long-period-grating. *Electronics Letters*, 48(4):235–236, 2012.

[20] S Khaliq. *Fibre Optic Long Period Gratings For Sensing Applications*. PhD thesis, Cranfield University, 2003.

[21] S Khaliq, S W James, and R P Tatam. Fibre optic liquid level sensor using long period gratings. *Optics Letters*, 26(16):1224–1226, 2001.

[22] R Falciai, A G Mignani, and A Vannini. Long period gratings as solution concentration sensors. *Sensors and Actuators B*, 74(1-3):74–77, 2001.

[23] S Korposh, R Selyanchyn, W Yasukochi, S W Lee, S W James, and R P Tatam. Optical fibre long period grating with a nanoporous coating formed from silica nanoparticles for ammonia sensing in water. *Materials Chemistry and Physics*, 133(2-3):784–792, 2012.

[24] X Shu and D Huang. Highly sensitive chemical sensor based on the measurement of the separation of dual resonant peaks in a 100-m-period fiber grating. *Optics Communications*, 171(1-3):65–69, 1999.

[25] T Allsop, L Zhang, and I Bennion. Detection of organic aromatic compounds in paraffin by a long-period fiber grating optical sensor with optimized sensitivity. *Optics Communications*, 191(3-6):181–190, 2001.

[26] M Smietana, W J Bock, P Mikulic, and J Chen. Pressure sensing in high-refractive index liquids using long-period gratings nanocoated with silicon nitride. *Sensors*, 10(12):11301–11310, 2010.

[27] H Tsuda and K Urabe. Characterization of long-period grating refractive index sensors and their applications. *Sensors*, 9(6):4559–4571, 2009.

[28] S M Topliss, S W James, F Davis, S P J Higson, and R P Tatam. Optical fibre long period grating based selective vapour sensing of volatile organic compounds. *Sensors and Actuators B: Chemical*, 143(2):629–634, 2010.

[29] C S Cheung, S M Topliss, S W James, and Tatam R P. Response of fibre optic long period gratings operating near the phase matching turning point to the deposition of nanostructured coatings. *Journal of the Optical Society of America B Optical Physics*, 25(6):897–902, 2008.

[30] X Lan, Q Han, T Wai, J Huang, and H Xiao. Turn-around-point long-period fiber gratings fabricated by CO_2 laser point-by-point irradiations. *IEEE Photonics Technology Letters*, 23(22):1664–1666, 2011.

[31] M Yan, S Luo, L Zhan, Y Wang, Y Xia, and Z Zhang. Step-changed period chirped long-period fiber gratings fabricated by CO_2 laser. *Optics Communications*, 281(10):2784–2788, 2008.

[32] R Kashyap. Fabrication of Bragg gratings. In R Kashyap, editor, *Fibre Bragg Gratings*, pages 349–377. 2009.

[33] S J Buggy, S W James, and R P Tatam. A long period grating based directional flow sensor. *Proceedings of the SPIE, 19th International Conference on Optical Fibre Sensors*, 7004:70045P–1–70045P–4, 2008.

[34] M Das and K Thyagarajan. Wavelength-division multiplexing isolation filter using concatenated chirped long period gratings. *Optics Communications*, 197(1-3):67–71, 2001.

[35] R P Murphy, S W James, and R P Tatam. Multiplexing of fiber-optic long-period grating-based interferometric sensors. *Journal of Lightwave Technology*, 25(3):825–829, 2007.

[36] B A L Gwandu, X Shu, T D P Allsop, W Zhang, L Zhang, D J Webb, and I Bennion. Simultaneous refractive index and temperature measurement using a cascaded long-period grating device. *Proceedings of IEEE Sensors*, 3(2):1032–1035, 2002.

[37] B H Lee and J N. Bending sensitivity of in-series long-period fiber gratings. *Optics Letters*, 23(20):1624–1626, 1998.

[38] Y G Han, B H Lee, W T Han, U C Paek, and Y J Chung. Fibre-optic sensing applications of a pair of long-period fibre gratings. *Measurement Science and Technology*, 12(7):778–781, 2001.

[39] O Duhem, J F Henninot, and M Douay. Study of in fiber Mach-Zehnder interferometer based on two spaced 3-dB long period gratings surrounded by a refractive index higher than that of silica. *Optics Communications*, 180(4-6):255–262, 2000.

[40] R Wu, Y Liu, J Zou, N Chen, F Pang, and T Wang. Fabrication of tilted long-period fiber gratings by CO_2 laser. *Proceedings of the SPIE*, 8307:83072D1–83072D–7, 2011.

[41] T Mizunami, H Kawashima, and A Hayashi. Wavelength tuning of long-period fiber gratings by fabrication using a tilted amplitude mask. *Optical Review*, 9(5):202–206, 2002.

[42] R Wu, Y Liu, N Chen, F Pang, and T Wang. Fabrication and sensing characteristics of tilted long-period fiber gratings. *Proceedings of the SPIE, Advanced Sensor Systems and Applications V*, 8561:85610G1–85610G7, 2012.

[43] K S Lee and T Erdogan. Fiber mode conversion with tilted gratings in an optical ber. *Journal of the Optical Society of America A*, 18(5):1176–1185, 2001.

[44] Y F Zhang, C C Chan, Y M Chan, and P Zu. Tilted long period gratings pressure sensing in solid core photonic crystal fiberss. *Sensors Journal, IEEE*, 12(5):954–957, 2012.

[45] H Ke, K S Chiang, and J H Peng. Analysis of phase-shifted long-period fiber gratings. *IEEE Photonics Technology Letters*, 10(11):1596–1598, 1998.

[46] S M Topliss. *Optical Fibre Long Period Grating Sensors with Nanostructured Coatings*. PhD thesis, University of Cranfield, 2011.

[47] Y Han. Transmission characteristics of multiply-cascaded phase-shifted long-period fiber gratings. *Journal of the Korean Physical Society*, 57(6):1751–1754, 2010.

[48] L Wang, Y Lie, M Zhang, D Tu, X Mao, and Y Liao. A relative humidity sensor using a hydrogel-coated long period grating. *Measurement and Science Technology*, 8(10):3131, 2007.

[49] S Kodaira, S Korposh, W Batty, S W James, and S W Lee. Fabrication of highly efficient fibre-optic gas sensors using SiO_2/polymer nanoporous thin films. *Proceedings of IEEE, 3rd International Conference on Sensing Technology*, 133:481–485, 2008.

Chapter 3

Fabrication of long period gratings

3.1 Introduction

3.2 Methods of fabrication

LPGs are fabricated by modifying the refractive index of the core of the optical fibre either by photo-induction, or by physically deforming the optical fibre [1]. The refractive index may be modified by locally exposing the fibre to the output from a high powered UV laser [2, 3], a CO_2 laser [4, 5], an infra-red femtosecond laser [6] or by ion implantation [7]. Deformation of the fibre can be caused mechanically (e.g. by inducing physical periodic corrugations on the fibre) [8], or by periodically tapering the fibre using a CO_2 laser [9] or an electrical arc discharge [10] as the heat source.

To inscribe gratings onto the core of an optical fibre using UV irradiation, the fibre must first be made photosensitive, i.e. the refractive index of the core should be sensitive to UV radiation. One method is to dope the core of the fibre during manufacture with, for example, germanium (Ge). In 1978, Hill et. al [11] were the first to observe and report the photosensitivity of Ge-doped optical fibres. By utilising the interference pattern of two counter propagating coherent beams a refractive index grating was formed inside the fibre core. The refractive index change in the fibre was caused by a two-photon process at wavelengths of 488 nm or 514.5 nm [11]. They were able to identify the presence of the grating by monitoring the increase in back reflections of the light couple into the fibre. UV radiation is a popular choice for writing gratings in optical fibre as it produces symmetrical coupling and has good repeatability in terms of fabrication [12, 13]. UV causes changes in the refractive index in Ge-doped silica as the wavelength of the radiation closely matches energy level transitions, which lead formation of germanium related defects [14].

UV irradiation at a wavelength of less than 200 nm of a single mode fibre with 3% germanium doping can induce refractive index changes of round 3 x 10^{-5} [15]. Other dopants which have been used include, but are not limited to, nitrogen [16], tin [17], cerium [18] and europium [19]. Another common method for improving photosensitivity is via hydrogen loading [20]; the doped fibre is kept at room temperature in a high pressure tank (150 bar) filled with hydrogen which, over time (typically 1-2 weeks), diffuses into the core of the optical fibre. Storing the fibre at a high pressure prevents the out-diffusion of hydrogen from the fibre. By introducing hydrogen to the optical fibre, the refractive index of the core and cladding increases. Hydrogen causes deeper bands as the disassociated hydrogen molecules (from UV light) react with the germanium in the fibre core, quenching the amount of hydrogen there is in the core. The hydrogen from the cladding will now migrate into the core to replace the depletion; the distribution of hydrogen is no longer uniform and there is a higher effective index in the core [21, 22]. When the hydrogen-loaded fibre is exposed to UV radiation, a greater refractive index modification can be achieved, leading to stronger coupling and deeper attenuation bands in the long period grating's transmission spectrum. However, over time (when the fibre is out of the high pressure environment) the hydrogen will gradually diffuse out of the fibre causing the refractive indices of the core and cladding to decrease, which leads to a shift in the central wavelengths of the attenuation bands. This can pose as a problem when carrying out long term experiments. This problem can be overcome by annealing the section of the fibre containing the LPG at an elevated temperature. This causes the hydrogen to diffuse rapidly out of the fibre and remove the unstable refractive index change in the fibre. The attenuation bands will then have a repeatable response to environmental perturbation, provided the temperature remains below the annealing temperature.

Amplitude masks can be used to introduce a spatial modulation of the intensity of the laser beam on the optical fibre. The quality of the masks used are not as stringent as those of phase marks often used for the fabrication of fibre Bragg gratings (FBG), due to the relaxed tolerance associated with the longer period [23]. The inscription of an LPG can also be carried out in a point-by point fashion which is a more flexible approach, allowing arbitrary choice of the grating period, allowing the period to be chirped, or the introduction of phase steps [23]. In the point-by-point approach, a section of fibre with a length typically equal to half the desired period is exposed to the UV irradiation for a set dwell time. The fibre or laser beam is translated by one period and the fibre exposed again. This process is repeated until

the required grating length is achieved. The approach is also used when fabricating LPGs using CO_2 laser irradiation. Amplitude masks may be more expensive as new masks have to be purchased each time a grating of a new period is required. However, an advantage of amplitude masks is that they have the possibility of writing a single grating quicker as the entire section can be irradiated at the same time. The use of a CO_2 laser can be versatile and cost effective as masks or photosensitive fibres do not need to be purchased [5].

LPGs can also be fabricated mechanically by placing the fibre between two plates, one flat and one with periodically separated grooves [8]. The pressure from the grooves induces a refractive index modulation as the optical properties of the fibre are changed via the photoelastic effect. By adjusting the pressure used, the depth of the indentation can be tuned which will lead to deeper attenuation bands in the spectrum of the LPG. This method works more successfully if the fibre jacket is not removed as the loss is reduced and spectra are cleaner [8]. Sohn and Peng [24] used strategically positioned metal wires to create the grooves in the fibre. The requirement of external pressure was replaced with the use of epoxy during cure to compress the wires onto the fibre. Mechanically induced LPGs have the advantage of being erasable, meaning the same length of fibre can be reused to create LPGs with varying periodicities [8, 24]. Tapered LPGs fabricated via electric arc discharge have also been demonstrated [13, 25]. A fibre is placed on a pulley system to ensure the optical fibre remains straight and an electric arc is discharged onto the fibre. As it is heated, the pulley stretches the fibre causing a small taper. This process is repeated periodically along the length of the fibre until the desired LPG length is achieved [25].

3.3 Experimental fabrication of long period gratings

3.3.1 Point-by-point technique

The experimental configuration used to fabricate the LPGs in this thesis is shown in figure 3.2. This method employs the point-by-point technique and is carried out using a UV laser. UV irradiation was chosen for fabricating LPGs as the system was readily available and it allowed gratings to easily be fabricated into photosensitive fibre. The system previously used at Cranfield University [26] to fabricate LPGs was modified with the aim of improving the quality and repeatability of the fabrication

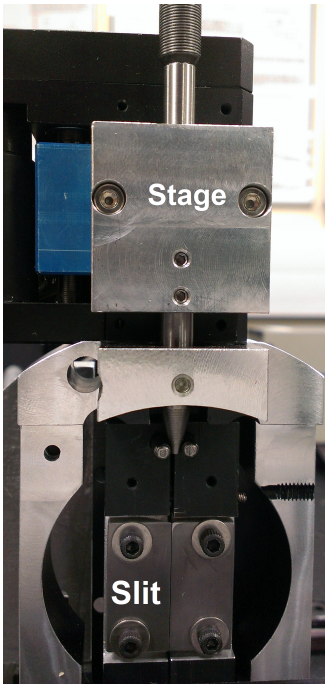

Figure 3.1: Photograph of the slit used in the setup for point-by-point fabrication. As the translation stage moves, a pointed dowel moves down towards the jaws, forcing them to open.

process. The modifications are highlighted in section 3.3.3.

The output from an Nd:YAG laser (injection-seeded, flashlamp-pumped Spectra Physics Quanta-Ray Nd:YAG Laser, repetition rate of 10 Hz, output energy of 110 mJ at 266 nm, pulse width 4-5 ns) was guided towards the fibre by a series of optical components (see figure 3.2). The average power output from the laser was 300 mW when injection seeded. Experience has shown that if the power density falling on the optical fibre is too high, the fibre can be damaged and become too fragile to handle. This indicated the importance of being able to control the power reaching the fibre. A variable attenuator was used as this gave reliable and repeatable control over how much power was incident on the fibre whilst the laser operated at the maximum of the gain efficiency curve for stable maximum output power. The variable attenuator was composed of a half-wave plate retarder and a polariser that worked at Brewster's angle. Only the p-polarised light was able to pass through the attenuator. A suitable beam dump (Optosigma 119-0785) was used to absorb the reflected energy from the unused s- polarised radiation transmitted by the device.

The output from the attenuator was reflected by a beam-splitter toward a circular plano-convex focusing lens of 70 mm, which was used to focus the beam down to a

9.5 μm beam waist diameter determined using Gaussian beam theory. Methods of determining the beam size on fibre include using a focussing lens [5, 27, 28] To change the period of the grating, the focal lens can be changed (which can be costly) or the fibre can be moved closer of further away in relation to the beam focus. However, the beam width is only well defined in the centre of the focal region and may affect the quality of the LPGs fabricated. A practical way to define the length of section to be exposed was to use a slit. This slit was positioned 9.5 mm beyond the focus of the beam, such that the beam diameter at the slit was 3.4 mm. The optical fibre was positioned 1 mm behind the slit. The use of this slit was beneficial as both jaws of the slit moved apart in unison (see figure 3.1) with the result that the central point always remained in the same position so that the alignment of the UV beam did not have to be adjusted when a different period was selected. The slit width was adjusted by means of a computer controlled linear translation stage (PI, M-110.1DG) with a resolution of 7 nm and maximum travel of 5 mm. The relationship between the movement of the linear translation stage and the width is $slit = 0.35 \times stage + 5.06$. This provided a significantly high resolution control over the slit width, which as shown in section 3.4, is of great importance when fabricating LPGs with periods near the phase matching turning point. The optical fibre was attached to a translation stage by a standard v-groove fibre holder and magnet. A high resolution (8 nm) translation stage (PI, M-150.11), with a maximum travel of 50 mm, was used. This translation stage was controlled by a LabView program to allow the fibre to be moved according to the period that was desired by the user. The program was developed to allow the user to not only choose the period, dwell time and length of the grating but also to allow the stage to be controlled such that chirped and phase shifted LPGs could be written, in addition to uniform period LPGs (see section below; 3.3.4). The time taken to write one LPG is dependent on the chosen grating pitch, the required grating length and dwell time for each period written. The power used to write gratings was around 60 mW (before the focusing lens), and typically the dwell time was 35 s for each period. Considering, for example a slit width of 50 μm, the average beam power incident on the fibre for the duration of the 35 s dwell time was calculated to be 3.87 mW. Before each LPG was fabricated, the period was verified by placing a length of fibre with its polyacrylate buffer jacket intact into the system and exposing the fibre for a period of 5 seconds. The exposed fibres were examined under an optical microscope and the period was measured.

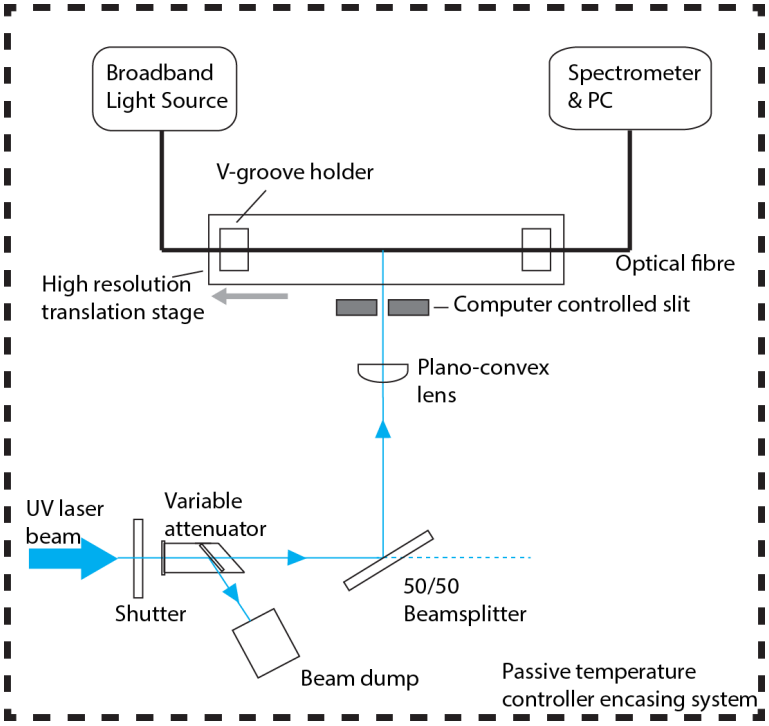

(a)

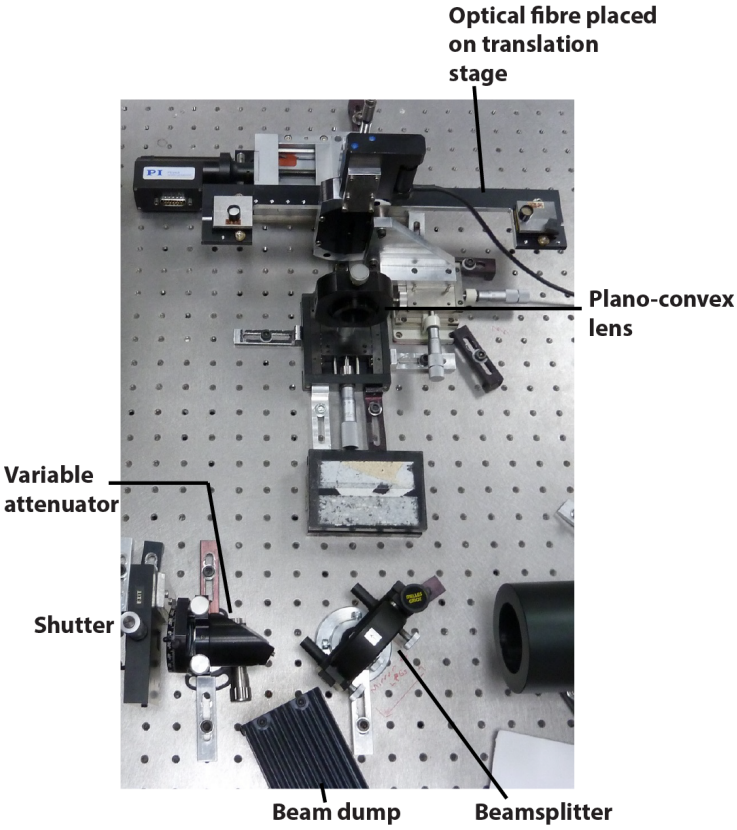

(b)

Figure 3.2: The (a) schematic and (b) photograph of the setup developed for fabricating LPGs using a UV laser beam and the point-by-point method. The width of the illuminating beam is set by the gap of the computer controlled slit and the translation stage moves periodically.

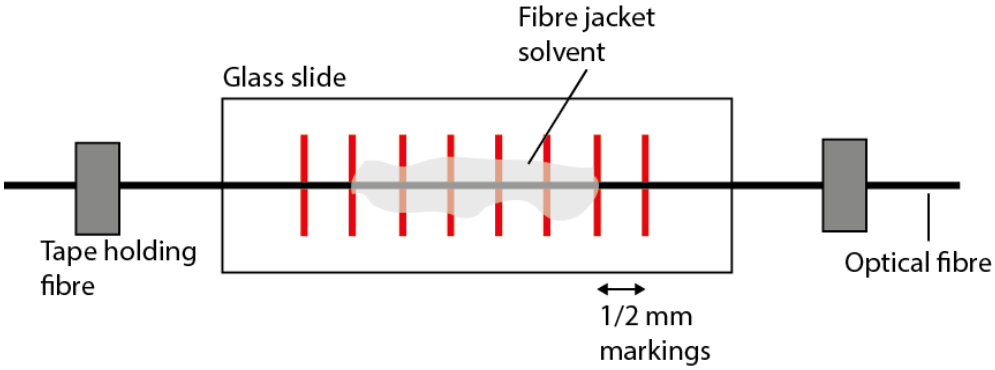

Figure 3.3: The process carried out for stripping an optical fibre used for fabricating LPGs.

3.3.2 Optical fibre preparation

To prepare the optical fibre for the fabrications of LPGs, the polymer buffer coating (usually made from PVC or polyurethane) of the section of the fibre where the grating is to be written must first be removed. This is because the coating absorbs the energy from the UV radiation, preventing it from reaching the glass fibre. The appropriate section of the fibre is placed on a microscope slide marked at 0.5 mm intervals. The interval markings allows the user to determine the desired length of the stripped section. The fibre is covered with a thin layer of 'Nitromors', which is a proprietary paint stripper with the active solvent ingredients dichloromethane and methanol (as shown in figure 3.3). By using this method, the coating can be removed without damaging the surface of the cladding and thus without affecting the mechanical integrity of the fibre. Other coating removal approaches, such as the use of mechanical strippers, can reduce the mechanical strength by, for example, scratching the surface of the cladding. The fibre is left in the solvent for 1 minute, after which the jacket and paint stripper are removed by wiping with a lens tissue. The bare fibre is then cleaned of any residue by wiping the surface with a lens tissue soaked with Isopropyl alcohol (IPA). After being cleaned, the optical fibre is attached to a translation stage by a v-groove fibre holder and magnet. The beginning of the stripped section was placed in line with the gap in the slit.

The evolution of the transmission spectrum of the LPG was monitored during fabrication by attaching one end of the fibre to a broadband tungsten-halogen light source and the other to an Ocean Optics CCD spectrometer (HR4000 with a wavelength range of 600 nm - 1050 nm and a resolution of 0.02 nm) via SMA bullet connectors (Newport). The spectrometer consists of a plane grating which diffracts in the incoming light and is sent to a linear CCD array. Each element of the array

has a corresponding pixel and the separation of these pixels gives the wavelength resolution; if there are a high number of pixels, the resolution of the spectrometer will be high [**?**]. As the LPG was being written, the transmission spectrum revealed resonance/attenuation bands as the light coupled between the guided core and the co-propagating cladding modes.

Variable parameters for fabrication setup
For a given grating length, changing the dwell time influences the change in refractive index in the core of the fibre. Increasing the dwell time will increase the amplitude of the refractive index modulation and therefore the depth of the attenuation bands in the LPG's transmission spectrum. However, having a long dwell time may potentially weaken the structure of the fibre, making the grating fragile to handle. The length of the grating affects the number of periods that contribute to the phase matching condition.

3.3.3 Development and evolution of the LPG fabrication setup

A versatile method for fabricating reproducible fibre optic LPG sensors was developed. The single system can be used to fabricate different LPG configurations. The following section describes the development of the system. Figure 3.4 shows the original setup used for writing LPGs before the changes were made.

A stepper-motor controlled stage with a resolution of 2 μm [26]) was previously used. A simple LabView program for controlling was available to control the movement of the stage to enable the fabrication of long period gratings with uniform periods. This system was replaced with a high 8 nm resolution translation stage (PI, M-150.11) which can travel a maximum of 50 mm. The LabView program was changed to enable the fabrication of different types of LPGs and the fabrication of LPGs with different duty cycles.

The cylindrical lens with a focal length of 75 mm was used to focus the laser beam in a horizontal line, acquired from a system previously used to fabricate LPGs using an amplitude mask, was replaced with a circular plano-convex lens. This allowed a circular beam profile to be incident on the slit, concentrating the laser power density more efficiently.

In order to overcome the limitations imposed by defining the length of the irradiated

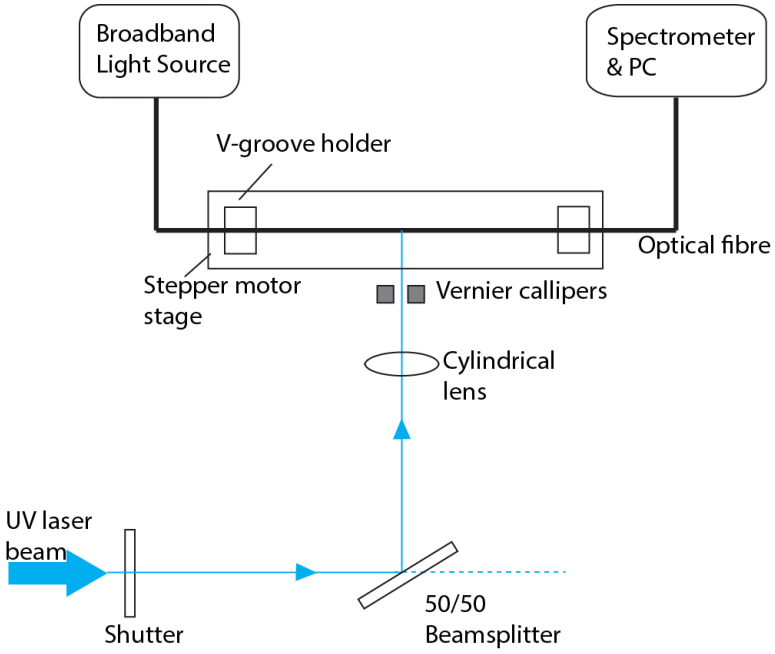

(a)

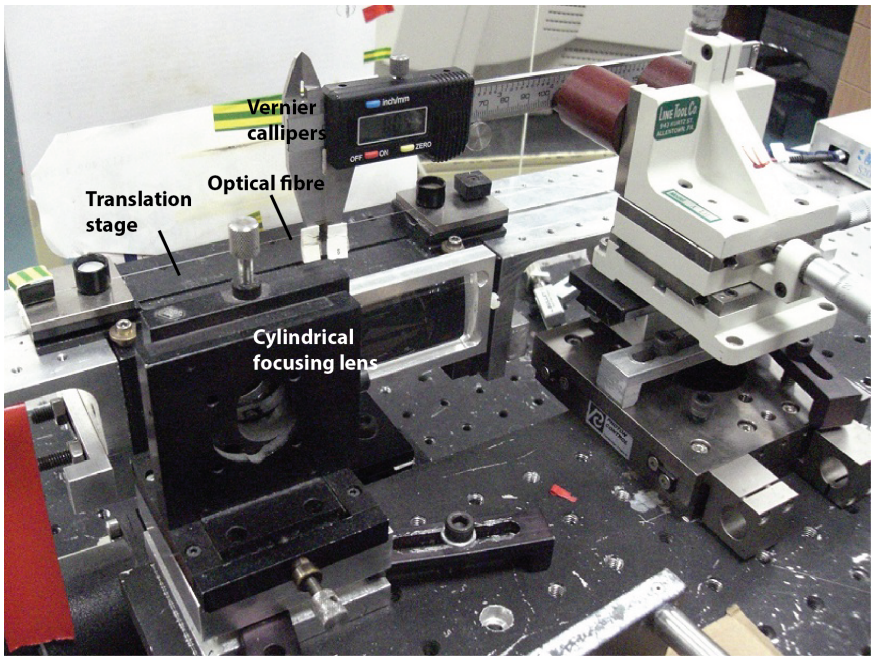

(b)

Figure 3.4: The (a) schematic and (b) photograph showing the original setup configured for fabricating LPGs using a UV laser beam and the point-by-point method.

section of the fibres with the vernier callipers initially a hand controlled mechanical slit was used. The callipers had a resolution of 10 μm which meant gratings could only be written provided their periods were divisible by 20 μm. The duty cycle of each grating may also not have been 50 % due to the limited accuracy in adjusting the callipers. The mechanical slit that was adjusted by hand had a finer resolution (1 μm) and unlike the callipers where only one jaw moved, both jaws moved apart in unison making the initial fibre alignment simpler. Eventually this was adapted to allow the slit to be computer controlled allowing for more consistent LPGs and did not have to rely on user intervention beyond entering the required LPG parameters in the LabView program. By computer controlling the slit with a more advanced LabView program, configurations of LPG such as chirped gratings, where the period does not remain constant for the entire length of the LPG, could also be written.

As mentioned in the previous section, 3.3.1, a variable attenuator was added to the system to allow control over the power output of the laser without requiring the flash lamp energy or SHG crystals to be altered which was found to lead to instabilities in the laser.

Passive temperature control of the environment, achieved by placing a thermally insulated box over the experimental setup, was added to reduce the temperature fluctuations and provide a more stable environment during the writing process. This helped improve the repeatability of the LPGs written with the temperature fluctuation reducing to $\pm$ 0.5 ^oC from more than 5 ^{o}C. The temperature was monitored by placing a wireless temperature logger (i-button® DS1923) within the system, in close proximity to the fibre.

3.3.4 Computer controlled fabrication

When LPGs of specific or unique characteristics are required, they are best produced using the point-by-point fabrication technique. This section discusses the properties of various types of LPGs, which was used to inform the development of a master LabView program to control the motion of the translation stages controlling the slit width and motion of the fibre.

3.3.4.1 Long period gratings with uniform periods

A uniform period LPG is depicted in figure 3.5 and is characterised by its constant period, Λ_0, along its entire length. Figure 3.6 shows the spectrum of a uniform

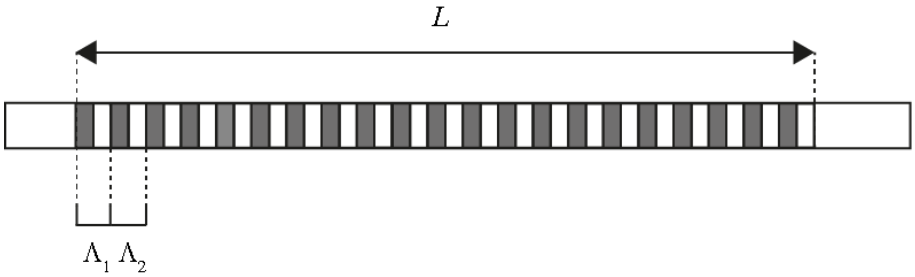

Figure 3.5: Uniform period LPG of length L and consisting of N periods. Λ_i; i^{th} period.

period LPG. The UV beam spot size which is defined via the slit and irradiates the fibre core, is configured to be $\Lambda_0/2$ (for a 50:50 duty cycle). After exposure of one section of fibre, the fibre is translated by a distance, Λ_0. This is repeated until the required number of periods have been fabricated. Equations 3.1 and 3.2 govern the fabrication of an uniform period LPG.

$$\Lambda_1 = \Lambda_2 = \Lambda_3 = ... = \Lambda_N = \Lambda_0 \tag{3.1}$$

$$L = \sum_{i=1}^{N} \Lambda_i \tag{3.2}$$

To verify the period of the LPG, a length of fibre was placed into the system. The outer polyacrylate buffer jacket of a single mode optical fibre was exposed to the laser beam through the slit. Figure 3.7 shows the fibre as it was examined under a microscope, after exposure to the UV beam with the system configured to write an LPG with a period of 400 μm.

3.3.4.2 Phase shifted long period gratings

When the periodicity of an LPG is broken, the LPG is said to be phase shifted. This behaviour may be implemented in one or multiple locations within the grating structure, leading to single or multiple phase shifts, respectively. Of interest is a π phase shift which, when inserted in the middle of the grating, leads to the attenuation bands of the LPG spectrum being split into two. Figure 3.8 shows the procedure used to create one or more phase shifts in the LPG during fabrication. In order to create a phase shift in the LPG, a section of the fibre core that is the length of the chosen period is irradiated entirely (as opposed to half the length as with a uniform period LPG), as seen in figure 3.9. Each grating period is constant along the entire length of the LPG, as in equation 3.1.

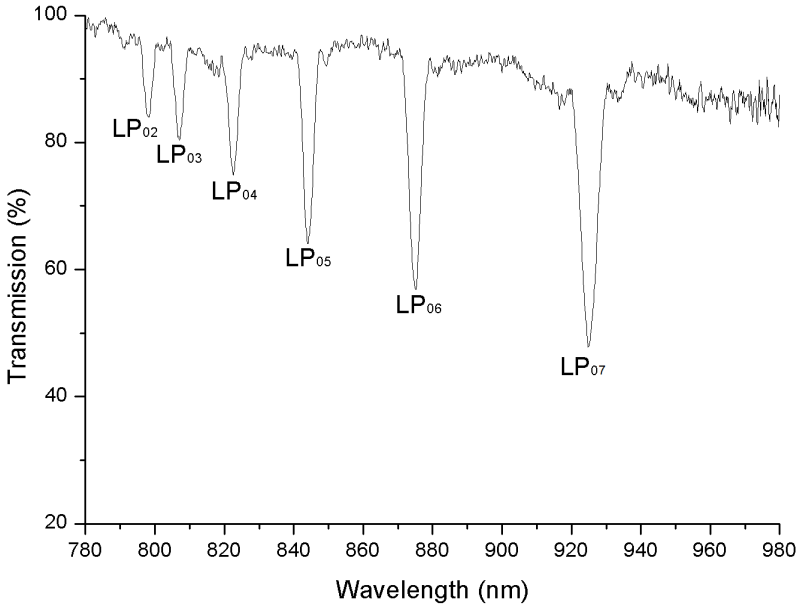

Figure 3.6: The transmission spectrum of a 400 μm period LPG, 35 mm in length written in PS750 fibre with a cutoff wavelength of 627 nm

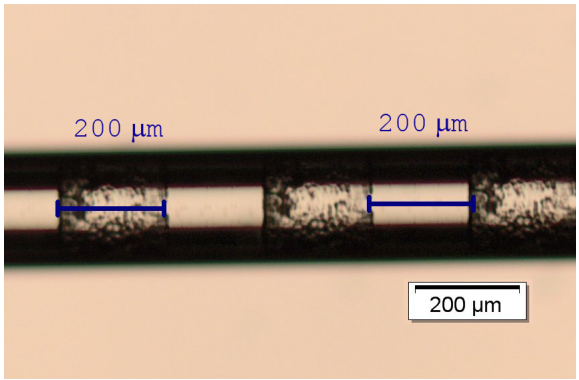

Figure 3.7: Optical images of the 400 μm period LPG inscribed on the fibre buffer jacket of a single mode fibre. The darker sections denote the regions exposed to the laser through the slit. Taken at magnification x5.

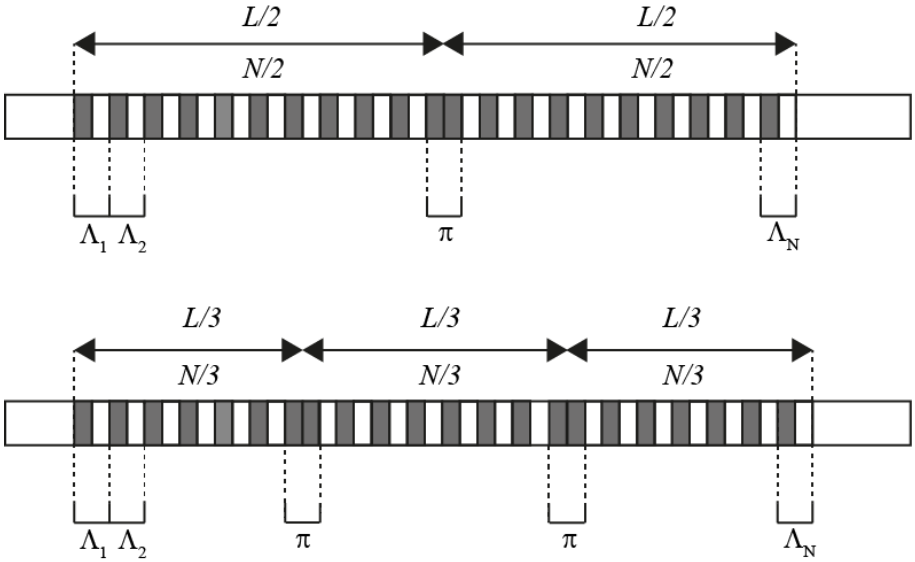

Figure 3.8: Phase shifted LPG of length L and consisting of N periods. (a) Single phase shift, (b) 2 phase shifts. π; phase shift, Λ_i; ith period.

A single phase shift in the centre of the LPG structure (figure 3.8) is inserted at

$$length\,position = \frac{L}{2} \tag{3.3}$$

$$period\,position = \frac{N}{2} \tag{3.4}$$

Two phase shifts in the LPG are inserted at

$$length\,position = \frac{L}{3}, \frac{2L}{3} \tag{3.5}$$

$$period\,position = \frac{N}{3}, \frac{2N}{3} \tag{3.6}$$

Equations 3.3, 3.4, 3.5 and 3.6 describe the physical locations where the phase shifts are to be inserted into a uniform period LPG. Collating these equations, the position of the n phase shifts, in a LPG can be represented by

$$length\,position = \frac{L}{(n+1)}, \frac{2L}{(n+1)}, ..., \frac{nL}{(n+1)} \tag{3.7}$$

$$period\,position = \frac{N}{(n+1)}, \frac{2N}{(n+1)}, ..., \frac{nN}{(n+1)} \tag{3.8}$$

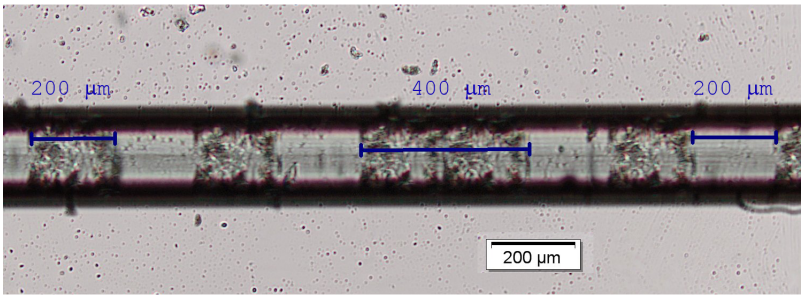

Figure 3.9: Optical images of a 400 μm period LPG with a single phase shift inscribed on the fibre buffer jacket of a single mode fibre. The darker sections denote the regions exposed to the laser through the slit. Taken at magnification x5.

Figure 3.10 shows an example of a 400 μm period LPG written with a single phase shift placed in the centre of the grating. As can be seen, the result is two narrow bands centred around a single LP mode (for a uniform period LPG only one band is present); this could lead to high resolution measurements.

3.3.4.3 Step chirped long period gratings

An LPG may be fabricated such that it consists of many different sections, with each section having the same period, and the size of the period changing from one section to the next. Such a grating device is referred to as a step chirped LPG (figure 3.11). The slit is set at $\Lambda_i/2$, such that as the period changes from section to section, so does the length of the irradiated section.

The step chirp is applied from one section to next and is represented by

$$step\,chirp = \Lambda_2 - \Lambda_1 = \Lambda_3 - \Lambda_2 = ... = \Lambda_N - \Lambda_{N-1} \tag{3.9}$$

where Λi is the grating period in the ith section of the step chirped LPG.

The following equations govern the fabrication of the step chirped LPG with the same number of periods in each section

$$\Lambda_i = \Lambda_1 + (i-1) \cdot chirp\,step \tag{3.10}$$

$$n = n_a = n_b = ... = n_N \tag{3.11}$$

$$l_1 = n \cdot \Lambda_i \tag{3.12}$$

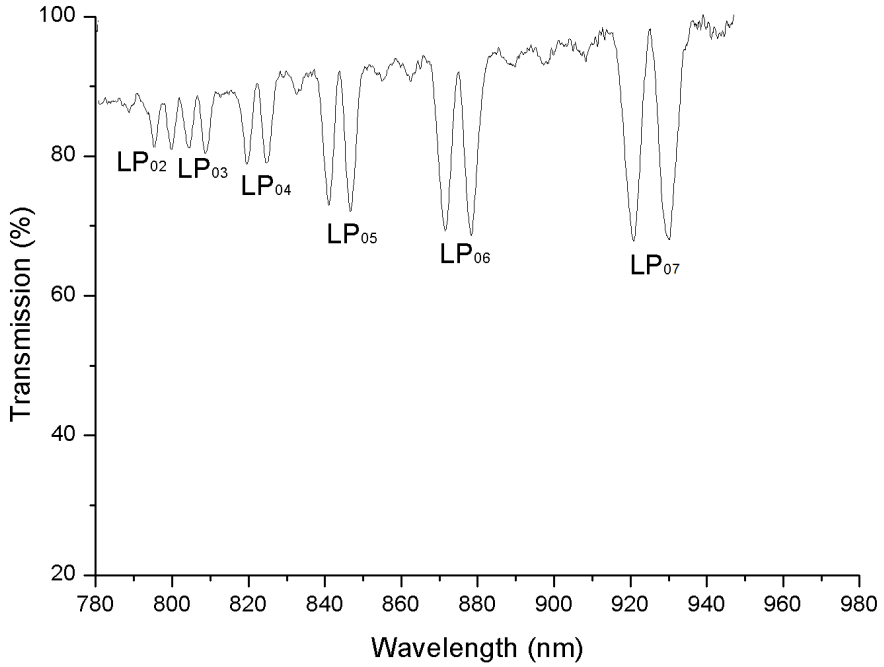

Figure 3.10: The transmission spectrum of a 400 μm period phase shifted LPG. A single phase shift was placed in the centre of the grating. The PSLPG (phase shifted long period grating) was 35 mm in length and was written in PS750 fibre with a cutoff wavelength of 627 nm.

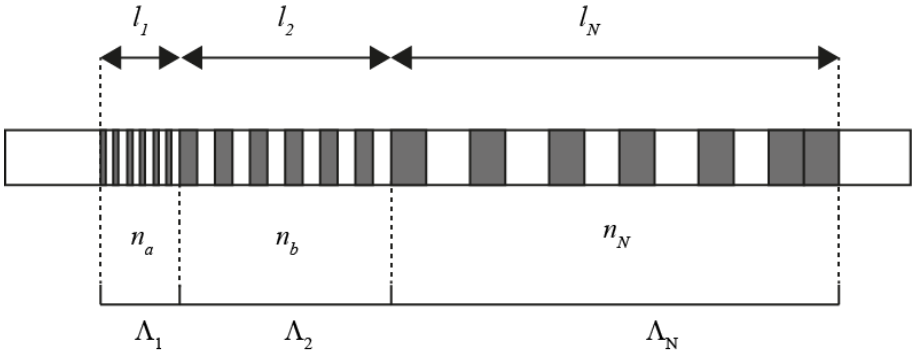

Figure 3.11: Step chirped LPG of length L and consisting of N sections. l_i; length of i^{th} section, Λi; period in the i^{th} section, n_i; number of periods in the i^{th} section.

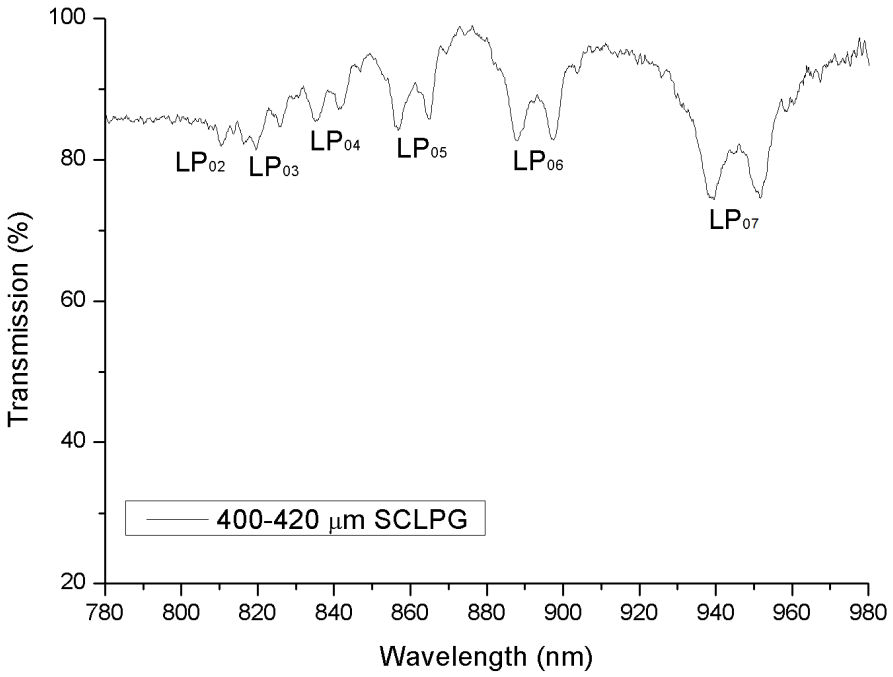

Figure 3.12: Transmission spectrum of a 400 - 420 μm period step chirped LPG with a step chirp of 2 μm. The LPG was 35 mm in length written in PS750 fibre with a cutoff wavelength of 627 nm.

$$L = \sum_{i=1}^{N} n \cdot \Lambda_i \tag{3.13}$$

where the number of periods in each section is n.

Equation 3.14 shows how to fabricate a step chirped long period grating with each section having the same length. The number of sections, N is set along with the length of each section (L/N). An example transmission transmission of a 400 - 420 μm period step chirped LPG (35 mm long) with a step chirp of 2 μm between each grating section is shown in figure 3.12.

$$n_i = \frac{L/N}{\Lambda_1 + (i-1) \cdot chirp\ step} \tag{3.14}$$

Figure 3.13 shows the microscope images of a 400 - 420 μm period chirped LPG. As the period was not constant through the entire length of the grating, only the beginning (figure 3.13 (a)) and end (figure 3.13 (b)) images are shown.

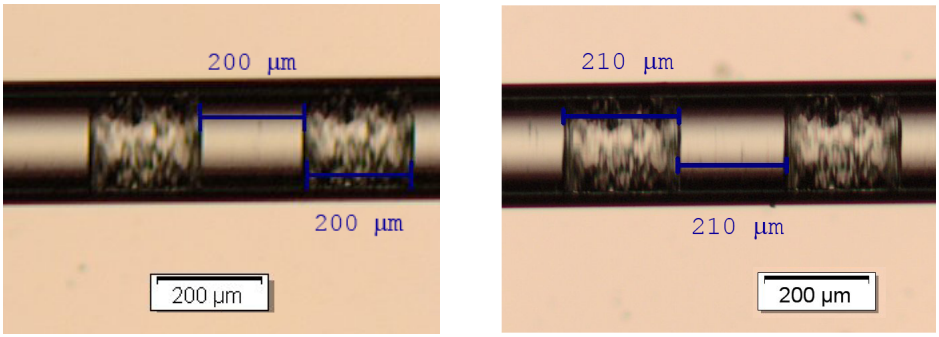

(a) (b)

Figure 3.13: Optical images of the chirped LPG with a period of 400 - 420 μm inscribed on the fibre buffer jacket of a single mode fibre showing the (a) beginning of the grating at 400 μmm and (b) end at 420 μm. The darker sections denote laser inscription. Taken at magnification x5.

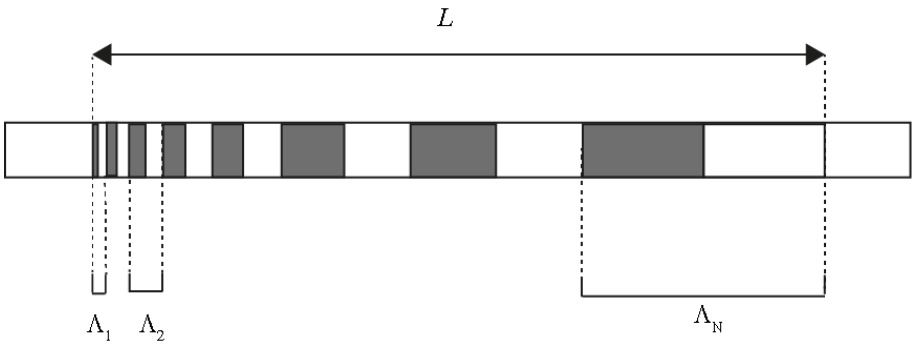

Figure 3.14: Continuously chirped LPG of length L and consisting of N periods. Λ_i; ith period.

3.3.4.4 Continuously chirped long period gratings

When an LPG is designed to have a period that varies continually from one end of the grating to the other according to some prescribed function which, for example, can be linear it is referred to as a continuously chirped LPG.

Figure 3.14 illustrates an LPG with continuous chirp which is a linear variation in the period of the LPG as a function of length.

The length, L, of the LPG, the initial period, Λ_1, and the end period, Λ_N, are the input parameters specified by the user. The other parameters required to write a continuously chirped LPG are determined with equations 3.15 - 3.18. For this configuration, both the translation stage and slit must move in conjunction with each other.

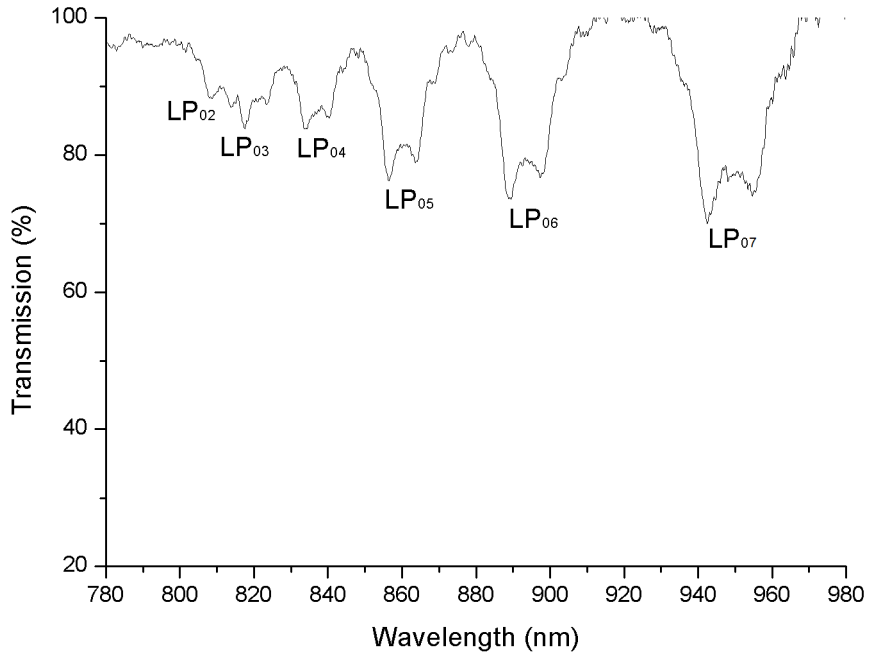

Figure 3.15: Transmission spectrum of a 400 - 420 μm period continuously chirped LPG. The LPG was 35 mm in length written in PS750 fibre with a cutoff wavelength of 627 nm.

$$\Lambda_{mean} = \frac{(\Lambda_1 + \Lambda_N)}{2} \tag{3.15}$$

$$N = \frac{L}{\Lambda_{mean}} \tag{3.16}$$

$$chirp\,rate = \frac{(\Lambda_N - \Lambda_1)}{(N-1)} \tag{3.17}$$

$$\Lambda_i = \Lambda_1 + (i-1) \cdot chirp\,rate \tag{3.18}$$

Just as with the step chirped LPG, figure 3.13 shows the beginning and end periods, 400 μm and 420 μm respectively, of the chirped LPG. Figure 3.15 shows the transmission spectrum of the continuously chirped LPG.

The shallow attenuation bands of the chirped LPGs are due to the broadened nature of these gratings. In simplified terms, they can be said to constitute many individual uniform period LPGs with short lengths. The attenuation bands of the CCLPG have more uniform broadening than that of the SCLPG due to the CCLPG having

a greater number of different sized periods.

3.3.5 Flowchart of computer control fabrication

The flowchart, figure 3.16 shows how the LabView program (Appendix A) works to control the translation stages used for LPG fabrication. It is possible to choose between the different kinds of LPGs mentioned above; uniform period, chirped and phase shifted.

3.3.6 Amplitude mask

For the fabrication of LPGs using an amplitude mask, a frequency quadrupled Nd:YAG laser (injection seeded Spectra Physics Quanta-Ray Nd:YAG laser, repetition rate of 30 Hz, output energy of 60 mJ at 266 nm, pulse width 8 ns) exposed the fibre through an amplitude mask made of aluminium with a period of 400 μm and 50:50 duty cycle (figure 3.17). A Galilean beam expander (Thorlabs ELU-25-5X-248), with the ability to collimate and expand the diameter of the input beam 5 times was used in conjunction with a mechanical slit to create an LPG of a suitable length which gave deep attenuation bands in the transmission spectrum and was easy to handle (35 mm). As for the point-by-point approach, a variable attenuator was used to control the amount of power that the fibre was exposed to. To help with alignment, a set of irises were used to ensure a perpendicular path from the beamsplitter. A cylindrical lens with a focal length of 75 mm was used to focus the beam onto the amplitude mask, producing a line focus aligned with the axis of the fibre. The beam waist along the axis of the fibre was calculated to be 1.2 mm. The fibre was held in place by two standard v-groove fibre holders and magnets. These holders were attached to a mechanical translation stage that had a maximum travel of 20 mm and a resolution of 10 μm (see figure 3.18 for apparatus). The translation stage was added to allow other LPG configurations, such as phase shifted or cascaded LPGs to be fabricated in the future.

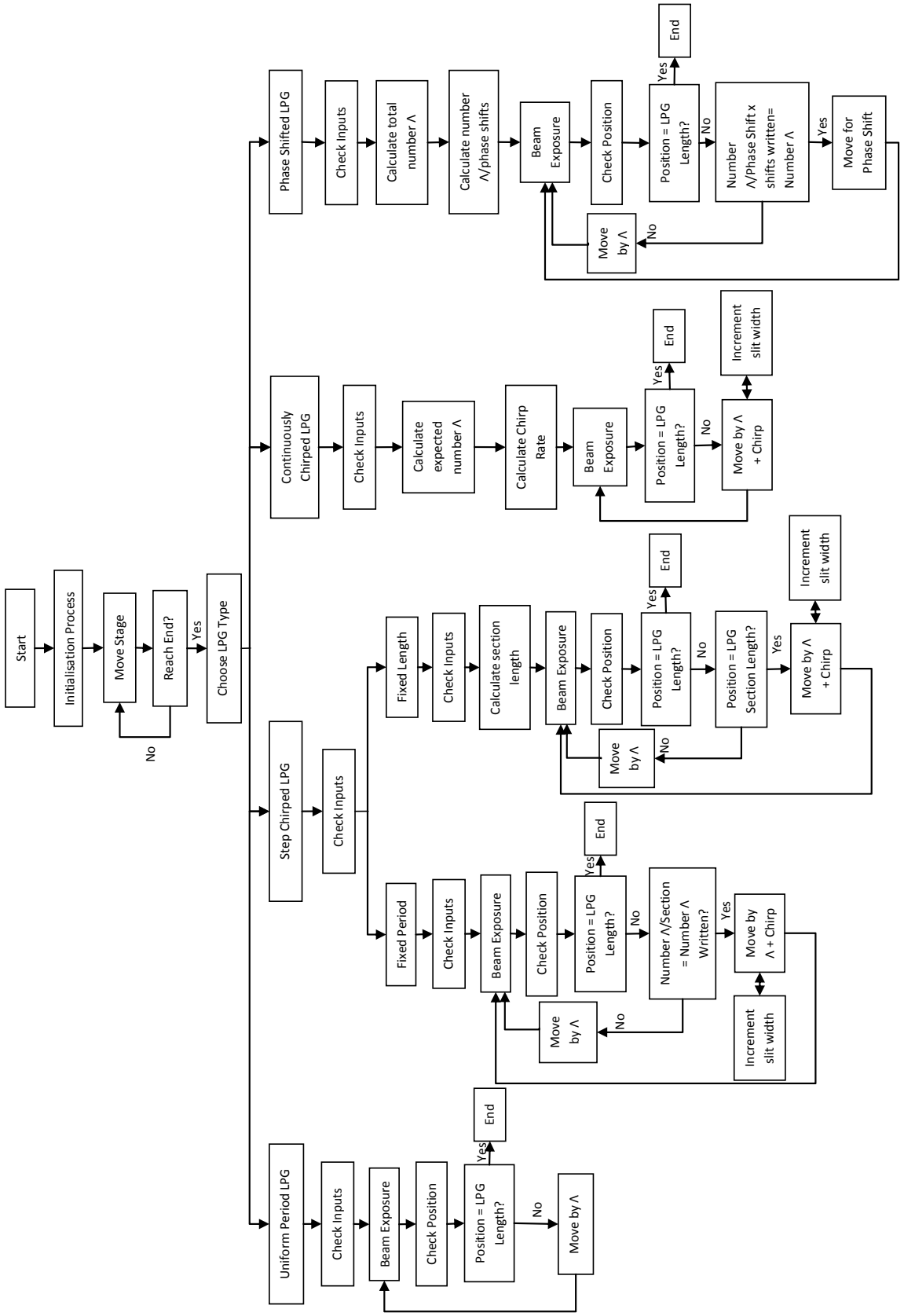

Figure 3.16: Flowchart representing the master program used to control the translation stage for LPG fabrication. It is possible to choose between four different types of LPGs; uniform period, step chirped, continuously chirped and phase shifted.

Figure 3.17: Photograph of amplitude mask used for fabricating 400 μm period LPGs with a 50:50 duty cycle. The "strips" in the mask denote the period and duty cycle of the LPG. The mask is placed closely in front of the optical fibre and the gaps in the mask allow UV light to pass and irradiate the fibre.

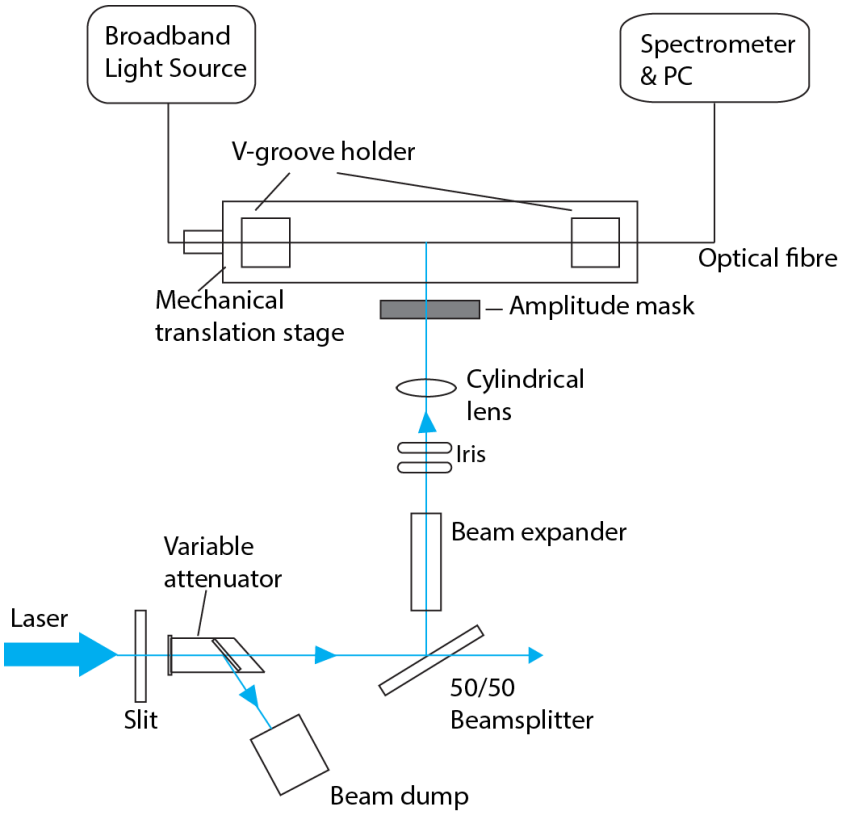

(a)

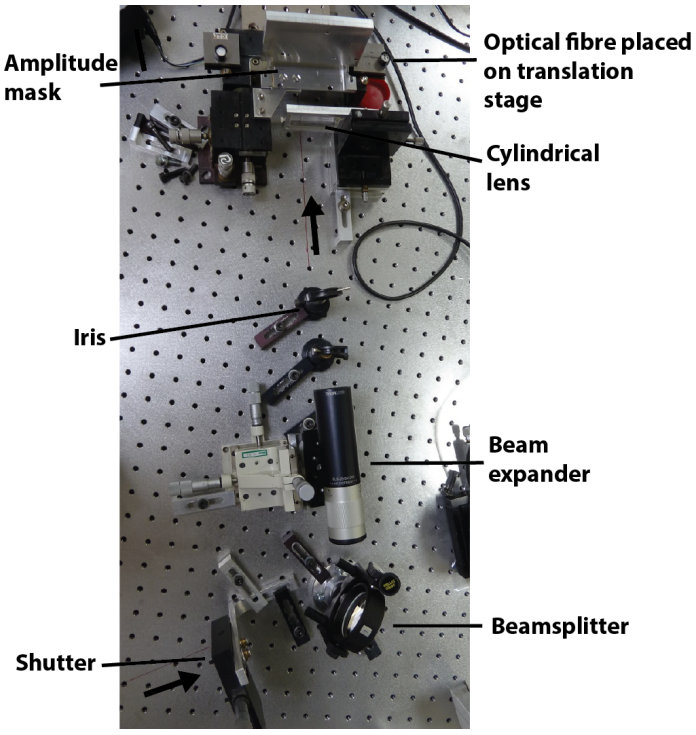

(b)

Figure 3.18: The (a) schematic showing the setup configured for fabricating LPGs using a UV laser beam and an amplitude mask with corresponding (b) photograph. The width of the illuminating beam is set by a slit and beam expander

3.4 Fabrication considerations of long period gratings at turning point using point-by-point

For shorter periods, when coupling to higher order modes, the phase matching condition contains a turning point where a cladding mode has two resonance wavelengths [29]. The sensitivity of the attenuation band is a maximum when the period is chosen such that phase matching occurs at the phase matching turning point. The transmission spectra of these LPGs are not only highly sensitive to the surrounding environment, but also small changes in period as can be seen from the evolution of the spectrum with increasing period shown in figure 3.19. Figure 3.19 shows that changes in period of less than 1 μm have a significant influence on the spectrum. This sensitivity places stringent demands on the system used to fabricate LPGs. To experimentally investigate the influence of grating period on the transmission spectrum of an LPG designed to operate near the phase matching turning point, a series of LPGs were fabricated using the point-by-point technique with periods lying in the range of 110 - 111 μm. By using the point-by-point fabrication technique, it allowed LPGs with small changes in period to be created easily. These periods were chosen by the phase matching dispersion curves from chapter 2, and this range of periods operate near and at the PMTP. The modes coupled to, shown in the transmission spectrum in figure 3.20 were also determined using the dispersion curves. Figure 3.20 shows that by changing the grating period by just 0.1 μm the attenuation bands in the transmission spectrum are significantly affected.

3.4.1 System reproducibility

The temperature of the fabrication system was passively maintained at 24 -24.5 ^{o}C by insulating the system, as described in section 3.3.1. A wireless temperature logger (i-button® DS1923) was placed next to the fibre to monitor the temperature. A grating with a period around the phase matching turning point region, 110.9 μm, was fabricated and repeated four times to determine the reproducibility of the set up. The average power output of the laser was also monitored throughout the fabrication process of each grating. This was carried out by monitoring the power of the redundant output coming from a beam splitter placed in the beam path. The spectra are shown in figure 3.21. The maximum difference between the resonance wavelengths recorded for the LP_{017} mode was 125 pm, and for the LP_{018} mode was 125 pm. For the LP_{019} mode, the maximum change in transmission depth was 6 %. The slight change in the extinction of the attenuation band could be due to a slight variation of environmental conditions or laser power (up to 3 mW).

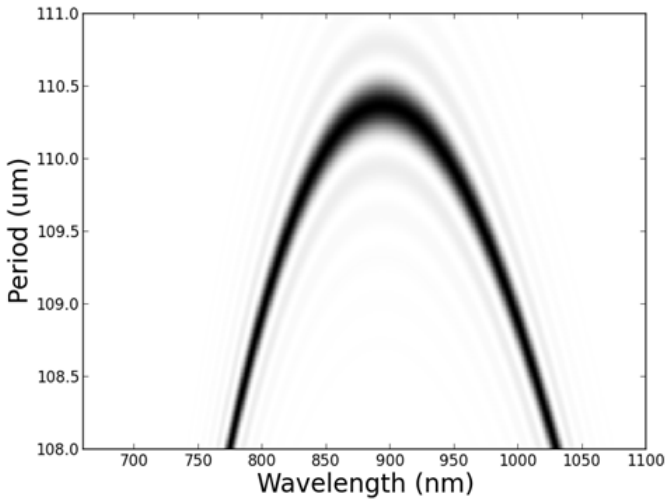

Figure 3.19: Simulated evolution of the resonance band corresponding to coupling to the LP_{019} cladding mode in response to changes in grating period. White and black represent 100% and 0% transmission, respectively.

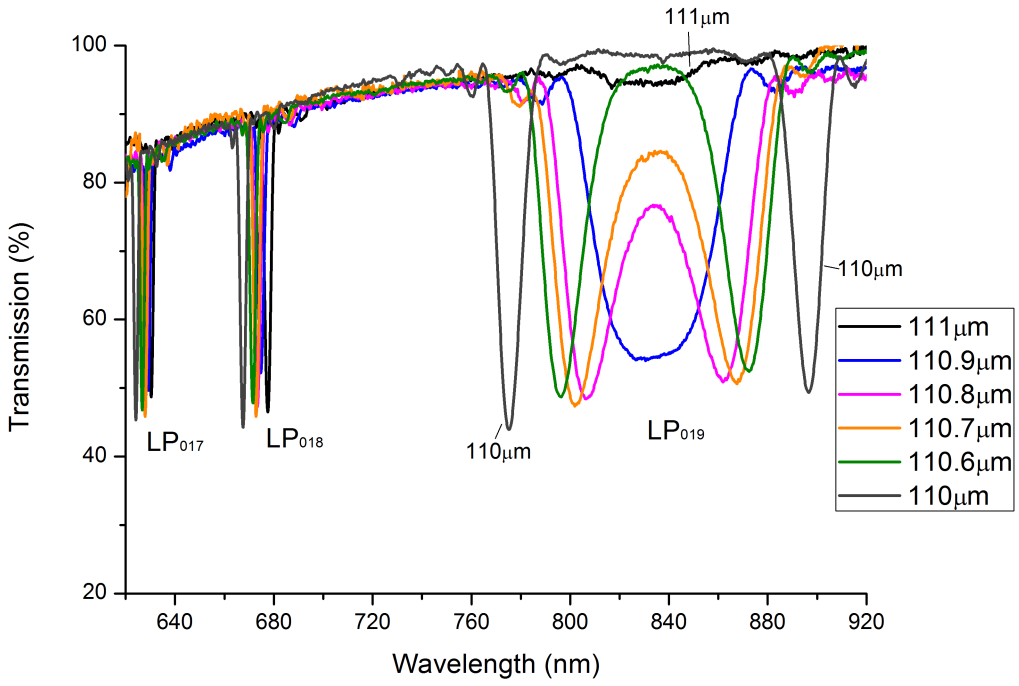

Figure 3.20: Transmission spectra of LPGs written at and around the phase matching turning point at six different periods ranging from 110 μm - 111 μm.

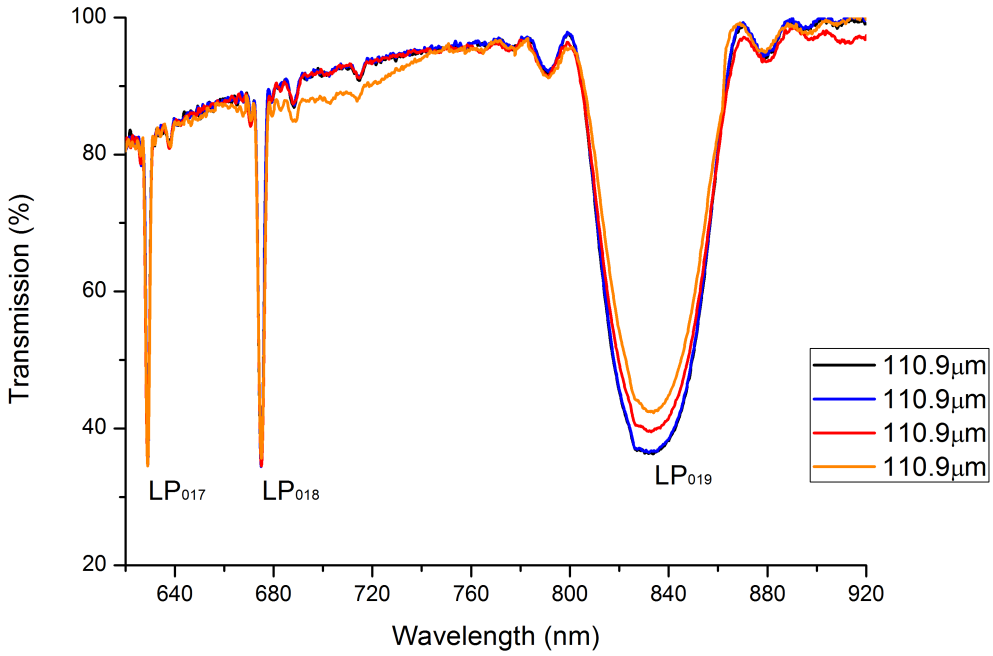

Figure 3.21: Transmission spectra of 4 LPGs, each of period 110.9 μm period, fabricated in an environment in which the temperature was controlled to 0.5 ^{o}C.

To further illustrate the importance on the control of the environment in which the LPG is fabricated, the insulation was removed, such that the temperature varied by up to 5 ^{o}C, and another 4 LPGs, each of period 110.9 μm, were fabricated. The extinction of the LP_{019} attenuation band exhibited changes of up to 28 %. This suggests that two of the LPGs were fabricated at the PMTP, two were fabricated where the band corresponding to the LP_{019} mode had 'fully formed', and one was where the dual resonance bands started to develop and separate. The attenuation bands corresponding to coupling to the LP_{017} and LP_{018} modes, away from the phase matching turning point, exhibit maximum wavelength shifts of 390 pm and 130 pm respectively (figure 3.22).

3.4.2 Effects of duty cycle

With the aim of studying the influence of duty cycle on the transmission spectrum, LPGs with differing duty cycles, 80:20, 70:30 and 50:50 (where the ratio is; irradiated section: non-irradiated section) were fabricated. The results are shown in figures 3.23 and 3.25 for LPGs of period 110.7 and 110.9 μm, respectively. Varying the duty cycle of the fabrication process produces gratings that can appear to

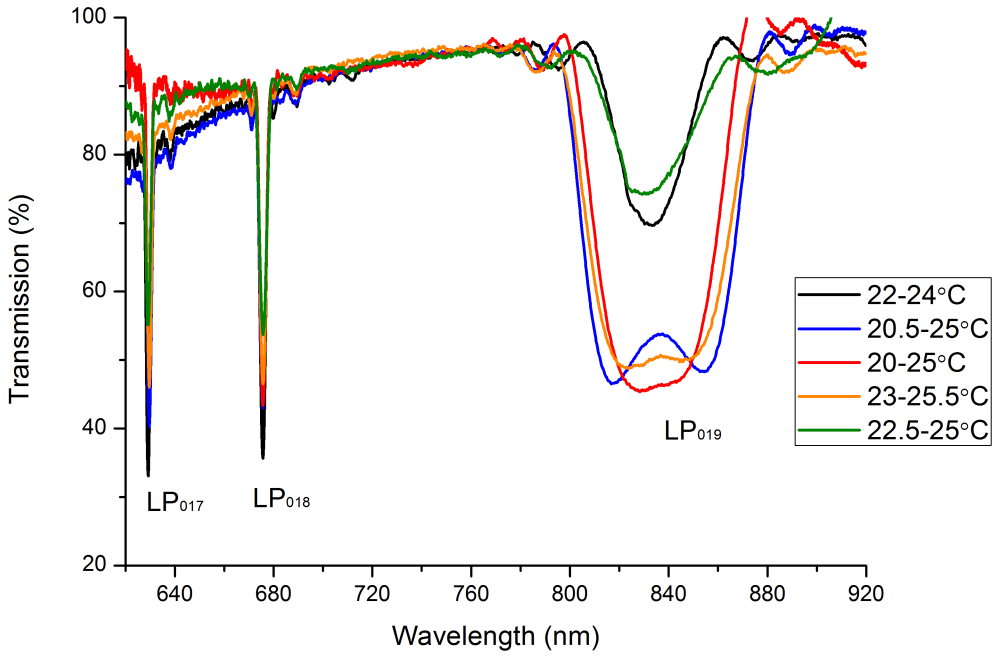

Figure 3.22: Transmission spectra of 4 LPGs, each fabricated with a period 110.9 μm where the temperature has not been controlled. The temperature varies from 20 25.5 ^{o}C.

be written at different periods. This is due to a different effective refractive index which is exhibited at duty cycles other than 50:50. To ensure that the programmed duty cycles were correctly fabricated, optical images were taken under a microscope of irradiated, un-stripped optical fibres as shown in figures 3.24 and 3.26 (PS750). Figure 3.24 shows the 110.7 μm period LPG and figure 3.26 shows the 110.9 μm period LPG. The strongest gratings (those in which the attenuation in the transmission spectra was greater) were fabricated when the duty cycle was set to 50:50. As can be seen the LP_{019} resonant band at the PMTP of the 110.9 μm period LPG the only appears with a 50:50 duty cycle. For the both gratings, the attenuation of the lower order modes, LP_{017} and LP_{018}, is reduced when the duty cycle is no longer equal and the central wavelengths differ.

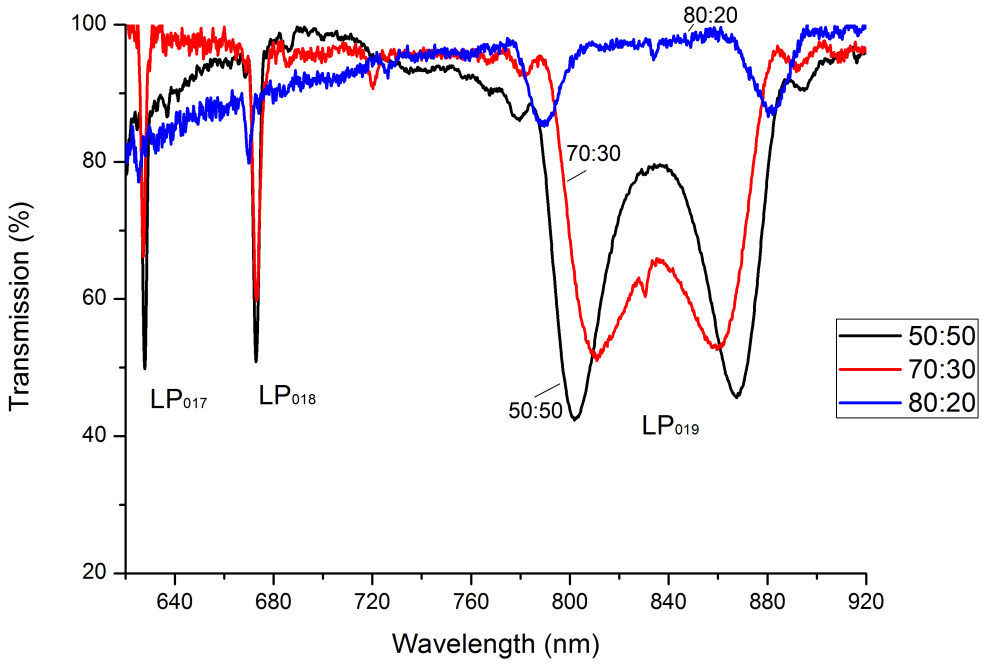

Figure 3.23: LPG with a 110.7 μm period with varying duty cycles of 50:50, 70:30 and 80:20 where the percentage ratio is irradiated section: non-irradiated section.

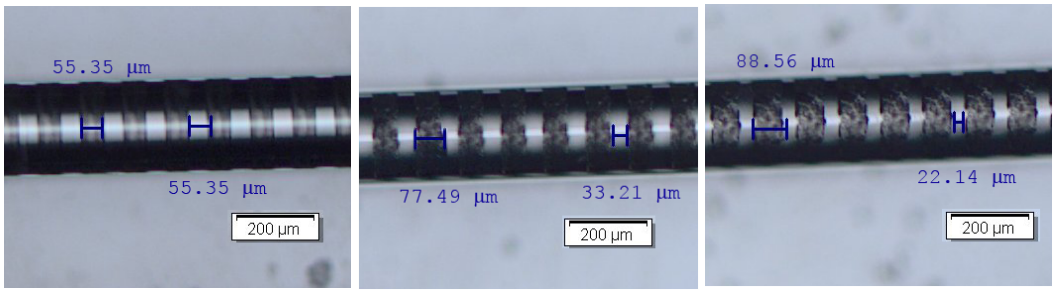

(a) (b) (c)

Figure 3.24: Optical images of a 110.7 μm period structure inscribed on the fibre buffer jacket of a single mode fibre with duty cycles (a) 50:50 (b) 70:30 and (c) 80:20. The darker sections denote the regions exposed to the laser through the slit.

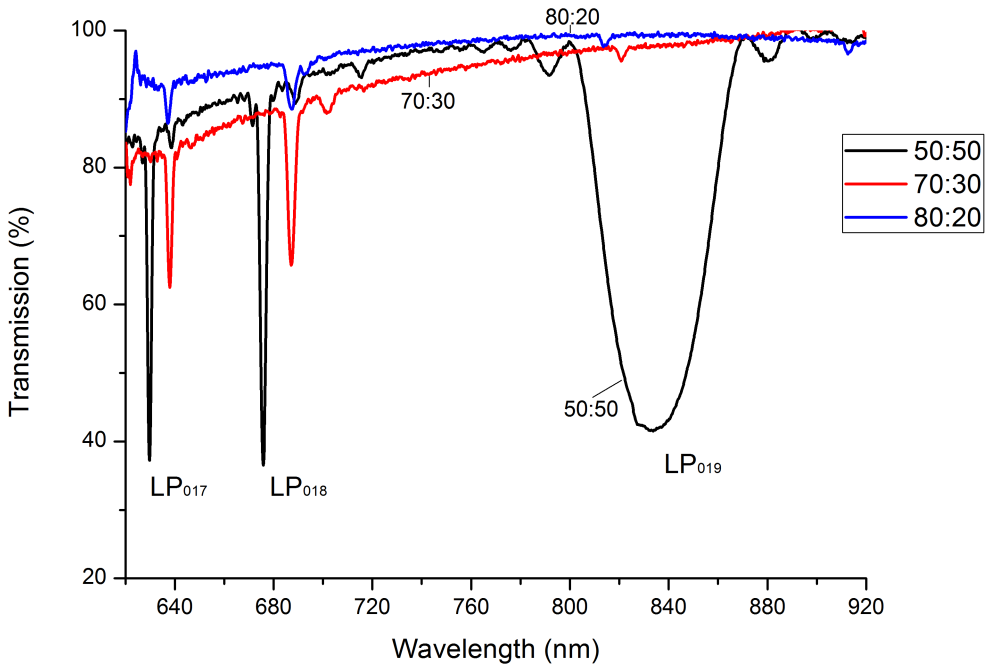

Figure 3.25: LPG with a 110.9 μm period with varying duty cycles of 50:50, 70:30 and 80:20 where the percentage ratio is irradiated section: non-irradiated section.

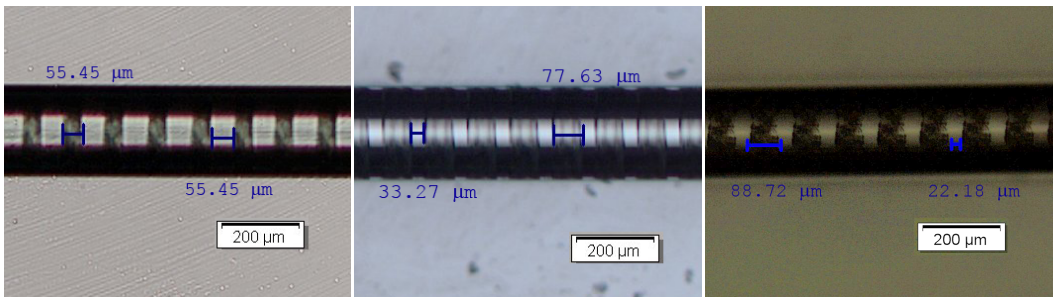

(a) (b) (c)

Figure 3.26: Optical images of a 110.9 μm period structure inscribed on the fibre buffer jacket of a single mode fibre with duty cycles (a) 50:50 (b) 70:30 and (c) 80:20. The darker sections denote the regions exposed to the laser through the slit.

3.5 Summary

The different methods of fabricating long period gratings and the two experimental processes for creating LPGs via UV-inscription, point-by-point method and use of an amplitude mask, are discussed. A versatile point-by-point fabrication system was developed, which created repeatable LPGs as well different configurations of LPGs. The amplitude mask method was also discussed. Finally LPGs created at the PMTP, which are highly sensitive to the environment, were presented. The section highlighted the requirements that should be taken into consideration when fabricating such LPGs, such as duty cycle and temperature.

References

[1] S W James and R P Tatam. Optical fibre long-period grating sensors: characteristics and application. *Measurement Science and Technology*, 14:R49–R61, 2003.

[2] V Bhatia, D K Campbell, D Sherr, T G D'Alberto, N A Zabaronick, G A Ten Eyck, K A Murphy, and R O Claus. Temperature-insensitive and strain-insensitive long-period grating sensors for smart structures. *Society of Photo-Optical Instrumentation Engineers*, 36(7):1872–1878, 1997.

[3] J Blows and D Y Tang. Gratings written with tripled output of Q-switched Nd:YAG laser. *Electronics Letters*, 36(22):1837–1839, 2000.

[4] C C Davis. *Lasers and Electro-Optics*. Cambridge University Press, 1996.

[5] X Lan, Q Han, T Wai, J Huang, and H Xiao. Turn-around-point long-period fiber gratings fabricated by CO_2 laser point-by-point irradiations. *IEEE Photonics Technology Letters*, 23(22):1664–1666, 2011.

[6] Y Kondo, K Nouchi, T Mitsuyu, M Watanabe, P Kazansky, and K Hirao. Fabrication of long-period fibre gratings by focused irradiation of infra-red femtosecond laser pulses. *Optics Letters*, 24(10):646–8, 1999.

[7] M Fujimaki, Y Ohki, J L Brebner, and S Roorda. Fabrication of long-period optical fiber gratings by use of ion implantation. *Optics Letters*, 25(2):88–89, 2000.

[8] S Savin, M J F Digonnet, G S Kino, and H J Shaw. Tunable mechanically induced long-period fiber gratings. *Optics Letters*, 25(10):710–712, 2000.

[9] G Kakarantzas, T E Dimmick, T A Birks, R Le Roux, and P St J Russell. Miniature all-fiber devices based on CO_2 laser microstructuring of tapered fibers. *Optics Letters*, 26(15):1137–1139, 2001.

[10] G Rego, O Okhotnikov, E Dianov, and V Sulimov. High-temperature stability of long-period fibre gratings using an electric arc. *Journal of Lightwave Technology*, 19(10):1574–1579, 2001.

[11] K O Hill, Y Fujii, D C Johnson, and B S Kawasaki. Photosensitivity in optical fiber waveguides: Application to reflection filter fabrication. *Applied Physics Letters*, 32(10):647–649, 1978.

[12] A I Kalachev, V Pureur, and D N Nikogosyan. Investigation of long-period ber gratings induced by high-intensity femtosecond uv laser pulses. *Optics Communications*, 246(1-3):107–115, 2004.

[13] M Smietana, W J Bock, and P Mikulic. Comparative study of long-period gratings written in a boron co-doped ber by an electric arc and uv irradiation. *Measurement Science and Technology*, 21(2):1–8, 2010.

[14] M Kristensen. Ultraviolet-light-induced processes in germanium-doped silica. *Physical Review B*, 64(14):144201/1–144201/12, 2001.

[15] V Bhatia. *Properties and Sensing Applications of Long-Period Gratings*. PhD thesis, Virginia Polytechnic Institute and State University, 1996.

[16] E M Dianov, K M Golant, V M Mashinskv, O I Medvedkov, I V Nikolin, O D Sazhin, and S A Vasiliev. Highly photosensitive nitrogen-doped germanosilicate fibre for index grating writing. *Electronics Letters*, 33(15):1334–1336, 1997.

[17] L Dong, J L Cruz, J A Tucknott, L Reekie, and D N Payne. Strong photosensitive gratings in tin-doped phosphosilicate optical fibers. *Optics Letters*, 20(19):1982–1984, 1995.

[18] M M Broer, R L Cone, and Simpson J R. Ultraviolet-induced distributed-feedback gratings in ce^{3+}-doped silica optical fibers. *Optics Letters*, 16(18):1391–1393, 1991.

[19] K O Hill, B Malo, F Bilodeau, and D C Johnson. Photosensitivity in optical fibers. *Annual Review of Materials Science*, 23:125–157, 1993.

[20] S Kannan and P Lemaire. Optical reliability of fiber gratings. In J M López-Higuera, editor, *Handbook of Optical Fibre Sensing Technology*, pages 421–431. 2001.

[21] K Fujita, Y Masuda, K Nakayama, M Ando, K Sakamoto, J Mohri, M Yamauchi, M Kimura, Y Mizutani, S Kimura, T Yokouchi, Y Suzaki, and S Ejima.

Dynamic evolution of the spectrum of long-period fiber Bragg gratings fabricated from hydrogen-loaded optical fiber by ultraviolet laser irradiation. *Applied Optics*, 44(33):7032–7038, 2005.

[22] T Mizunami and T Fukuda. Fem calculation and the effects of hydrogen diffusion in fabrication processes of long-period fiber gratings. *Optical Communications*, 259(2):581–586, 2006.

[23] L Zhang, W Zhang, and I Bennion. In-fiber grating optic sensors. In S Yin, P B Ruffin, and F T S Yu, editors, *Fiber Optic Sensors, Second Edition*, pages 109–162. 2008.

[24] K R Sohn and G D Peng. Mechanically formed loss-tunable long-period fiber gratings realized on the periodic arrayed metal wires. *Optics Communications*, 278(1):77–80, 2007.

[25] W J Bock, J Chen, P Mikulic, and T Eftimov. A novel fiber-optic tapered long-period grating sensor for pressure monitoring. *IEEE Transactions on Instrumentation and Measurement*, 56(4):1176–1180, 2007.

[26] S M Topliss. *Optical Fibre Long Period Grating Sensors with Nanostructured Coatings*. PhD thesis, University of Cranfield, 2011.

[27] B Li, L Jiang, Wang S, H L Tsai, and H Xiao. Femtosecond laser fabrication of long period ber gratings and applications in refractive index sensing. *Optics and Laser Technology*, 43(8):1420–1423, 2011.

[28] L A Everall, R W Fallon, J A R Williams, L Zhang, and I Bennion. Flexible fabrication of long-period in-fiber gratings. *Proceedings of the IEEE, Conference on Lasers and Electro-Optics*, pages 513–514, 1998.

[29] C S Cheung, S M Topliss, S W James, and Tatam R P. Response of fibre optic long period gratings operating near the phase matching turning point to the deposition of nanostructured coatings. *Journal of the Optical Society of America B Optical Physics*, 25(6):897–902, 2008.

Chapter 4

Characterisation of long period grating sensors

4.1 Introduction

LPGs can be used to detect measurands such as temperature, strain, pressure, refractive index changes, and, by coating with an appropriate functional material, specific chemical analytes [1]. LPGs have been used for multi-parameter sensing as the numerous attenuation bands in the transmission spectrum show different sensitivities to the same environmental parameters and can therefore be processed to allow the monitoring of multiple parameters at the same time [2]. The exact responses and sensitivities are dependent on the period of the LPG, which determines the cladding modes to which energy is coupled and the position on the phase matching curve, as discussed in chapter 2.

This chapter investigates the sensitivities to temperature, refractive index and strain of a uniform period LPG, an LPG at the phase matching turning point and a continuously chirped LPG. For all fibres, the transmission spectra were recorded by coupling the output from a tungsten-halogen light source into the fibre and monitoring the transmission via an Ocean Optics CCD spectrometer (HR4000 with a resolution capability of 0.02 nm) connected to a PC. The error bars for each reading were calculated from repeated measurements.

4.2 Characterisation of a uniform period long period grating

A 35 mm long LPG with a period of 400 μm was written in a photosensitive fibre (Fibercore PS750) with a cut-off wavelength of 627 nm, using the approach detailed in Chapter 3. This period was chosen as it typifies an LPG with a period at the larger end of the typical range. A set of attenuation bands are produced which correspond to the modes that are being coupled to; LP_{02} to LP_{07}.

4.2.1 Temperature sensitivity

As the temperature of the LPG changes, the dimensions of the fibre no longer remain constant, causing the period and effective refractive index of the fibre to change.

4.2.1.1 Experiment

To measure the LPG's sensitivity to temperature, the LPG was placed inside a 40 mm long cylindrical ceramic heating furnace (Eurotherm 2132) (whilst keeping the fibre taut) whose temperature was monitored by a thermocouple stabilised using a PID circuit to $\pm$ 0.5 ^{o}C (see figure 4.1). The length of the grating was chosen to ensure that it would fit entirely inside the heater. To maintain the temperature of the LPG, 4 cm long copper pieces (chosen as copper is a good conductor of heat) were placed inside the cylinder. The insulation of the system was also passively controlled by covering the system with aluminium. Readings were taken from room temperature (24 °C) to 95 °C.

4.2.1.2 Results and discussion

The change in the wavelengths of the attenuation bands have a linear response to changes in temperature (as shown in figure 4.2), over the temperature range investigated. The attenuation bands corresponding to coupling to the higher order modes experienced a greater blue shift in wavelength, with the respective sensitivities ranging from (from lower to higher order modes) -125 $\pm$ 1.6 pm$(^{\circ}C)^{-1}$ to -174 $\pm$ 2.3 pm$(^{\circ}C)^{-1}$. The sensitivities for all 6 bands are summarised in table 4.1. Previous results [3] have shown sensitivities as high as -164 pm$(^{\circ}C)^{-1}$ for an LPG with a period of 400 μm at a resonance wavelength of 950 nm in boron co-doped photosensitive fibre (Fibercore PS750).

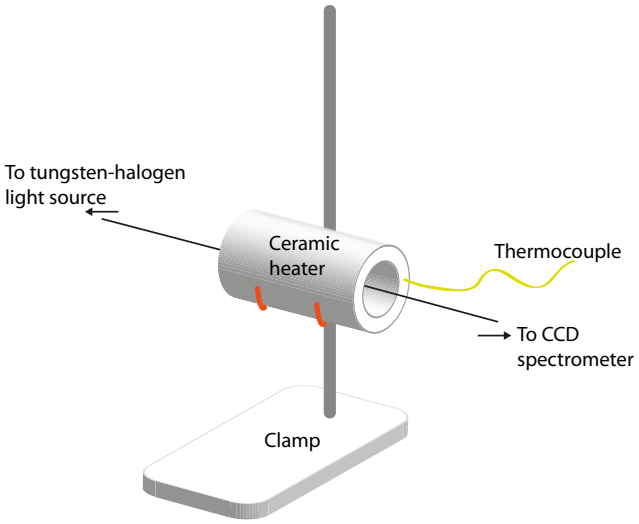

Figure 4.1: Experimental configuration used for characterising the temperature sensitivity of an LPG of uniform period 400 μm. The fibre was held inside a ceramic heater where the temperature was monitored by a thermocouple and maintained at the set temperature using a PID circuit.

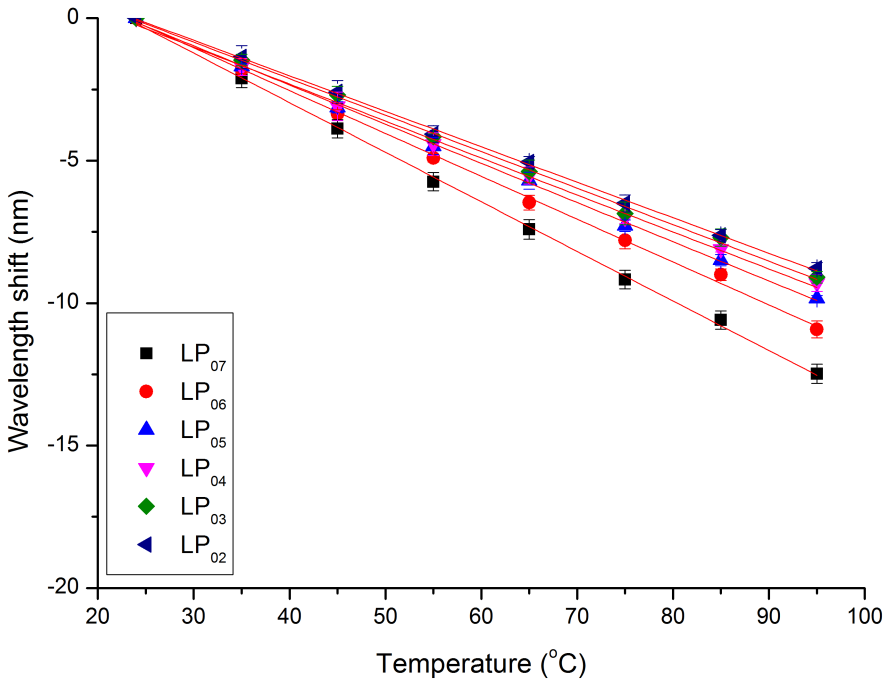

Figure 4.2: Shift in wavelength of the attenuation bands LP_{02} to LP_{07} of an LPG of uniform period of 400 μm as a function of temperature. Linear fits (using least squares method) give an indication to the sensitivities of the bands of the LPG.

Table 4.1: Temperature sensitivity of the attenuation bands of an LPG with a uniform period of 400 μm.

Mode	Temperature sensitivity $(\mathrm{pm}(^{\circ}C)^{-1})$
LP_{02}	-125 ± 1.6
LP_{03}	-128 ± 2.2
LP_{04}	-130 ± 2.4
LP_{05}	-138 ± 1.6
LP_{06}	-150 ± 2.6
LP_{07}	-174 ± 2.3

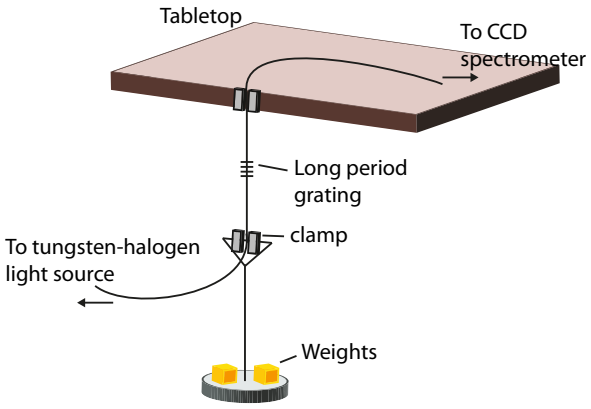

Figure 4.3: Experimental configuration used for characterising the strain sensitivity of an LPG of uniform period of 400 μm. The fibre is strained by progressively adding weights the the free end of the fibre.

4.2.2 Strain sensitivity

When an axial strain is applied to an LPG, the dimensions of the fibre change causing the period and refractive index of the fibre to change as it is stretched.

4.2.2.1 Experiment

The optical fibre containing the LPG was clamped at both ends, with one side suspended from a table top surface and the other hanging freely, as shown in figure 4.3. Weights ranging from 55 g to 530 g were added to the free end to impose a force on the grating. The weights were added until the LPG broke.

To calculate the strain, ε, experienced by the loaded grating, the following equation was used:

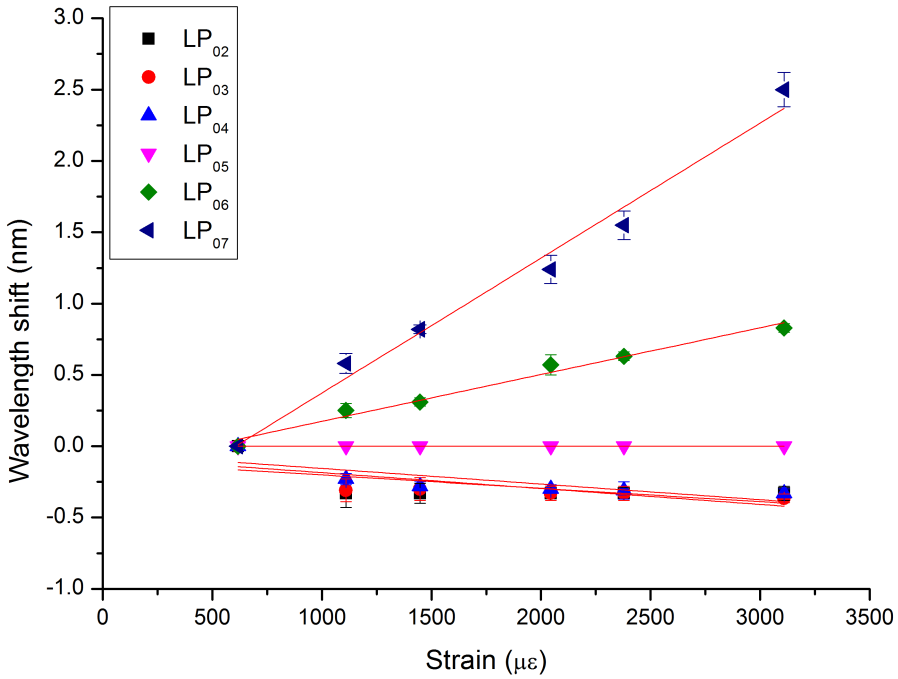

Figure 4.4: Shift in wavelength of the attenuation bands LP_{02} to LP_{07} of a 400 μm uniform period LPG as a function of axial strain. The linear fits (using least squares method) give an indication of the sensitivities of the bands of the LPG.

$$\varepsilon = \frac{mg}{EA} \tag{4.1}$$

where m is the mass applied, g is the gravitational acceleration, 9.81 ms^{-2}, E is Young's modulus of elasticity, 73 GPa [4], and A is the cross sectional area of the optical fibre.

Readings were taken at applied strains ranging from 600 $\mu\epsilon$ to 3500 $\mu\epsilon$.

4.2.2.2 Results and discussion

As with temperature, each attenuation band experiences a different response to the strain applied. The was still a linear relationship between change in attenuation band wavelength and axial strain as shown in figure 4.4.

As can be seen, there was a positive response to increasing strain for bands LP_{07} and LP_{06}. The LP_{05} mode showed no change to the applied strain and the lower modes

showed a small negative response. The negligible sensitivity to strain and a sensitivity to temperature (-130 ± 2.4 pm°C^{-1}) of the attenuation band corresponding to the coupling of the LP_{03} mode demonstrates the multi-parameter measurement capabilities of LPGs. This could also be exploited for use as a strain insensitive temperature sensor [5]). LPGs with a periodicity greater than 100 μm tend to be strain insensitive [2]. Bhatia et al. [5] showed a strain sensitivity of 0.04 pm$(\mu\epsilon)^{-1}$ for a 340 μm period LPG. Table 4.2 shows the sensitivities of the different attenuation bands to the applied strain.

Table 4.2: Strain sensitivity of the attenuation bands of a 400 μm period LPG.

Mode	Strain sensitivity (pm$(\mu\epsilon)^{-1}$)
LP_{02}	-0.094 ± 0.058
LP_{03}	-0.11 ± 0.050
LP_{04}	-0.11 ± 0.040
LP_{05}	0.00 ± 0.00
LP_{06}	0.33 ± 0.023
LP_{07}	0.95 ± 0.060

4.2.3 Refractive index sensitivity

The effective indices of an LPG's cladding modes change depending on the difference between the cladding refractive index and the refractive index of the fibre's surroundings [2]. The central wavelengths of the LPG's attenuation bands are therefore also dependent on the fibre cladding's surrounding medium.

4.2.3.1 Experiment

Liquids (Cargille Series AA and A) with known refractive indices (measured at a wavelength of 589 nm) were used to characterise the sensitivity of the LPG to changes in surrounding RI. The LPG was placed in a Teflon cell-type holder that allowed the entire grating to be completely submerged in the liquid. V-grooves were fashioned into the sides of the holders so that the fibre could be held taut in position (figure 4.5). The refractive indices used ranged from 1.400 to 1.500 ± 0.0012. The refractive indices were wavelength corrected using the Cauchy equations and data sheets provided by Cargille Ltd. [6].

Between each immersion, the previously used liquid was first removed from the trough via an extractor pump. The LPG was then cleaned thoroughly by filling the trough initially with acetone to remove the RI liquid from the surface of the

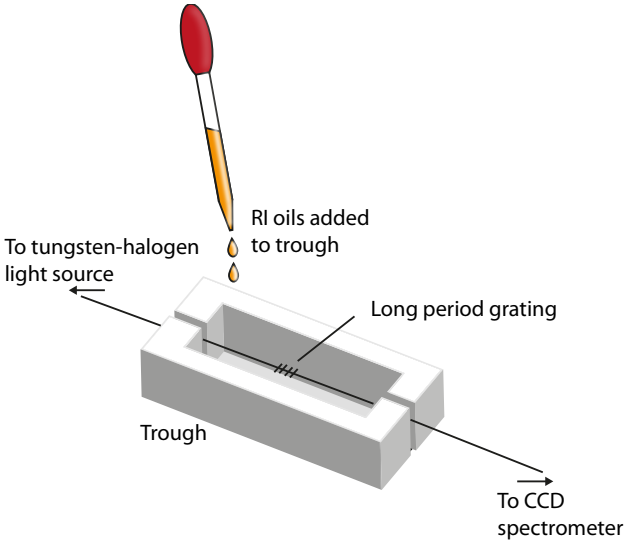

Figure 4.5: Setup used for characterising the RI sensitivity of a 400 μm uniform period LPG. The LPG is contained within a Teflon cell where different RI liquids are added.

grating and the holder. The bath was then filled with isopropyl alcohol (IPA) to remove any excess RI liquid that may have remained and any residue left by acetone. The grating and holder were subsequently dried using compressed air. This process was repeated until the attenuation bands of the grating returned to the wavelength recorded prior to immersion in the liquid.

4.2.3.2 Results and discussion

The higher order modes experienced a greater wavelength shift and the highest sensitivity was achieved at refractive indices approaching that of the fibre cladding. This can be explained as these high order modes possess an evanescent field that extends further in the the surrounding environment. As shown in figures 4.6 and 4.7, when the surrounding RI is the same as the cladding RI, the cladding appears to be infinite and therefore no discrete modes are supported. For surrounding refractive indices higher than the cladding, there is a much smaller red shift in attenuation band wavelength. For surrounding refractive indices higher than that of the cladding, the attenuation bands are a results of coupling to leaky modes, corresponding to Fresnel reflections at the interface of the cladding and the surrounding interface [7, 8]. The maximum wavelength shifts of the attenuation bands (measured at a surrounding RI of 1.445 $\pm$ 0.0012) are shown in table 4.3.

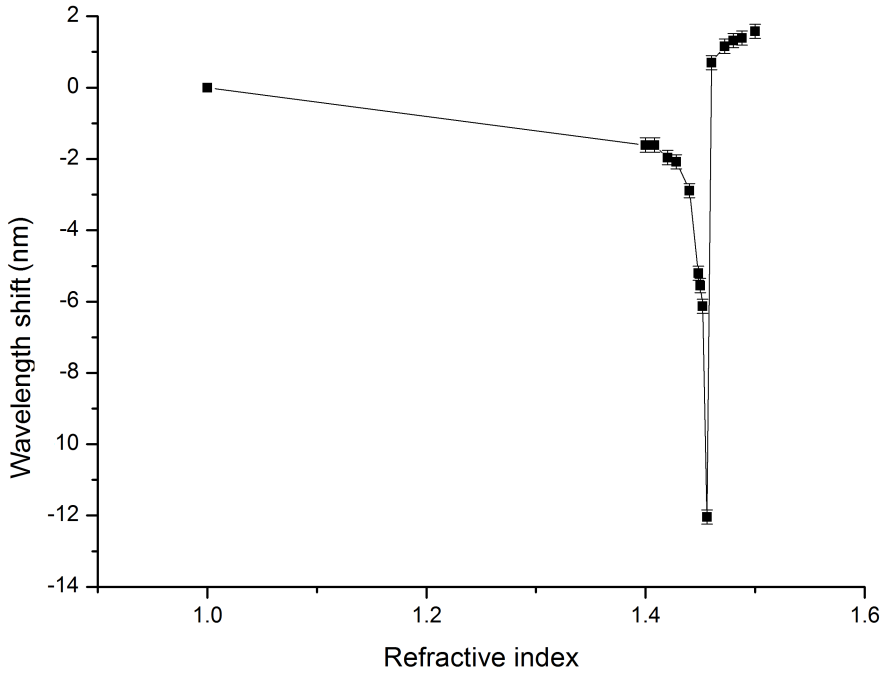

Figure 4.6: Wavelength shift against refractive index of surrounding liquid (Cargille Series A) of the LP_{07} mode of a 400 μm period LPG. The LPG was written in Fibercore PS750 fibre with a cutoff wavelength of 627 nm. The line acts as a guide to the eye.

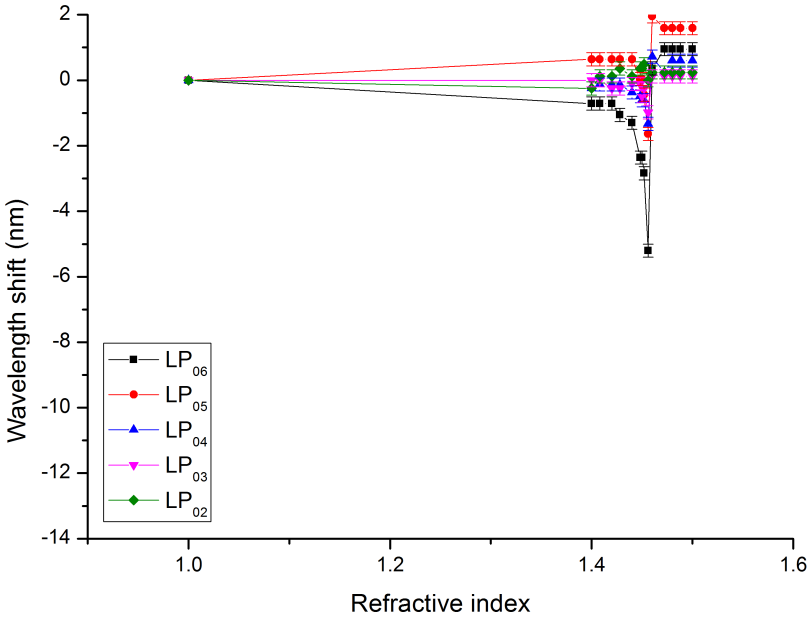

(a)

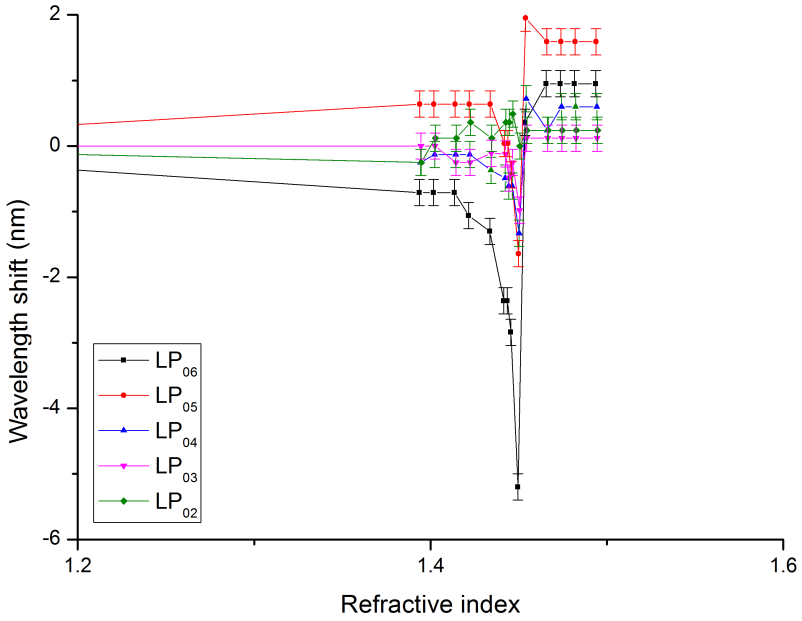

(b)

Figure 4.7: Wavelength shift against refractive index of surrounding liquid (Cargille Series AA and A) of the LP_{06} to LP_{02} modes of a 400 μm period LPG. The LPG was written in Fibercore PS750 fibre with a cutoff wavelength of 627 nm. The line joining the points is used as a guide to show the change in wavelength. (b) shows a close up of (a).

Table 4.3: Maximum wavelength shift of the attenuation bands of a 400 μm uniform period LPG due the surrounding refractive index (1.445).

Mode	Maximum wavelength shift (nm)
LP_{02}	0 ± 0
LP_{03}	-1.0 ± 0.2
LP_{04}	-1.4 ± 0.2
LP_{05}	-2.8 ± 0.2
LP_{06}	-5.2 ± 0.2
LP_{07}	-12.0 ± 0.2

4.3 Characterisation of a long period grating at a phase matching turning point

Two LPGs were fabricated with periods of 111 μm and 110.8 μm in photosensitive fibre (Fibercore PS750) with a cut-off wavelength of 627 nm. These periods were chosen as they couple to the same mode (LP_{019}) and therefore the same PMTP. The experimental procedures used to gain the data in this section are as those described in 4.2.

4.3.1 Temperature sensitivity

At room temperature, the resonant mode did not exhibit an attenuation band (111 μm period LPG). This period was chosen as an LPG with a period of 111 μm is close to a PMTP and would be highly sensitive to external stimuli. With an increase in temperature, a single LP_{019} attenuation band begins to develop and deepen (figure 4.8) as, when the coupling mode is slightly off the PMTP the transmission of the band changes instead of the resonance wavelengths. The transmission depth changes from 1.0 to 0.5 from 25 ^{o}C to 65 ^{o}C with the transmission depth remaining constant until 45 ^{o}C. As the surrounding temperature is increased further, the LP_{019} band will eventually split, producing two bands which will shift in opposite directions. This separation of wavelengths is not linear due to the curved nature of a mode around the PMTP. Figure 4.9 shows the evolution of the dual attenuation bands and their shifts with increasing temperature. Figure 4.10 shows the blue shifted wavelength shifts of the LP_{018} and LP_{017} modes, exhibiting temperature sensitivities of -157 ± 2.0 pm$(^\circ C)^{-1}$ and -112 ± 1.3 pm$(^\circ C)^{-1}$, respectively. These sensitivities are consistent with that of a long period grating with a uniform period not at the phase matching turning point.

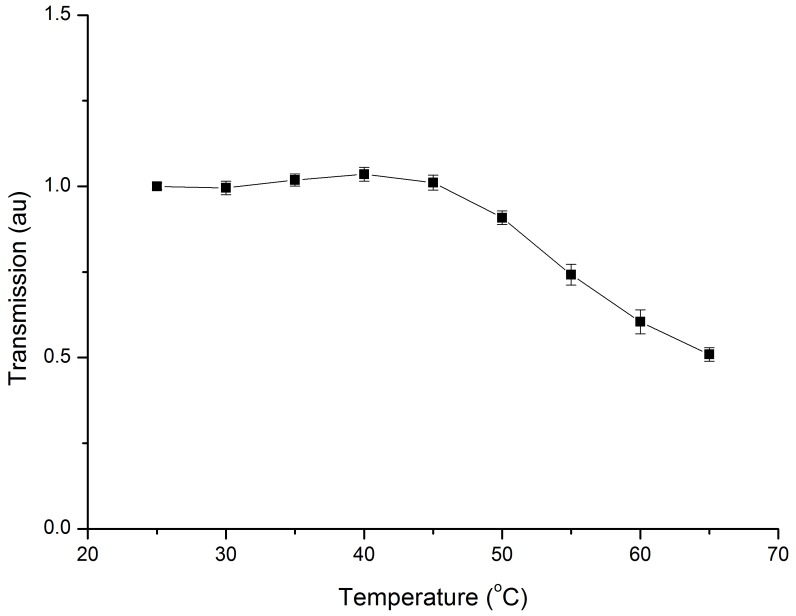

Figure 4.8: Transmission depth of a 111 μm period LPG at the PMTP as a function of temperature from 25 ^{o}C to 65 ^{o}C. The line used to join the data points act as a guide to show the shift of wavelength of the bands.

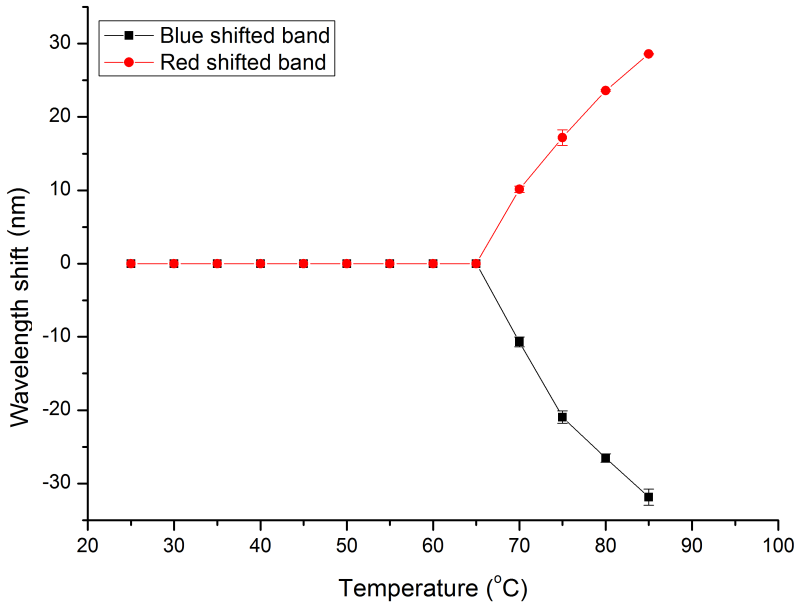

Figure 4.9: Shift in wavelength separation of the dual attenuation bands of a 111 μm period turning point LPG as a function of temperature. The lines used to join the data points act as a guide to show the shift of wavelength of the bands.

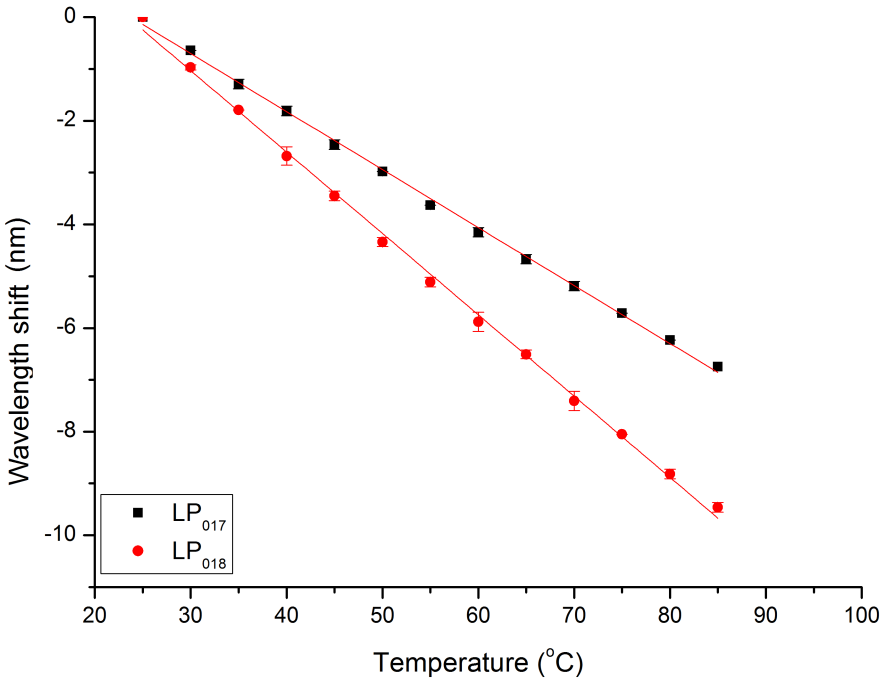

Figure 4.10: Shift in wavelength of the LP_{018} and LP_{017} modes of a 111 μm PMTP LPG as a function of temperature. The best fit line was calculated using the least squares method and help to give an indication of the sensitivities of the bands.

4.3.2 Strain sensitivity

To evaluate the strain sensitivity, the 110.8 μm period LPG was used. This period was chosen as the initial transmission spectrum (without weights) was shown to have dual attenuation bands. Previous studies show that with increasing strain, the dual bands will move closer together [9]. As the strain is increased, the separation of the bands reduced. The wavelength separation of the dual attenuation bands plotted as a function of strain can be seen in figure 4.11. There is a near linear trend with a decreasing wavelength separation with increasing strain. The sensitivity is calculated from the the best fit line (using least squares method) of the measured data and was found to be -11.1 $\pm$ 0.6 pm$(\mu\epsilon)^{-1}$. The strain sensitivities of the LP_{018} and LP_{017} modes are 0.30 $\pm$ 0.02 pm$(\mu\epsilon)^{-1}$ and 0.54 $\pm$ 0.02 pm$(\mu\epsilon)^{-1}$, respectively (figure 4.12).

4.3.3 Refractive index sensitivity

In air, the resonant LP_{019} mode did not exhibit a band (111 μm period LPG) and when immersed in refractive index oils with increasing refractive indices, the band began to deepen and separate. The rate at which the dual attenuation bands sep-

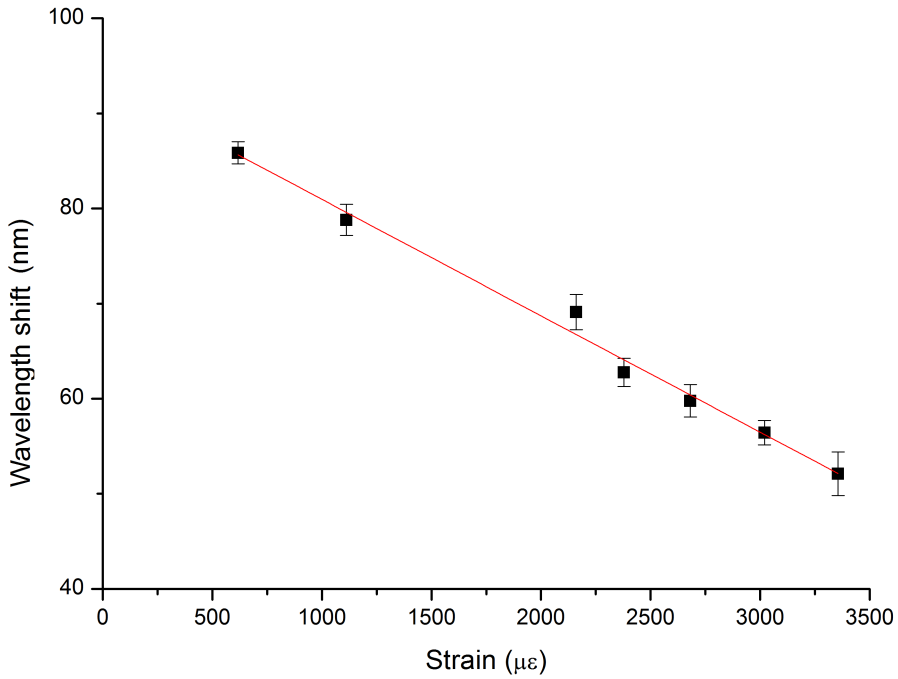

Figure 4.11: Shift in wavelength separation of the dual attenuation bands of a 110.8 μm turning point LPG as a function of strain. The best fit line was calculated using the least squares method and help to give an indication of the sensitivities of the bands.

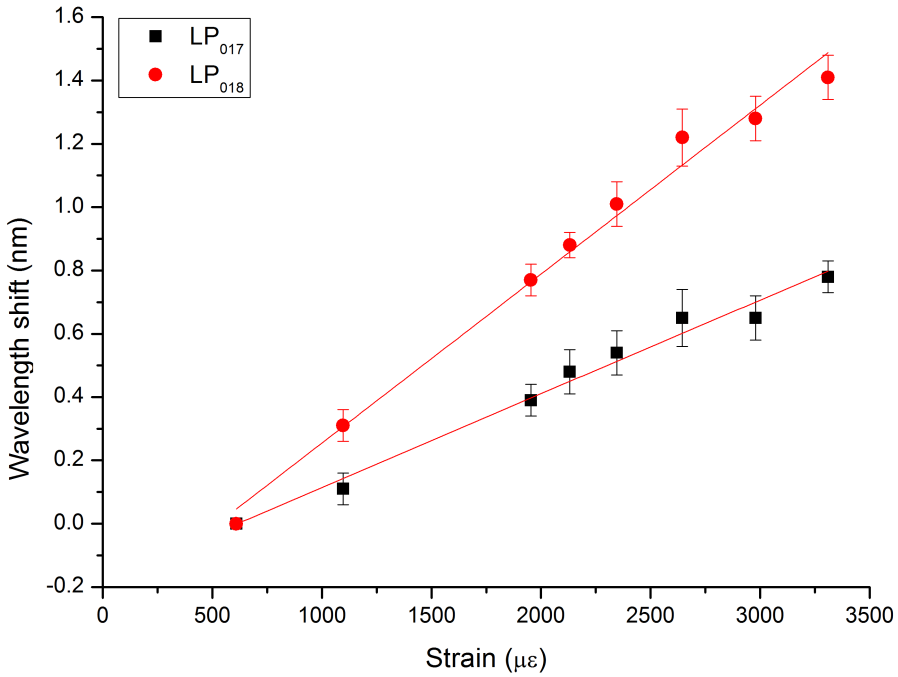

Figure 4.12: Shift in wavelength of the LP_{018} and LP_{017} modes of a 110.8 μm turning point LPG as a function of strain. The best fit line was calculated using the least squares method and help to give an indication of the sensitivities of the bands.

arated increased with increasing refractive index. Eventually, the red shifted band started to disappear out of the range of the spectrometer as the index was increased even further. The red shifted band was more sensitive than the blue shifted band. As figure 4.13 shows, when there is an increase of refractive index from 1 to 1.445, the red shifted attenuation band had a wavelength change of 133 $\pm$ 1.3 nm whereas the blue shifted attenuation band had a wavelength shift of 70 $\pm$ 0.8 nm. This is expected as the phase matching curves are not symmetrical about the phase matching turning point. This agrees with the trends shown in [9]. At surrounding refractive indices matching that of the of the cladding or higher, the PMTP band was no longer evident. Figure 4.14 shows the wavelength shifts of the bands corresponding to coupling to the LP_{018} and LP_{017} modes, with the maximum shifts of -15.85 and -8.05 at a surrounding RI of 1.445 $\pm$ 0.0012. The trend of the measured wavelength shifts are consistent with that of a long period grating with a uniform period not at the phase matching turning point.

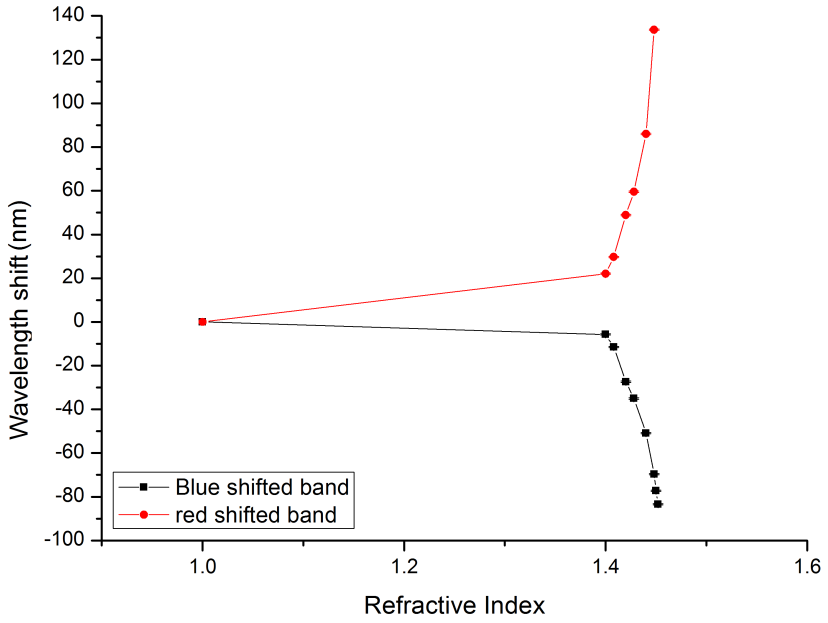

Figure 4.13: Shift in wavelength separation of the dual attenuation bands of a 111 μm turning point LPG as a function of refractive index. The lines used to join the data points act as a guide to show the shift of wavelength of the bands.

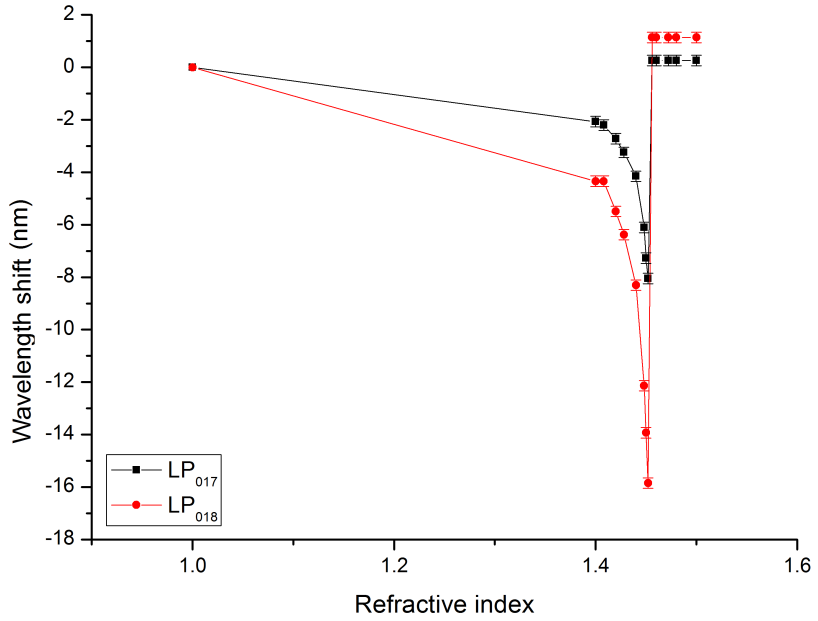

Figure 4.14: Shift in wavelength shifts of the LP_{018} and LP_{017} modes of a 111 μm turning point LPG as a function of surrounding refractive index. The lines used to join the data points act as a guide to show the shift of wavelength of the bands.

4.4 Characterisation of a chirped long period grating

A continuously chirped LPG with a period linearly ranging from 400 - 420 μm over a length of 35 mm was fabricated in a photosensitive fibre (Fibercore PS750) with a cut-off wavelength of 627 nm. This LPG was fabricated using the approach detailed in chapter 3. The experimental procedures for the following chapter are as those described in 4.2. The sensitivities of the bands corresponding to coupling to the LP_{03} and LP_{02} modes are not shown as, due to the nature of the broadened bandwidth of attenuation bands, the bands corresponding to the lower order modes had overlapped making it difficult to resolve them as shown in figure 4.15. Characterisation was only carried out using the CCLPG and not the SCLPG, because their sensitivities to external measurands were expected to be the same. This is valid only for the case where the measurands affect the entire length of the sensor uniformly.

4.4.1 Temperature sensitivity

The higher order modes experienced a greater blue shift in wavelength with increasing temperature, with the respective sensitivities (from lower to higher order modes) from -124 ± 2.9 pm$^{\circ}C^{-1}$ to -193 ± 4.9 pm$^{\circ}C^{-1}$. The sensitivities of the attenuation bands are shown in figure 4.16. The characterisation results are shown in table 4.4. This indicates the CCLPG has a similar sensitivity to temperature than that of the uniform period LPG.

Table 4.4: Temperature sensitivity of the attenuation bands of a continuously linearly chirped LPG of length 35 mm with a period ranging from 400 μm to 420 μm.

Mode	Temperature sensitivity (pm$(^{\circ}C)^{-1}$)
LP_{04}	-124 ± 2.8
LP_{05}	-136 ± 4.4
LP_{06}	-160 ± 4.7
LP_{07}	-193 ± 4.9

4.4.2 Strain sensitivity

Evaluation of the response of the CCLPG to strain reveals that is relatively insensitive to axial strain, as compared to its sensitivity to other measurands such as temperature and refractive index, as shown in figure 4.17. The LP_{07}-LP_{05} modes

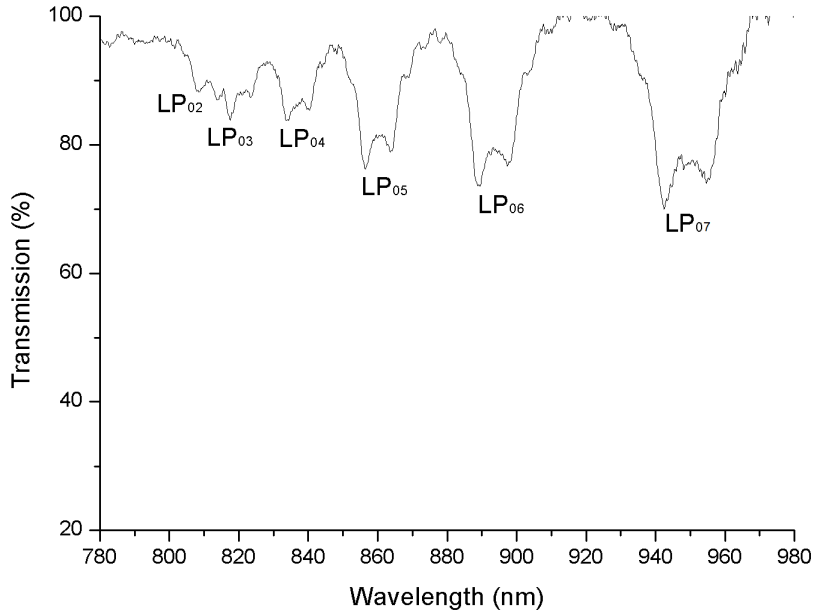

Figure 4.15: Transmission spectrum of a 400 - 420 μm period continuously chirped LPG. The LPG was 35 mm in length written in PS750 fibre with a cutoff wavelength of 627 nm.

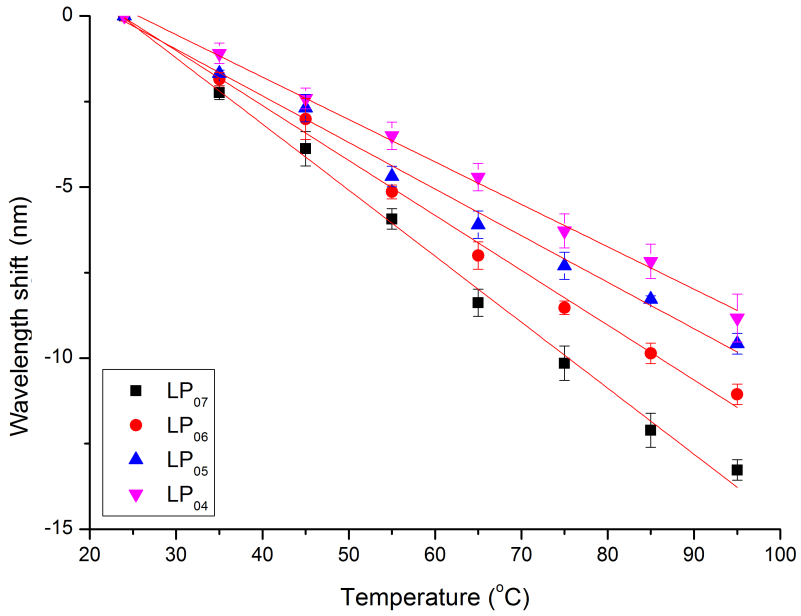

Figure 4.16: Shift in wavelength of the attenuation bands LP_{04} to LP_{07} of a continuously linearly chirped LPG of length 35 mm with a period ranging from 400 μm to 420 μm as a function of temperature. The best fit line was calculated using the least squares method and help to give an indication of the sensitivities of the bands.

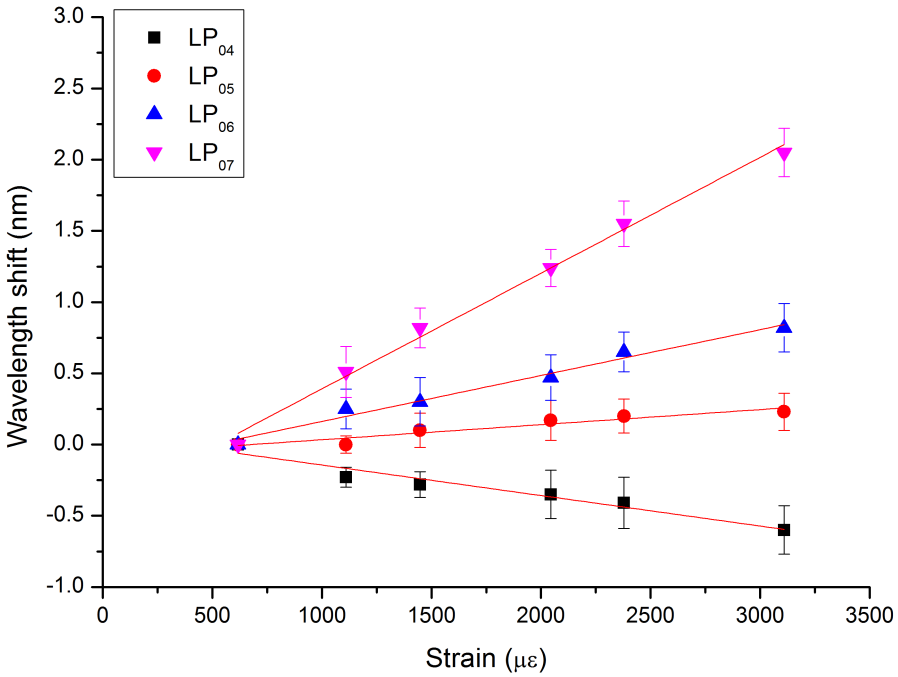

Figure 4.17: Shift in wavelength of the attenuation bands LP_{03} to LP_{06} of a continuously linearly chirped LPG of length 35 mm with a period ranging from 400 μm to 420 μm as a function of axial strain.The best fit line was calculated using the least squares method and help to give an indication of the sensitivities of the bands.

have a positive sensitivity and the LP_{04} shows a negative sensitivity to strain. The results are shown in table 4.5. Compared with the uniform period LPG, where the LP_{04} mode has no sensitivity to axial strain, the LP_{04} mode for the CCLPG has a strain sensitivity of 0.106 ± 0.02 pm$(\mu\epsilon)^{-1}$. This indicates the CCLPG has a similar sensitivity to strain than that of the uniform period LPG.

Table 4.5: Strain sensitivity of the attenuation bands of a continuously chirped LPG with a period of 400 μm to 420 μm.

Mode	Strain sensitivity (pm$(\mu\epsilon)^{-1}$)
LP_{04}	-0.21 $\pm$ 0.03
LP_{05}	0.11 $\pm$ 0.02
LP_{06}	0.32 $\pm$ 0.02
LP_{07}	0.81 $\pm$ 0.03

4.4.3 Refractive index sensitivity

The sensitivity of the LP_{07} mode is shown in figure 4.18 and has a similar sensitivity trend to that of the 400 μm period LPG, from section 4.2.3. As the surrounding

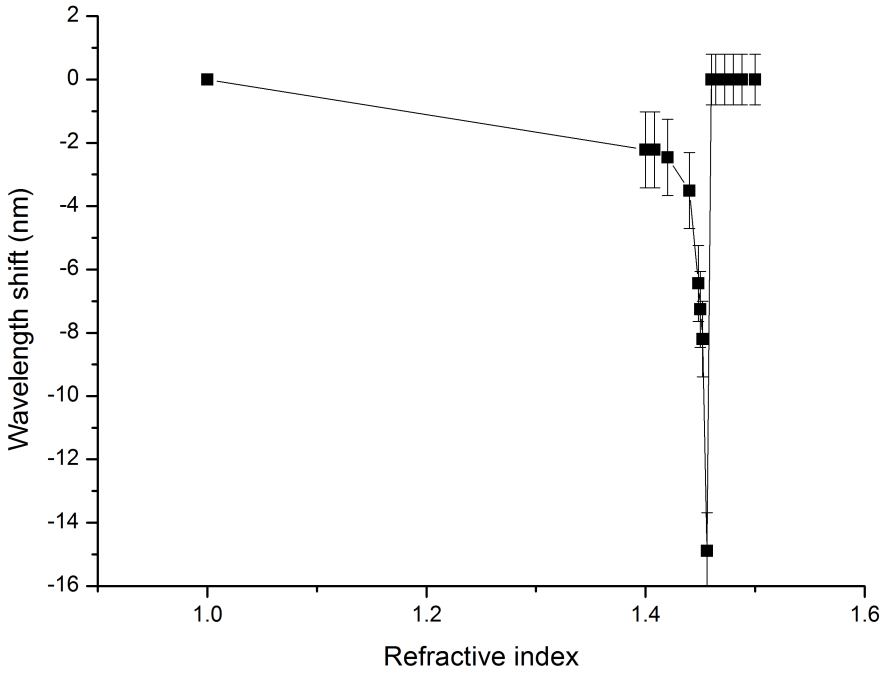

Figure 4.18: Wavelength shift against refractive index of surrounding liquid (Cargille Series A) of the LP_{07} mode of a 400 μm to 420 μm period continuously chirped LPG. The LPG was written in Fibercore PS750 fibre with a cutoff wavelength of 627 nm. The lines used to join the data points act as a guide to show the shift of wavelength of the bands.

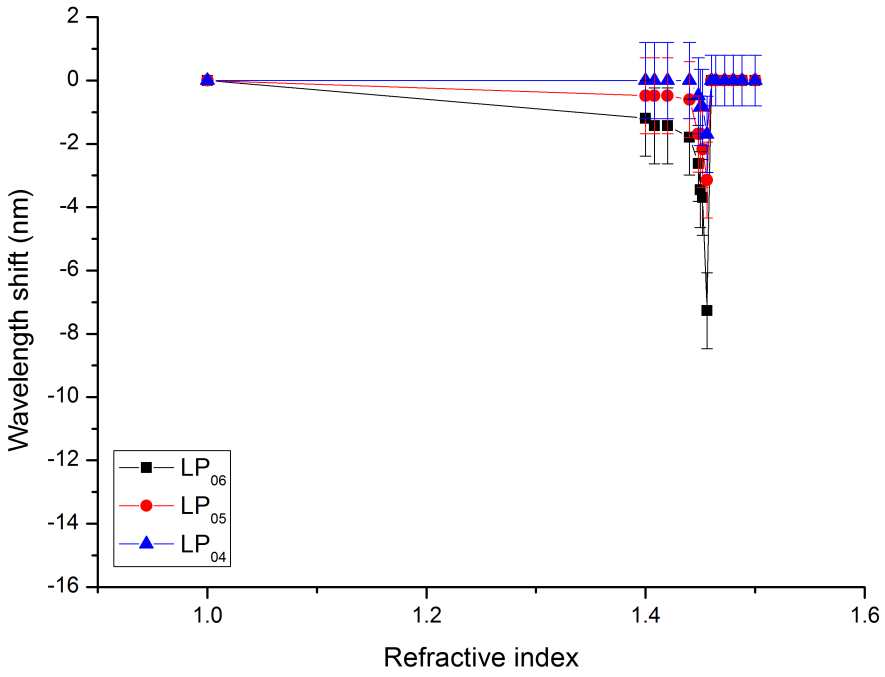

Figure 4.19: Wavelength shift against refractive index of surrounding liquid (Cargille Series A) of the LP_{06} to LP_{04} modes of a 400 μm to 420 μm period continuously chirped LPG. The lines used to join the data points act as a guide to show the shift of wavelength of the bands.

refractive index approaches that of the fibre cladding, the CCLPG experiences the highest sensitivity. Figure 4.19 shows the sensitivities of the LP_{06} - LP_{04} modes. There is no change in attenuation band wavelength with surrounding refractive indices greater than the cladding refractive index. Table 4.6 shows the maximum wavelength shifts for the different attenuation bands.

Table 4.6: Maximum wavelength shift of the attenuation bands of a 400 μm to 420 μm period LPG due the surrounding refractive index (1.456).

Mode	Maximum wavelength shift (nm)
LP_{04}	-2.1 $\pm$ 1.2
LP_{05}	-2.9 $\pm$ 1.2
LP_{06}	-7.0 $\pm$ 1.2
LP_{07}	-14.9 $\pm$ 1.2

4.5 Hydrogen loaded long period gratings

A common method for improving or inducing photosensitivity in an optical fibre is via high pressure hydrogen loading [10, 11]; the fibre is kept at room temperature

in a high pressure tank filled with hydrogen and, over time, it diffuses into the core of the optical fibre.

4.5.1 Experiment

An LPG with a uniform period of 400 μm and a length of 35 mm was written in hydrogen loaded photosensitive fibre (Fibercore PS750) using the point-by-point method. Hydrogen loading was carried out by placing the fibre in a high pressure tank (150 bar) filled with hydrogen for 3 weeks at room temperature. The LPG was fabricated within 10 minutes of being removed from the tank. The grating was left at room temperature for 5 days and the spectrum was monitored continuously using the broadband tungsten-halogen light source and the Ocean Optics spectrometer (SD 2000, resolution approximately 10.0 nm). The evolution of the transmission spectrum of the LPG was tracked and recorded in order to investigate the effects of hydrogen out-diffusion on the LPG spectrum over time.

4.5.2 Results and discussion

Figure 4.20 shows the evolution of the attenuation bands over time, as the hydrogen diffused out of the fibre; the attenuation bands experience wavelength shifts. The refractive index in the core is higher so the coupling wavelengths vary and as the hydrogen diffuses, the effective index changes and so do the coupling wavelengths. For the LP_{07} attenuation band, there was a maximum positive wavelength shift of 34 nm after 1800 minutes.

As the hydrogen first diffuses out of the cladding there is a reduction in the effective refractive index of the cladding modes. When the hydrogen begins to diffuse from the fibre core, the resonance wavelength begins to decrease after around 30 hours (1800 minutes) and the effective refractive index of the fundamental core mode decreases. From the initial starting wavelength to the final resting wavelength of the LP_{07} attenuation band, there was an overall negative shift of 22 nm.

Other LPGs written in hydrogen loaded fibre were annealled at a temperature of 50 ^{o}C for 1 hour. This was carried out by inserting the LPG into a cylindrical ceramic heating furnace whose temperature was monitored using a thermocouple and stabilised by a temperature controller (Eurotherm 2132). Figure 4.21 shows the effects of annealling on a 97 μm period LPG. An LPG at the PMTP was chosen as the effects of hydrogen were expected to be amplified. By annealling a hydrogen

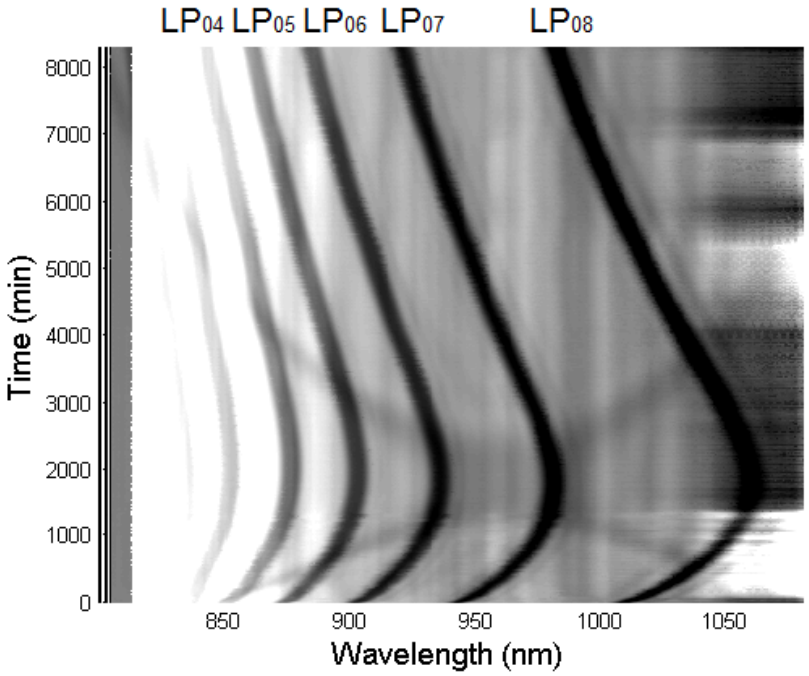

Figure 4.20: Greyscale plot showing wavelength shift against temperature of a 400 μm period hydrogen loaded PS750 LPG over a length of about 5 days. The greyscale represents the evolutionof the transmission spectrum, where white is 100% transmission and black is 0% transmission.

loaded LPG, the diffusion of hydrogen from the fibre is quickened, making the LPG more stable in the long term [12].

Figure 4.22 shows two LPGs written with an 80μm period, where one was fabricated in photosensitive fibre (Fibercore PS750) that was hydrogen loaded and the other was simply written in photosensitive fibre (Fibercore PS750). These LPGs were fabricated to determine the effects of hydrogen loading on LPGs at a period further away from the PMTP. These gratings were fabricated in near identical conditions with the exposure duration kept at 35 s per period and a power of 60 mW (before the focussing lens). It can be seen that the attenuation bands in figure 4.22 (a) are much deeper than in (b) due to stronger coupling influenced by the greater change in refractive index modification in the core of the hydrogen loaded fibre.

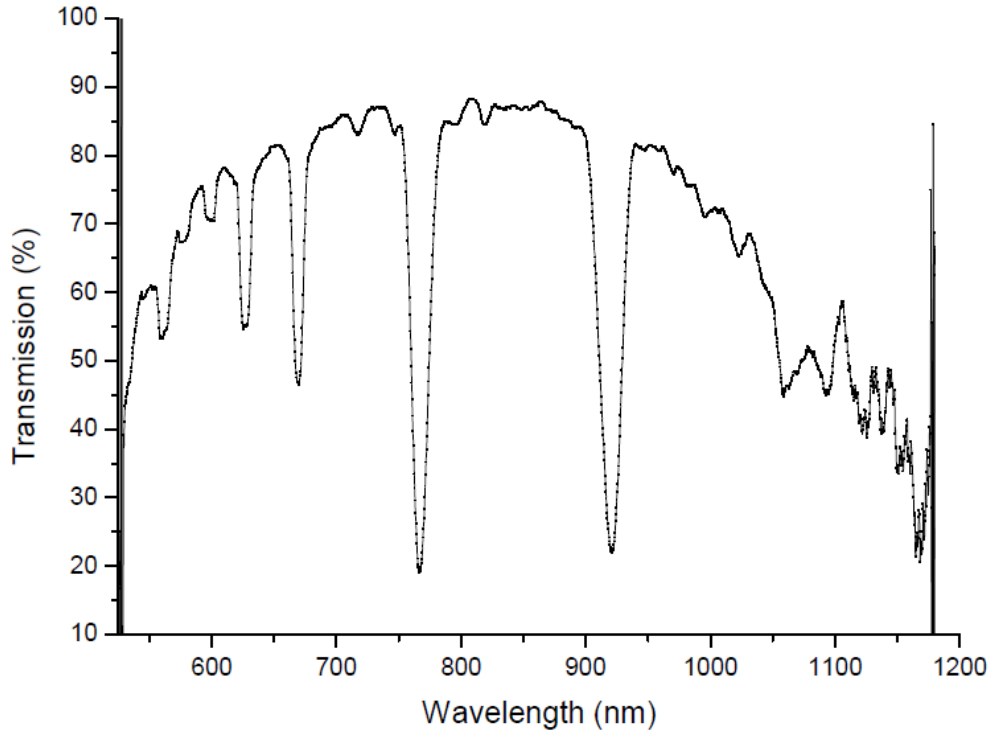

(a)

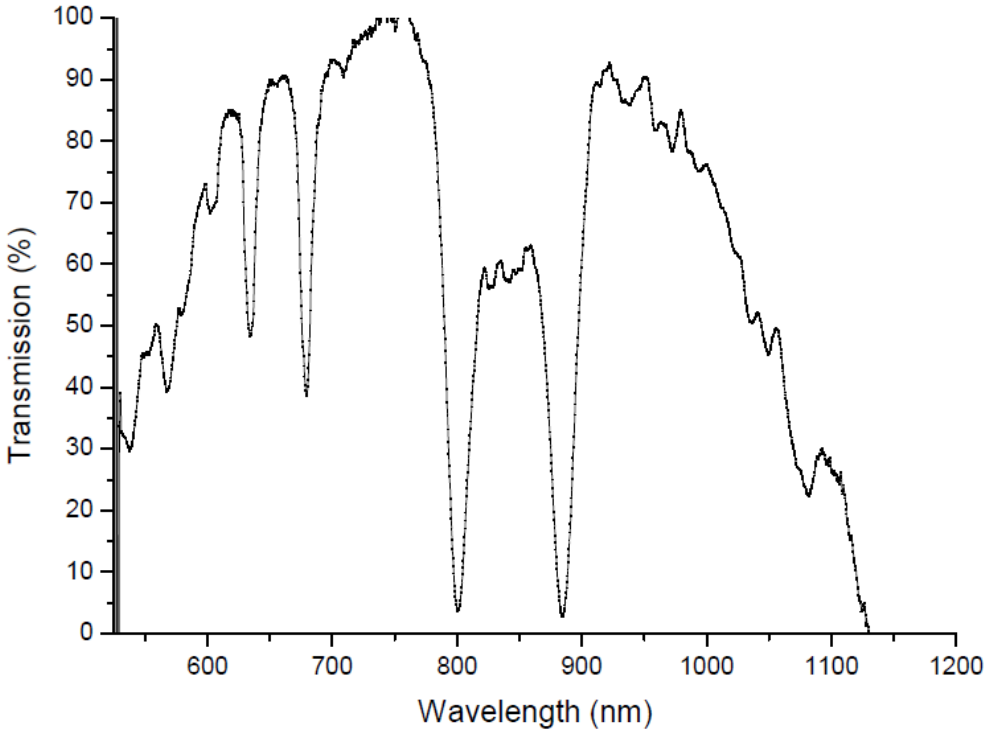

(b)

Figure 4.21: The effects of annealling at a temperature of 50^{o}C for 1 hour on a 97 μm period LPG. (a) shows the spectrum before annealling (b) is the result of annealling. The attenuation bands corresponding to coupling to the LP_{021} mode can be seen to move towards each other.

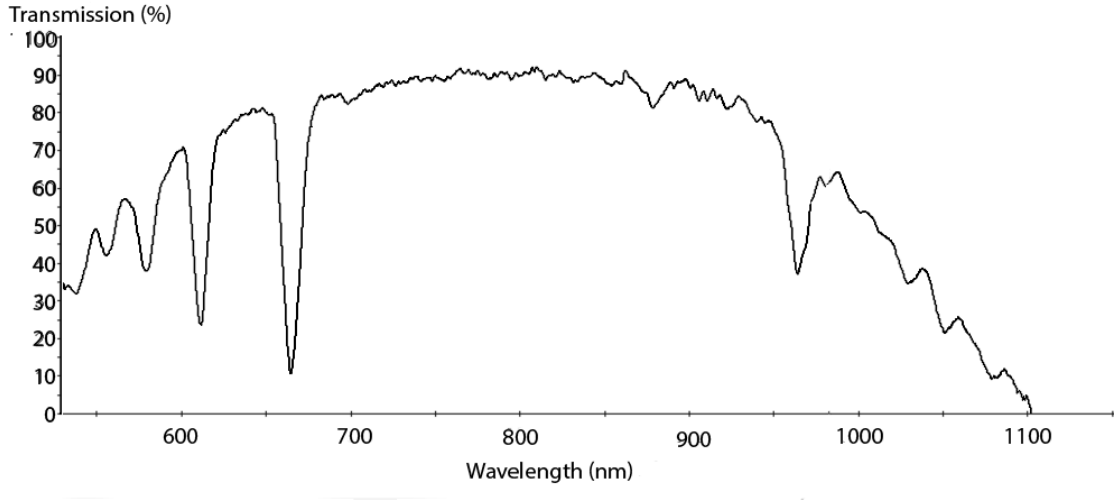

(a)

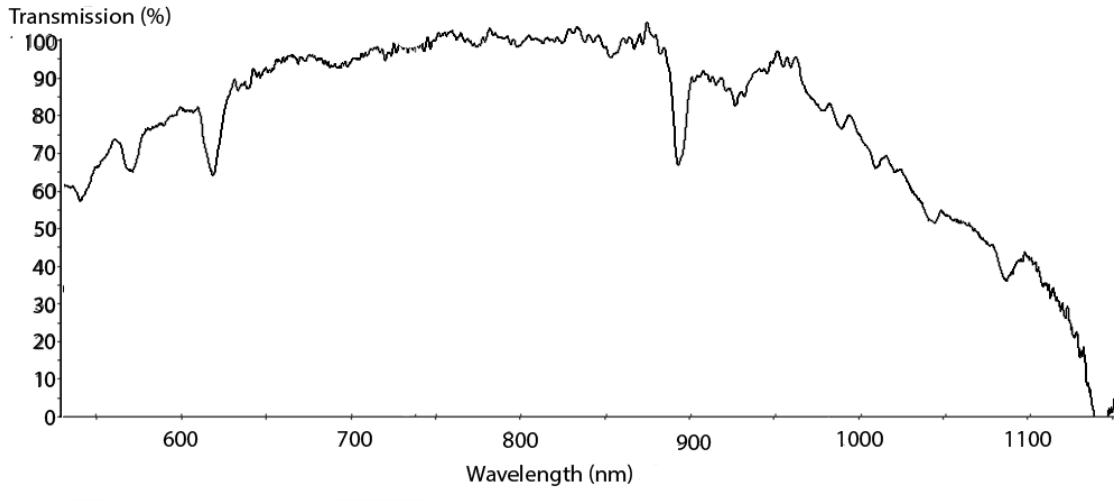

(b)

Figure 4.22: 80μm period LPGs written in (a) hydrogen loaded photosensitive fibre and (b) photosensitive fibre. The attenuation bands of the transmission spectrum are much deeper in (a) due to stronger mode coupling.

4.6 Summary and conclusion

The characteristics of various types of LPGs were investigated. In response to the different measurands, it was shown that LPGs written at the phase matching turning point exhibited a greater sensitivity to temperature, strain, and RI when compared to the uniform period and continuously chirped LPGs. The uniform period and continuously chirped LPGs were also shown to have a much lower sensitivity to strain compared to their sensitivity to the other measurands, temperature and surrounding refractive index. This was indicated by the shift in wavelengths of the attenuation bands, with smaller shifts evident when strain measurements were carried out. Compared to an FBG strain sensor (typical sensitivity of 1.2 $\pm$ 0.0161 pm$(\mu\epsilon)^{-1}$ at a Bragg wavelength of 1550 nm [13]), these LPG's have at least an order of magnitude lower sensitivity. An LPG's ability to couple the fundamental mode to the outer cladding modes causes it to have a larger reaction to environmental changes, such as temperature or refractive index. The core and cladding modes have a large difference in thermal and RI sensitivity as the core is doped but the cladding is not. As the LPG response depends on the difference between the core and cladding responses, the thermal response is greater. The dopant, however, does not have a significant effect on the strain response. With the surrounding refractive index of 1.445 $\pm$ 0.0012 the maximum shifts were 203 $\pm$ 2.1 nm for the LPG at the PMTP, 14.9 $\pm$ 0.4 nm for the uniform period LPG and 12.0 $\pm$ 0.2 nm for the continuously chirped LPG. This confirms that the LPG at the PMTP has a much higher sensitivity due to the dual resonance bands. Table tab:comptab summarises the sensitivities (by comparing wavelength shifts) of temperature, strain and refractive index for the three gratings where the maximum shifts of the CCLPG and LPG are comparable. The LPG at the PMTP had an order magnitude larger wavelength shift across all three measurands.

The influence of hydrogen loading on the properties of the LPG has been investigated. Hydrogen increases the photosensitive properties of an optical fibre, which, under the same exposure conditions, leads to stronger coupling between the core and cladding modes than would be obtained in non-hydrogen loaded fibre, and is represented by deeper attenuation bands in the transmissions spectrum of the LPG. However, after writing an LPG in hydrogen loaded, the coupling of the cladding modes varied as diffusion of hydrogen from the fibre occurred. This could potentially skew results during an experiment. To encourage rapid removal and to stabilise the transmission spectrum, annealling can be carried out.

Table 4.7: Comparison of the wavelength shift of different configurations of LPGs for different measurands.

Type	**Temperature at 85^{o}C**	**Strain at 3000 $\mu\epsilon$**	**Refractive index at 1.445**
	Wavelength shift (nm)	Wavelength shift (nm)	Wavelength shift (nm)
Uniform period LPG	10.6 ± 0.2	2.85 ± 0.1	12.04 ± 0.2
LPG at phase matching turning point	60.5 ± 2.0	56.4 ± 1.3	203 ± 2.1
Continuously chirped LPG	10.59 ± 0.5	2.43 ± 0.27	14.89 ± 1.2

References

[1] O Frazão, L A Ferreira, and F M Araújo. Applications of fiber optic grating technology to multi-parameter measurement. *Fiber and Integrated Optics*, 24(3):227–244, 2005.

[2] S W James and R P Tatam. Optical fibre long-period grating sensors: characteristics and application. *Measurement Science and Technology*, 14(5):R49–R61, 2003.

[3] C C Ye, S W James, and R P Tatam. Simultaneous temperature and bend sensing with long-period fiber gratings. *Optics Letters*, 25(14):1007–1009, 2000.

[4] Crystran Ltd. Silica glass data sheet. accessed [27 mar 2014]. *http://www.crystran.co.uk/userfiles/files/silica-glass-sio2-data-sheet.pdf*, 2012.

[5] V Bhatia, D K Campbell, D Sherr, T G D'Alberto, N A Zabaronick, G A Ten Eyck, K A Murphy, and R O Claus. Temperature-insensitive and strain-insensitive long-period grating sensors for smart structures. *Society of Photo-Optical Instrumentation Engineers*, 36(7):1872–1878, 1997.

[6] Cargille Ltd. Cauchy equations data sheet.

[7] H J Patrick, A D Kersey, and F Bucholtz. Analysis of the response of long period fiber gratings to external index of refraction. *Journal of Lightwave Technology*, 16(9):1606–1612, 1998.

[8] D B Stegall and T Erdogan. Leaky cladding mode propagation in long-period fiber grating devices. *IEEE Photonics Technology Letters*, 11(3):343–345, 1999.

[9] X Shu, L Zhang, and I Bennion. Sensitivity characteristics of long-period fiber gratings. *Journal of Lightwave Technology*, 20(2):255–266, 2002.

[10] P J Lemaire, R M Atkins, V Mizrahi, and W A Reed. High pressure H_2 loading as a technique for achieving ultrahigh UV photosensitivity and thermal

sensitivity in GeO_2 doped optical fibres. *Electronics Letters*, 29(13):1191–1193, 1993.

[11] S Kannan and P Lemaire. Optical reliability of fiber gratings. In J M López-Higuera, editor, *Handbook of Optical Fibre Sensing Technology*, pages 421–431. 2001.

[12] S J Buggy. *Composite material process monitoring using optical fibre gratings sensors*. PhD thesis, Cranfield University, 2008.

[13] A Othonos. Fiber Bragg gratings. *Review of Scientific Instruments*, 68(12):4309–4341, 1997.

Chapter 5

Species-specific chemical sensing using an LPG with a molecularly imprinted coating

5.1 Introduction

5.1.1 Coated LPGs as chemical sensors

As well as the core, the cladding also acts as a waveguide. Their optical intensities usually dissipate after they propagate a short distance due to bends in the fibre, scattering and absorption from the fibre jacket which designed to remove the cladding modes by attenuating them. When the jacket is removed, the cladding mode evanescent field is able to extend into the surrounding environment and the properties of the modes can be influenced by the local refractive index; by applying functional coatings to the surface of the cladding it is possible to influence the coupling of modes to improve the sensitivity of an optical fibre sensor. This makes them a viable chemical sensing platform. Nanoscale precision is required as coatings in the order of a few 100 nm have been seen to have a significant influence on the transmission spectrum of an LPG [1, 2, 3]. The techniques that have been employed for the deposition of such functional coatings with nano-scale control over the thickness of the coating include the Langmuir-Blodgett deposition [4, 5], electrostatic self assembly [6, 7], atomic layer deposition [8], dip coating [9] and liquid phase deposition [10].

The chemical sensing capabilities of LPGs have been employed in a number of areas. For example they have been used for detecting volatile organic compounds (VOC). VOCs can come from gases formed from fuel or petroleum products, paints

and inks, combustion processes and in nature and farming [11]. LPGs have been used to detect compounds such as toluene [12], benzene [12], chloroform [13], xylene and cyclohexane [14]. By applying a functional coating to the LPG the refractive index of the coating is influenced by particular compounds and is represented in the transmission spectrum [12]. Korposh et al. demonstrated a sensor coated with a mesoporous SiO_2 film that is infused with a functional material could be used to detect particular chemical species in water with a quick response time within 10 s [15]. Coated LPGs have also been used as pH sensors, where changes in pH levels change the refractive index or thickness of the coating, and again the information is relayed by changes in the transmission spectrum [16].

5.1.2 Molecular imprinting

There is significant interest in developing species specific chemical sensors by coating LPGs with functional materials, however achieving high selectivity is still a challenge. The molecular imprinting technique is a versatile platform for creating artificial receptors where the properties of the receptor can be easily controlled and tailored to a specific need. Molecular imprinting is a process used to create binding sites in host matrices. The physical shape and functionality of the binding site is specific such that it can be used to recognise particular templates (analytes) (see figure 5.1) [17].

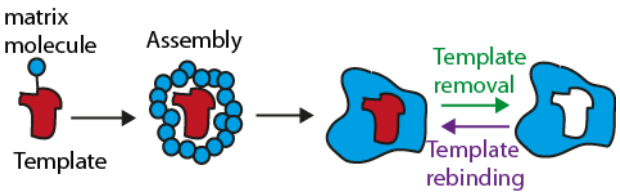

Figure 5.1: The basic principles of molecular imprinting are shown along with the removing and rebinding of the template (based on [17]).

In 1949, Dickey [18] reported his work on molecular imprinting based on the formation of antibodies with antigen as a template which was proposed originally by Pauling [19]. Dickey prepared a silica gel in the presence of different alkyl oranges and showed that a particular alkyl orange was more readily adsorbed in the silica gel that had initially been formed with that particular alkyl orange template. Since then, the development of molecular imprinting has expanded vastly and have potential uses in the medical field for detecting disease biomarkers [10, 17, 20] and for

detecting gases or chemicals [21, 22].

Molecular imprinting in metal oxide matrices

Processes that are often used to create metal oxide nanoscale films for molecular imprinting include, but are not limited to, the surface sol-gel deposition process [21, 23, 24], dip coating [25, 26], spin coating [27, 28] and liquid phase deposition [10]. The surface sol-gel deposition procedure is where the film is created layer-by-layer, and the aqueous solutions used gradually take a gel-like form [21, 23]. The molecules of the film are covalently bonded and are made with alternate layers of metal alkoxides and a hydroxyl to hydrolyse the alkoxide. To remove the excess solutions, the substrate is rinsed and dried between each layer [23]. Dip coating is a process where the substrate is immersed in a solution for a period of time whilst the layer deposits itself. The substrate is then removed, rinsed and dried. This procedure is repeated until the desired coating thickness is achieved [25]. Spin coating involves depositing the desired film (in solution) onto the centre of the substrate and then spinning the substrate at a high speed, typically 3000 rpm [28]. The acceleration causes the solution to spread out until a thin film is formed on the surface of the substrate. The film thickness is determined by the spin speed, acceleration, spin time, viscosity of the film material.

Liquid phase deposition allows the film to be created from aqueous solutions [10] using a metal-fluoro complex that is hydrolyzed by water, boric acid (H_3BO_3) or aluminium [29]. Boric acid and aluminium act as fluoride scavengers to form the oxide whereas the addition of water directly causes the formation of an oxide [29]. Homogeneous layers build up on the substrate by a chemical equilibrium reaction of two particular compounds mixed together, with the thickness of the layer being dependent on the duration of the immersion of the substrate is immersed in the solution. To create the actual template/metal oxide matrix, the particular template molecules (that is to be detected by the film) are mixed with the solutions used to create the metal oxide film. The bound template is then removed from the matrix, usually with a solvent such as hydrochloric acid (HCl) or ammonia [23], by heating [30] or by O_2 plasma treatment [28]. To test the successfulness of the process, similar compounds are bound to the film. The original template molecule will tend to have the greatest binding efficiency [17, 23], showing the film to be stable and having good selectivity.

Metal oxides are popular choices to create matrices as they are generally stable with

rigid structures and readily accept guest molecules. The desired binding holes can be created to carry out molecular imprinting without the film structure breaking down [10, 23].

TiO_2 photocatalysis under UV light

It has been reported that TiO_2 has photocatalytic properties when exposed to UV light [31, 32]. When TiO_2 is exposed to UV irradiation (which has an equal to or greater energy than the bandgap level), negative electron and positive hole pairs are produced as the electrons are excited to the conduction band. The electrons react with oxygen molecules to form oxide anions and the holes react with pollutants/template or water and release radical hydroxyl ($^{\bullet}OH$) particles which are powerful oxidation agents [33], see figure 5.2. The radical particles combine with the pollutant/template, decompose it and thereby removing it.

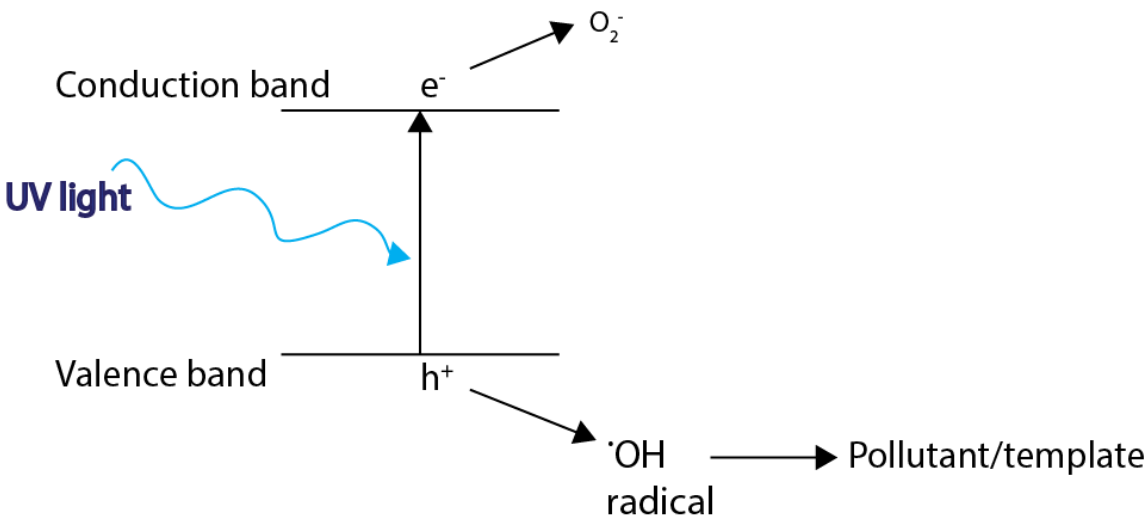

Figure 5.2: Representation of mechanism of TiO_2 photocatalysis under UV light. e^- represents the electrons and h^+ represents the holes.

This work describes a coated LPG sensor in which the functional material is a composite nanoscale film consisting of a molecularly printed ceramic. The goal was to demonstrate a selective method for porphyrin detection. As only the target molecule fits into the binding site, only the signature target molecule can influence the optical properties of the material. In this case, the binding of the target molecule into the cavity results in a change in the refractive index of the coating, which is sensed by monitoring changes in the properties of the attenuation bands that characterise the transmission spectrum of an LPG. The target molecule in this work is a porphyrin, a member of a group of chemicals that help form many important substances in

the body, including haemoglobin which is vital for enabling the body's cells to use oxygen. The detection of porphyrins are important as they can help determine diseases such as porphyria, which affects the skin or nervous system [34]. Liquid phase deposition was used to create the nanoscale coating on the cladding of an optical fibre containing an LPG. Liquid phase deposition is simple and reproducible technique for creating thin films with nanometer precision. This is also a versatile way of customising an LPG sensor depending on the compound that needs to be detected.The following experiments were carried out as a visiting researcher at the University of Kitakyshu, Japan and were extended at a later date upon return to the University of Cranfield, UK.

5.2 Experiment

97 μm and 96 μm period LPGs, each with a length of 35 mm were written in single mode, photosensitive fibres with a cut-off wavelength of 627 nm (Fibercore PS750). These periods were chosen as they promote coupling to the LP_{021} mode at the phase matching turning point, which has been shown to offer the highest sensitivity to changes in the properties of the coatings deposited onto an LPG [1]. The LPG transmission spectra were monitored by connecting the optical fibre to an Ocean Optics tungsten-halogen light source and an Ocean Optics CCD spectrometer (HR2000CG-UV-NIR). The LPG was placed in a Teflon holder. It effectively acted as a cell or bath so the LPG could be be fully immersed in the solutions that were used.

Fabrication of composite nanoscale film

The LPG was initially immersed into a solution of potassium hydroxide (KOH) for 30 minutes to prepare and activate the surface of the fibre for deposition. To prepare the matrix of the composite film, a 1:1 ratio of 500 μM of boric acid (H_3BO_3) and 100 μM of ammonium hexafluorotitanate ($(NH_4)_2TiF_6$) in aqueous solution were used. The titanium dioxide (TiO_2 or titania) solution was formed via the chemical reaction between the H_3BO_3 and $(NH_4)_2TiF_6$. The mechanism is described as follows [35]:

$$TiF_6{}^{2-} + 2\,H_2O \rightleftarrows TiO_2 + 4\,H^+ + 6\,F^- \tag{5.1}$$

$$BO_3{}^{3-} + 4\,F^- + 6\,H^+ \rightarrow BF_4{}^- + 3\,H_2O \tag{5.2}$$

The two following equations are an expansion and a more detailed description of equation 5.1:

$$\mathrm{TiF_6}^{2-} \xrightarrow{nOH^-} \mathrm{TiF_{6-n}(OH)_n^{2-}} + \mathrm{nF^-} \xrightarrow{(6-n)OH^-} \mathrm{Ti(OH)_6^{2-}} + 6\,\mathrm{F^-} \tag{5.3}$$

$$\mathrm{Ti(OH)_6^{2-}} \rightarrow \mathrm{TiO_2} + 2\,\mathrm{H_2O} + 2\,\mathrm{OH^-} \tag{5.4}$$

The increase in F^- moves the equilibrium of equation 5.1 to the left, while the addition of H_3BO_3 as the fluoride scavenger (as seen in equation 5.2) moves the equilibrium of equation 5.1 to the right. Equation 5.3 shows that when fluorinated titanium ions (TiF_6^{2-}) are placed in an aqueous solution, they eventually form titanium hydroxide ions ($Ti(OH)_6^{2-}$). TiO_2 is formed from these titanium hydroxide ions as the concentration of OH^- is gradually replaced with F^- ions [35].

To create the molecularly imprinted film, 100 μM of the 5, 10, 15, 20 Tetrakis-(N-methyl-piridinium-4-yl)-21H, 23H-porphine tertakis (p-toluenesulfonate) [TMPyP] porphyrin template in solution was incorporated into the TiO_2 matrix. The LPG was removed from the TiO_2/TMPyP solution when the dual attenuation band of the LP_{021} mode appeared in the transmission spectrum, which occurred after 4-5 hours. The mechanism of interaction between the template and the matrix is electrostatic attraction between the negative TiF_6^{2-} and the positive $TMPyP^+$.

Subsequently, the template was removed from the molecularly imprinted film by submerging the coated LPG into 0.1 M hydrochloric acid (HCl). The template was then rebound the the LPG coating by placing the fibre sensor into a TMPyP solution (concentration of 100 μm). The removal and rebinding of the template was carried out twice with the LPG being pre-treated with 1 wt% ammonia solution (NH_3) prior to the second template rebinding attempt to check the effects of NH_3 solution on the molecular imprinting process.

In between each process, the LPG was rinsed in distilled water and dried with compressed air to remove any excess solution and make sure the LPG was ready for the addition subsequent materials. To ensure that the influence on the transmission spectrum of the LPG were only due to changes in the refractive index of the molecularly imprinted coating, transmission spectra were recorded when the LPG was immersed in distilled water. Given the refractive index sensitivity of LPGs, it is important to ensure that the spectra were recorded with the same surrounding bulk

refractive index. The stability of the spectra was also determined by immersing the grating in distilled water for 2 minutes; this process was repeated 3 times. All the measurements were carried out at room temperature

5.2.1 SEM images of TiO_2 film and TiO_2/TMPyP composite film

In order to determine the dependence on thickness of the TiO_2 coating on immersion time, a bundle of optical fibres were placed together in the same holder and immersed in the TiO_2 solution. Over a period of 5 hours, after every hour, one fibre was removed from the holder. The fibres were viewed using a high resolution Hitachi S-5200 field emission scanning electron microscope (FE-SEM) (resolution of 1.8 nm at 1 kV and 0.5 nm at 30 kV). SEM images of the deposition of TiO_2 and TMPyP every hour, for five hours were also compared with each other. The coated sections of the fibre were first coated with a thin layer of platinum particles, to charge the surface. A Hitachi E-1030 ion sputter was used for this purpose.

Figures 5.3 - 5.4 show the growth of the TiO_2/TMPyP composite nano thin film on the optical fibre, over the course of 5 hours. Figure 5.3 (a) shows that after one hour of material growth, there are still gaps in the coating and only after 3 hours 5.3 (c) is there a more uniform film covering the substrate. This indicates why the transmission spectrum of the LPG begins to respond after this time, as shown in figure 5.7. The thickness of the film after a 5 hour period is shown in figure 5.5. An image was also taken of the TiO_2 thin film.

Figure 5.4 shows the difference between a fibre coated with just TiO_2 and a fibre coated with a TiO_2/TMPyP film. As can be seen, the addition of the template TMPyP into the TiO_2 matrix leads to the growth of a more uniform film on the optical fibre. Figure 5.4 (a) shows large clusters of varying size built up on the surface, whereas figure 5.4 (b) shows the nanoparticles distributed more evenly with the TiO_2 particles having a smaller diameter. This indicates that TMPyP helps to control the growth of the TiO_2 nanoparticles leading them to have a smaller diameter

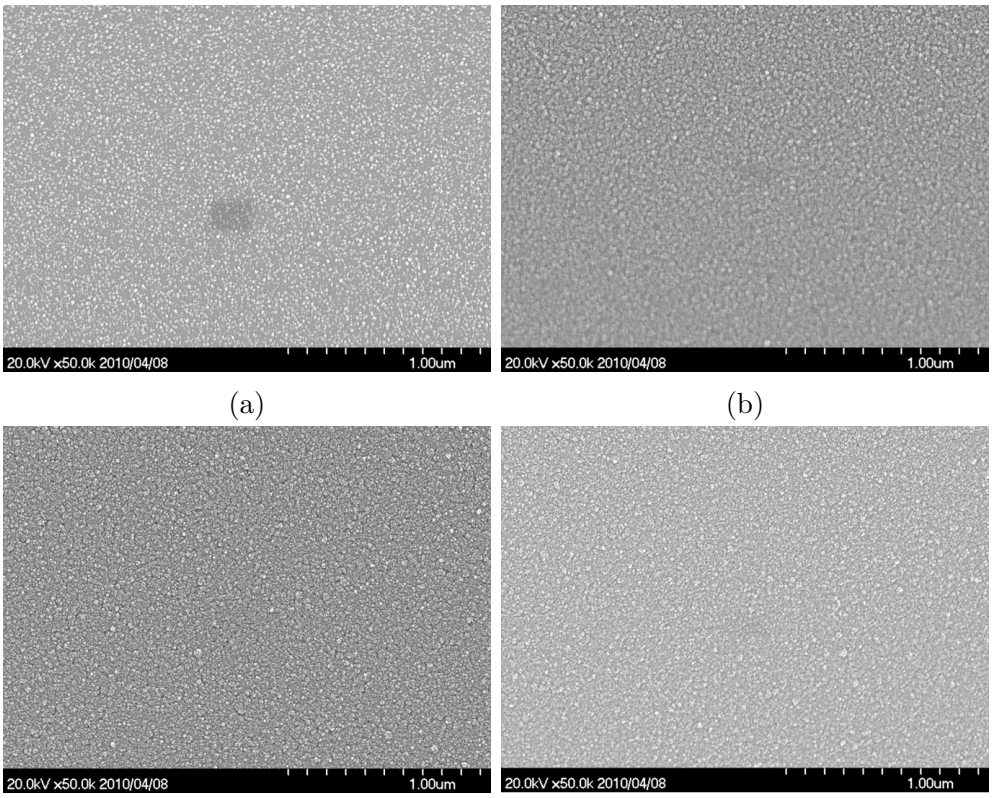

Figure 5.3: SEM images of the film deposited with a TiO_2/TMPyP composite nano thin film. Taken at (a) 1 hour (b) 2 hours (c) 3 hours and (d) 4 hours using a Hitachi S-5200 FE-SEM.

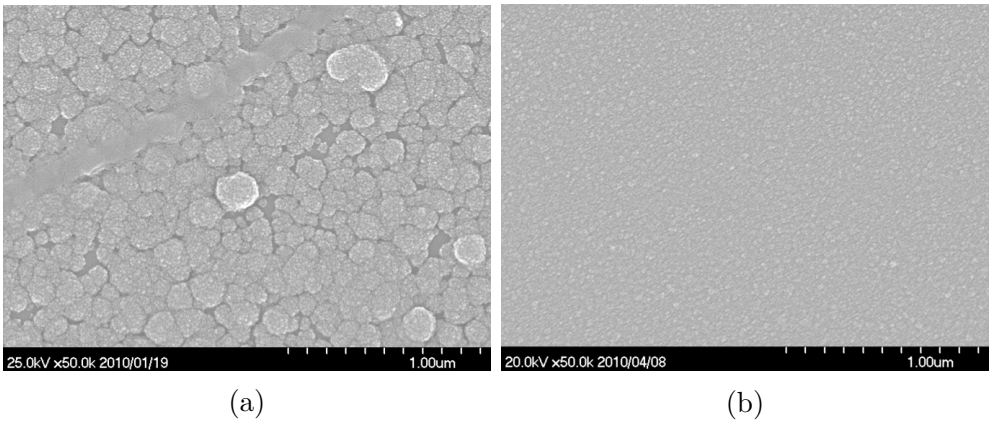

Figure 5.4: SEM images of the film deposited with (a) TiO_2 and (b) TiO_2/TMPyP nano thin film. Taken after 5 hours using a Hitachi S-5200 FE-SEM.

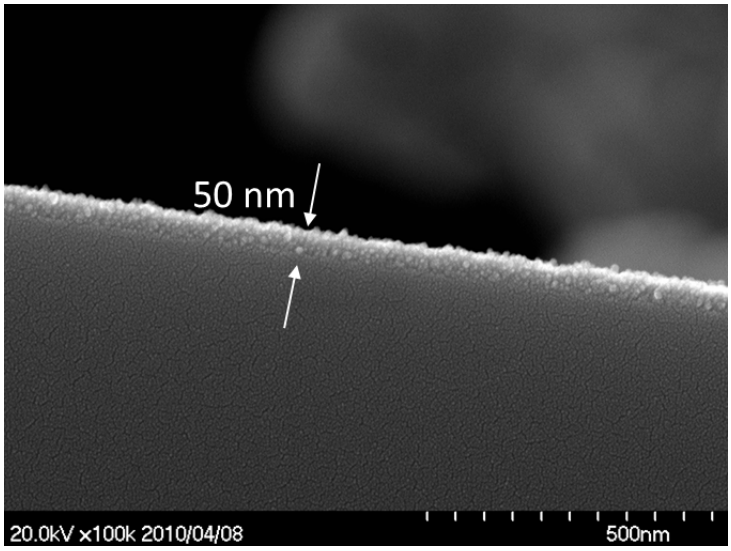

Figure 5.5: SEM image of a TiO_2/TMPyP composite nano thin film after 5 hours, with a thickness of 50 nm. Taken using a Hitachi S-5200 FE-SEM.

5.3 Results and discussion

5.3.1 Removing/rebinding the TiO_2 template

Figure 5.6 shows the changes in the transmission spectrum of the coated LPG as the TMPyP template (concentration of 100 μM) was removed from and rebound to the TiO_2/TMPyP film. After the LPG was immersed in HCl, the depth of the dual attenuation band centred at around 788 nm decreased as the TMPyP was being removed, indicating a reduction in the refractive index of the film. After the first removal and immediate rebinding of the template, the band depth was seen to increase slightly but did not reach the original TiO_2/TMPyP depth. This indicated that the rebinding efficiency was low.

The TMPyP template had a much greater binding efficiency with the coating when the coated LPG (without template) was first immersed in the solution of NH_3. An increase in attenuation band depth of the attenuation band at the PMTP was observed, indicating an increase in the refractive index of the coating. The NH_3 neutralised the film, as the exposure of the film to HCl changed the surface charge of the TiO_2/TMPyP film matrix. The improvement in the binding efficiency after treatment with NH_3 further supports the proposition that the binding mechanism is electrostatic interaction. As highlighted in Section 4.3.3 in Chapter 4, where the LPG's refractive index response was characterised, the depth and split of the attenuation band at PMTP increases as the refractive index increases.

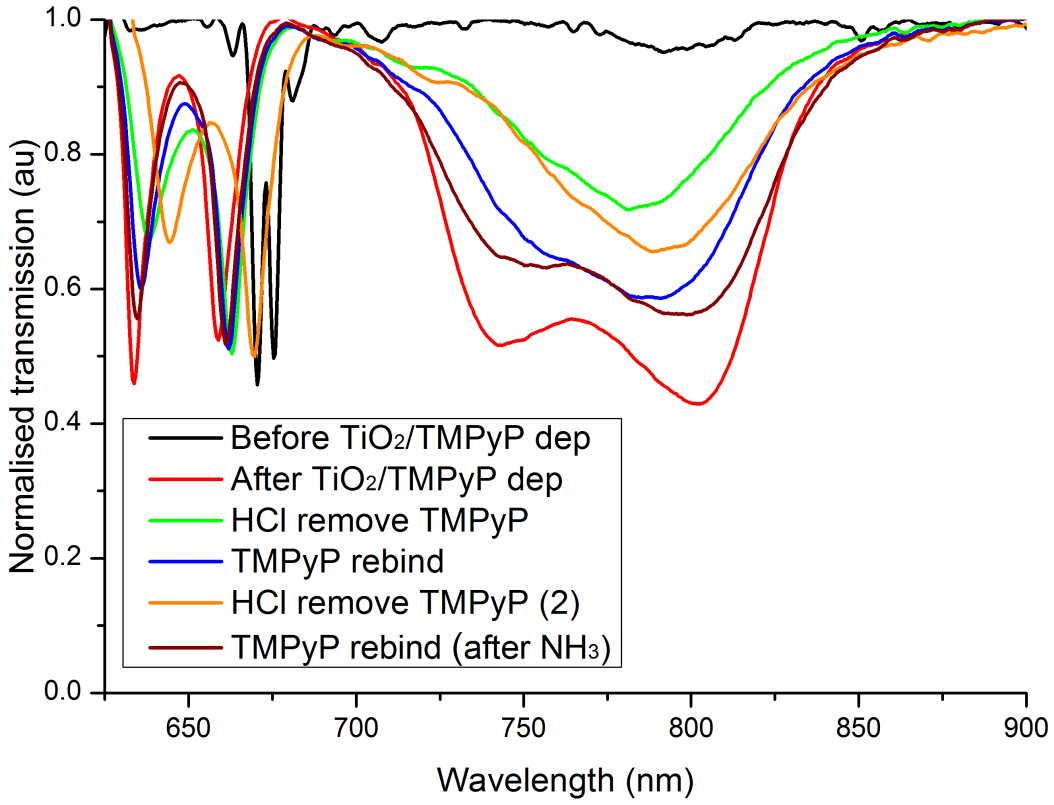

Figure 5.6: Transmission spectra of 97 μm period long period grating with removal/rebinding of TMPyP (100 μM) from/to the TiO_2/TMPyP film in solution.

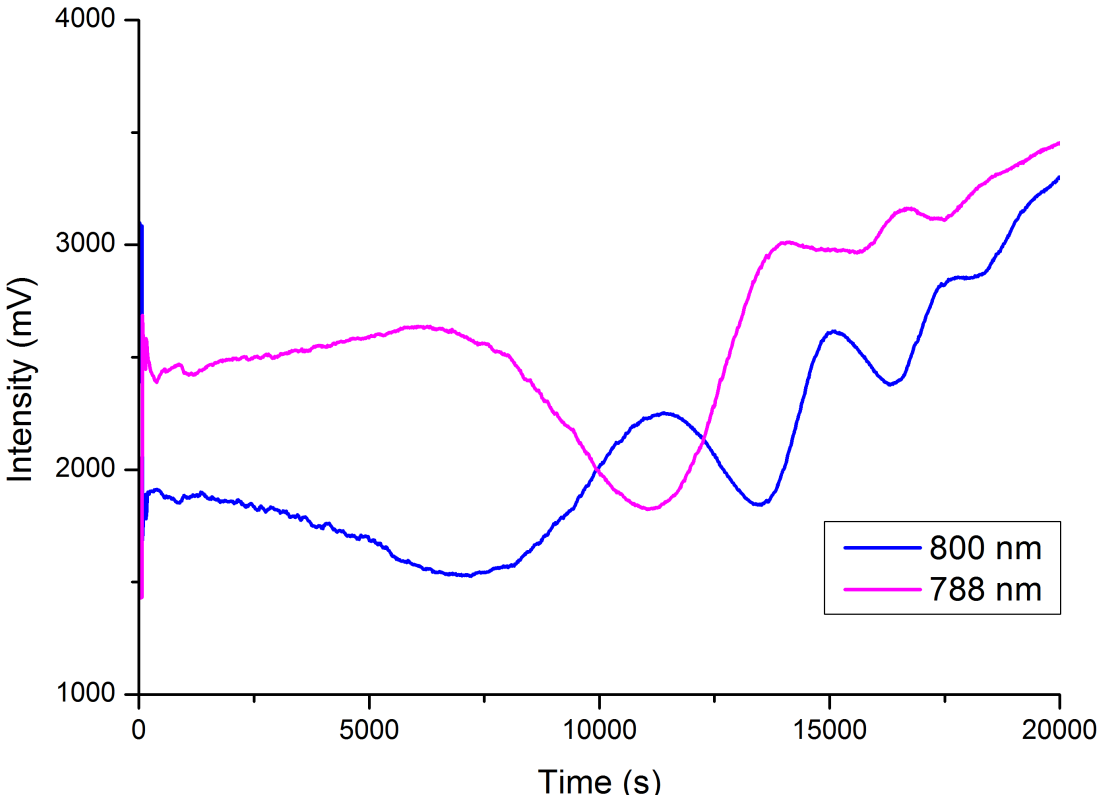

Figure 5.7: Change of the transmission, measured at 800 nm and 788 nm of TiO_2/TMPyP film coated 97 μm period LPG.

Though there was stronger TMPyP rebinding after exposure to NH_3, the attenuation band did not return to the original TiO_2/TMPyP depth. This could be attributed to the influence of the HCl solution on the film surface or thickness.

Figure 5.7 shows the evolution two wavelengths as the LPG was being coated. These wavelengths were close to the wavelength where the PMTP band of the 97 μm period LPG developed (720 - 820 μm). From figure 5.7 it can be seen that the attenuation band grew to a maximum after 10800 seconds (3 hours) before it began to split after 12600 seconds (3.5 hours) of the film developing.

When the experiment was repeated using a 96 μm period LPG, figure 5.8 shows that the reaction of the dual attenuation band had the same trend as that of the 97 μm period LPG as they are near the PMTP. Here, TMPyP also rebound much

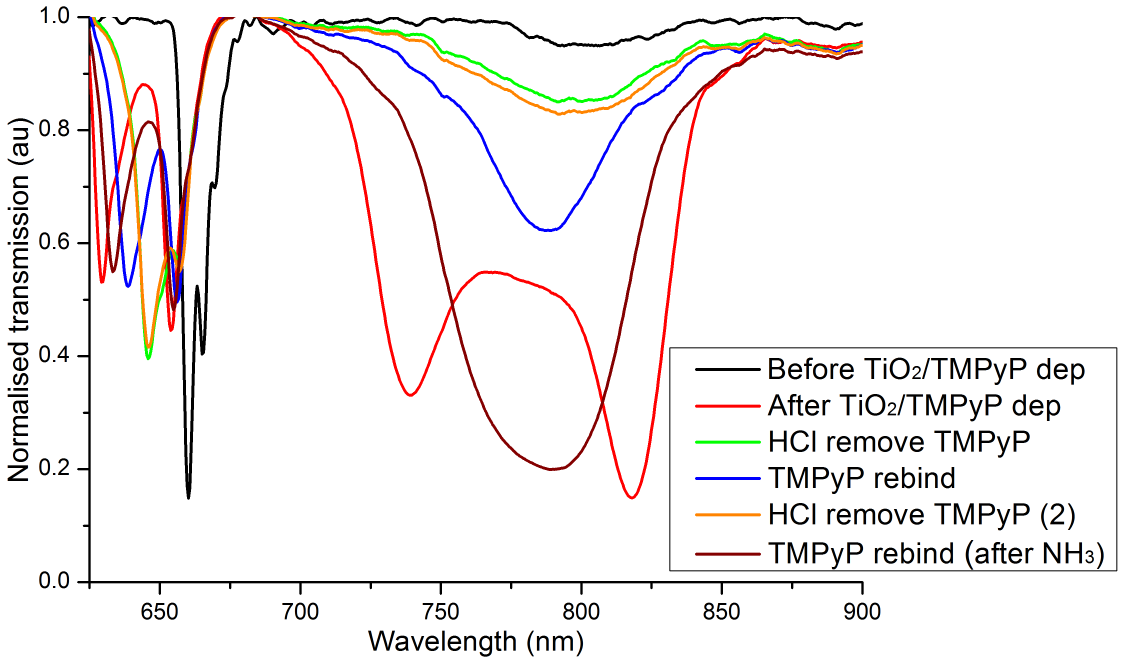

Figure 5.8: Transmission spectra of 96 μm long period grating with removal/rebinding of TMPyP (100 μM) from/to the TiO_2/TMPyP film in solution.

better with the matrix when the fibre was first treated with ammonia.

Figure 5.9 shows the change of the transmission of the attenuation band at a wavelength of 810 nm; as the thickness of the film increased, the depth of the attenuation band also decreased and the band began to split at around 3.5 hours and can be seen by the development of the right side of the PMTP band (LP_{021} mode) at 845 nm.

5.3.2 Assessment of the specificity

To assess the specificity of the molecular imprinting process, the LPG was also exposed to a porphyrin which was structurally similar to the template porphyrin (with the chemical structures shown in figure 5.10). The coated LPG, following NH_3 treatment, was immersed in a solution of 100 μM of the porphyrin Tetrakis-(4-sulfophenyl) porphine [TSPP] for 15 minutes. The change in the transmission spectrum was recorded and compared with the effects of the original template, TMPyP. This test was carried out with both the 96 μm and 97 μm period LPGs.

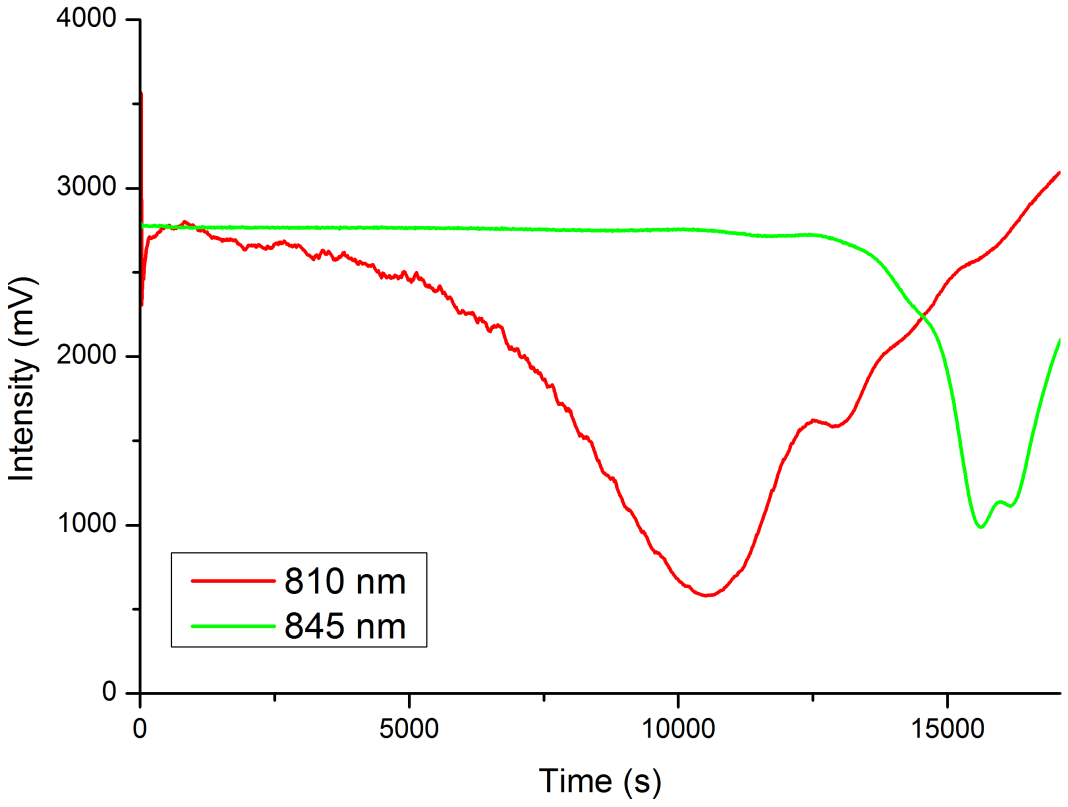

Figure 5.9: Change of the 810 nm and 845 nm wavelengths of TiO_2/TMPyP film as it was grown on the 96 μm period LPG.

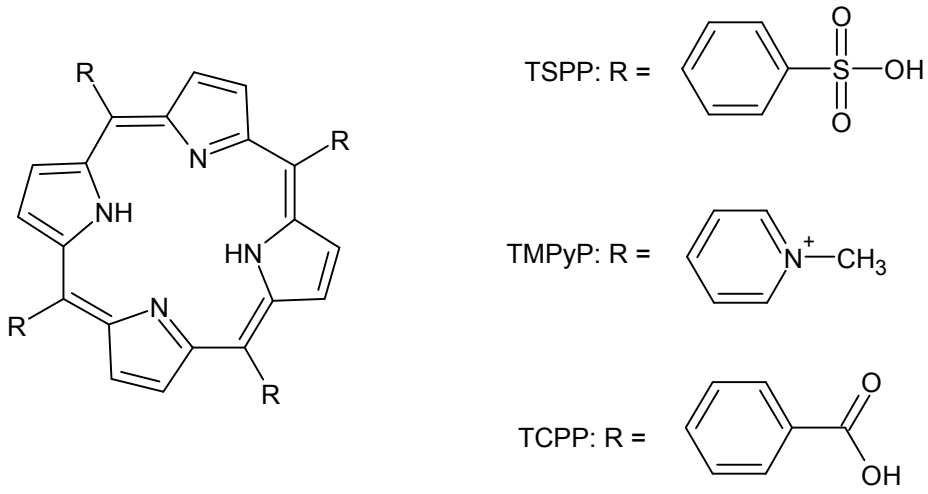

Figure 5.10: Chemical structure of the porphyrin compounds TMPyP (used as template), TSPP and TCPP

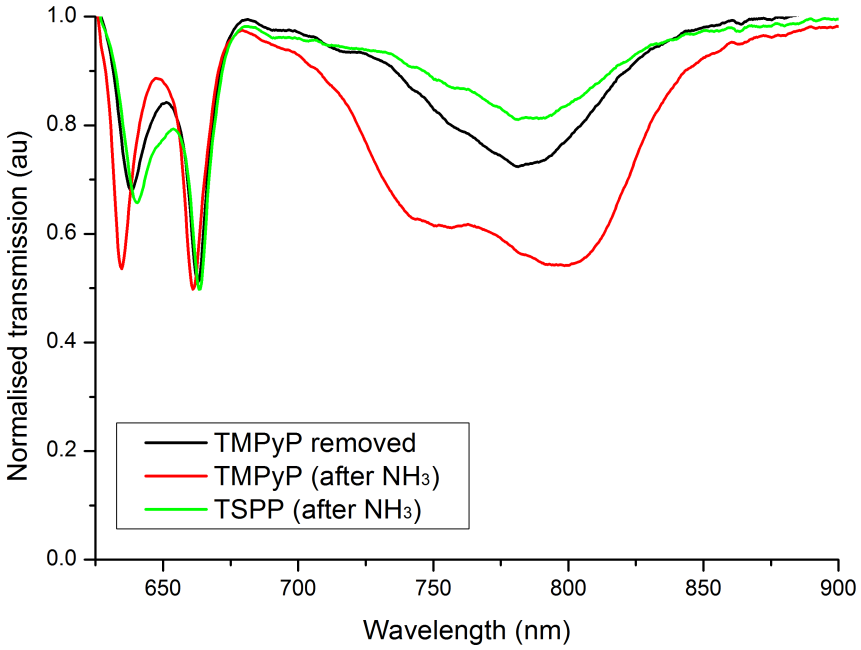

Figure 5.11: Spectrum of the 97 μm period LPG at rebinding of different porphyrins, TSPP and TMPyP (the template) (100 μM) to the TiO_2/TMPyP coating in solution. The transmission spectrum of the TiO_2/TMPyP coating without a porphyrin is also shown for comparison.

Figures 5.11 and 5.12 show the selectivity of the modified grating sensor, showing that the efficiency of binding the template material TMPyP was significantly greater than that of the other porphyrin, TSPP. There is little change in the attenuation band depth after exposure to TSPP.

Figure 5.13 shows the additional work carried out at Cranfield University. The response to additional structurally similar porphyrins (see figure 5.10 for chemical structure) was assessed using a 111 μm LPG coated with the TiO_2/TMPyP film. The spectra recorded after exposure to each of the porphyrins are shown in figure 5.13. This period was chosen as it promotes coupling to a cladding mode close to a phase matching turning point and would therefore show the greatest sensitivity to a refractive index change. As this work was carried out at a later date, the LPG used was fabricated in a new batch of fibre (though same specifications from the manufacturer) as the old reel had been used up. By using a new fibre reel, there may have been slight variations in the fibre properties such as refractive index, fibre dimensions and uniformity of the dopant. This means that the period at which the PMTP occurs will be different. In this case, the PMTP was achieved at a period of 111 μm. The porphyins used were 4, 4', 4", 4"'-(21H, 23H-Porphine-5,

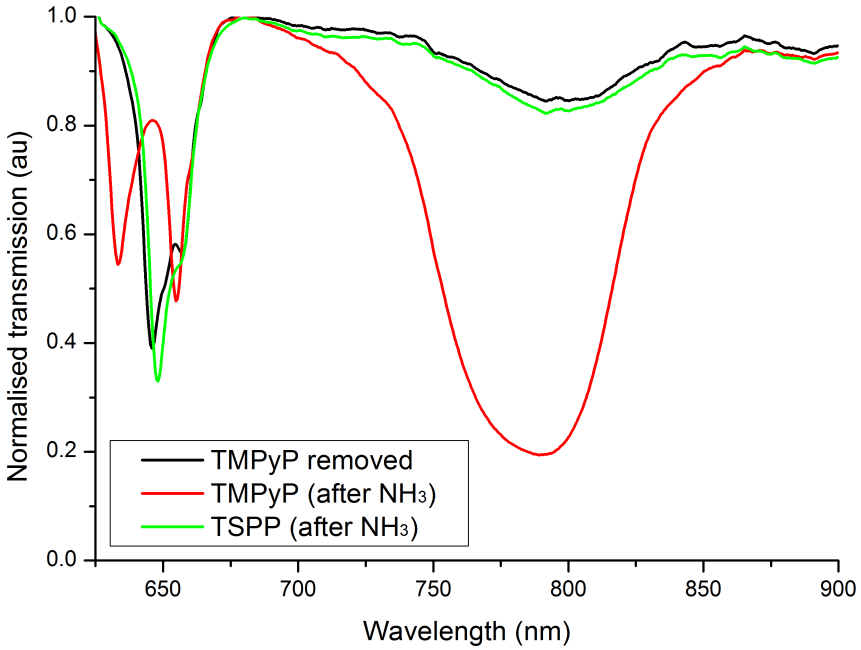

Figure 5.12: Spectrum of the 96 μm period LPG at rebinding of different porphyrins, TSPP and TMPyP (the template) (100 μM) to the TiO_2/TMPyP coating in solution. The transmission spectrum of the TiO_2/TMPyP coating without a porphyrin is also shown for comparison.

10, 15, 20-tetrayl) tetrakis (benzoic acid) [TCPP] and 5, 10, 15, 20 Tetrakis-(4-suslfophenyl)-21H, 23H, porphine manganese (III) chloride [MnTSPP]. Figure 5.13 confirms the selectivity of the coating as, just as with the porphyrin TSPP, there is little change in the response of the LPG's transmission spectrum. There is low binding efficiency for those porphyrins which were not the original template.

5.3.3 UV effects on rebinding/removing the TiO_2 template

In addition to the use of HCl, UV irradiation was also investigated as a method for template removal. As explained in section 5.3.1, the application of HCl may have been damaging the surface of the coating, reducing the rebinding capabilities. UV irradiation was used to check it's effectiveness as an alternative and viable method for the removal of the template. The effects were monitored using the same composite film but with different concentrations of the TMPyP compound (10 μM and 20 μM), to investigate the role that concentration plays on the time taken to break down the template.

A long wave UV lamp operating at 365 nm (Spectroline EN - 140L/J) was placed 5 cm above the grating. The LPG (with TiO_2/TMPyP coating) was placed in a so-

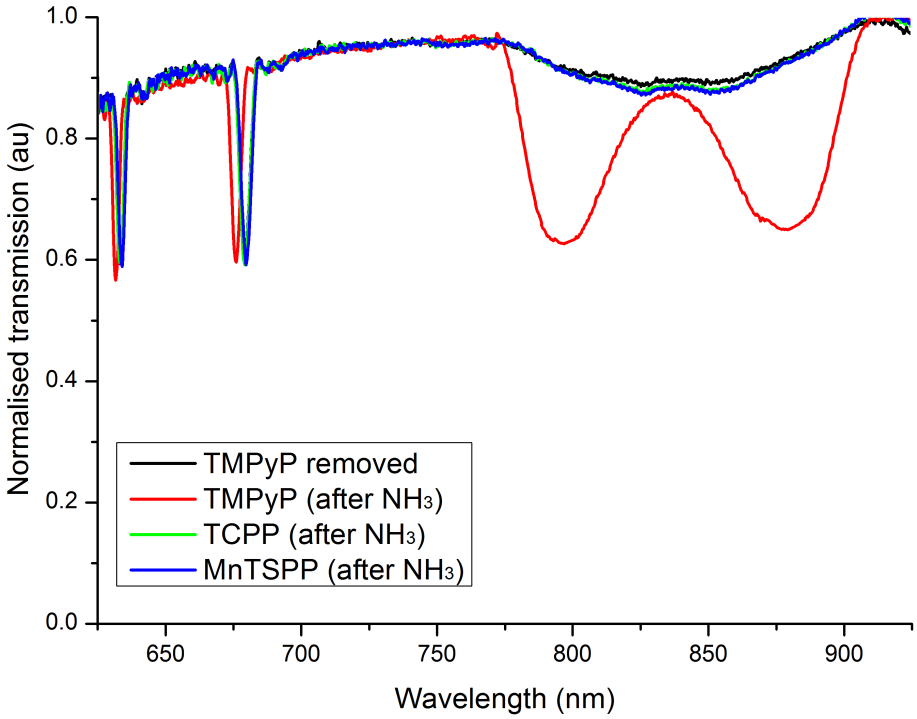

Figure 5.13: Spectrum of the the TiO_2/TMPyP coated 111 μm period LPG at rebinding of different porphyrins, TCPP, MnTSPP and TMPyP (the template) (100 μM) to the TiO_2/TMPyP coating in solution. The transmission spectrum of the TiO_2/TMPyP coating without a porphyrin is also shown for comparison.

lution of the TMPyP and the rebinding process was carried out whilst also exposing it to the UV light. Spectra were recorded every 15 minutes during an experiment with a total duration of 120 minutes.

The absorbance spectrum of TMPyP (10 μM) was monitored as it was rebound with the film, with and without the influence of UV light. The LPG was immersed in a solution of 800 μl of TMPyP for 15 minutes. The solution was then removed using a pipette, placed in a $1cm^2$ cuvette which was connected to a spectrometer (Ocean Optics USB2000) and the absorbance spectrum was recorded. The grating was then re-immersed in the same solution after the rebound template was removed from the film with HCl and the surface of the grating treated with NH_3. This time the rebinding process was carried out under UV light with the solution of TMPyP removed and absorbance curve recorded after 15, 30 and 90 minutes.

When the coated LPG (with template) was exposed to UV light, it indirectly led to

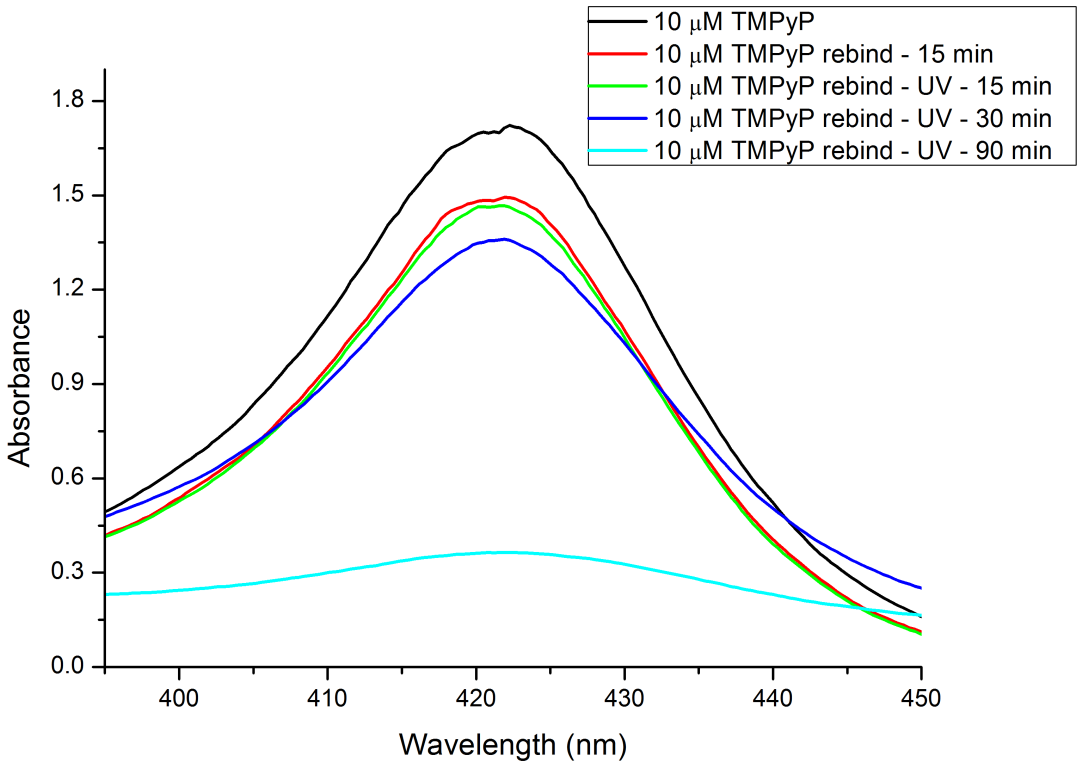

Figure 5.14: Absorbance spectrum of TMPyP (10 μm) after rebinding with TiO_2/TMPyP film with and without UV light. Measurements were taken before rebinding (black), after 15 minutes rebinding with no UV light present (red), and after 15, 30 and 90 minutes rebinding under UV light (green, blue and cyan respectively).

the decomposition of the TMPyP template and therefore removal from the film as described in section 5.1.2. The radical hydroxyls combine with the cationic TMPyP and and due its strong oxidising capabilities breaks down the template into harmless molecules such as water and carbon dioxide. To check this, the coated LPG (without template) was immersed in a solution of TMPyP solution to rebind the template with and without the influence of UV light. After a rebinding attempt, the same TMPyP solution was removed from the trough and placed in a cuvette so the absorbance spectrum could be measured. This same solution was then used to re-immerse the coated LPG for the next rebinding attempt. This process was repeated 4 times as illustrated in Figure 5.14. This figure shows the absorbance spectrum of TMPyP, showing the influence of rebinding to the TiO_2/TMPyP film under UV light. After 90 minutes, the absorbance was greatly reduced to around 0.3 at 420 nm indicating the successful breakdown of TMPyP from the film. Without the presence of TiO_2, the TMPyP is not affected by UV irradiation.

Figures 5.15 and 5.16 show how the presence of UV light affected the rebinding of different concentrations of TMPyP, 10 μm and 20 μm respectively, to the TiO_2/TMPyP film. The deepest attenuation band shows the TMPyP being rebound without the influence of UV light, as a point of reference. When UV light was placed over the fibre, it can be seen that the TMPyP had bound to the film as the band deepened in the first 15 minutes. However, after 15 minutes, this band gradually became shallower as the influence of the UV light became greater than the TMPyPs ability to bind to the film. This could indicate that, after the film became saturated and no more of the template could be rebound, the UV light began to be the dominant factor in breaking down the bonds of the template and the film. The time taken for the reaction to occur could also have been influenced by the need for an accumulation of enough electrons to the conduction band before enough ($^{\bullet}OH$) particles were released to react with the template [33].

Figure 5.17 shows the dynamic change of the TiO_2/TMPyP film measured at 788 nm. It confirmed that, after the film became saturated with TMPyP, the UV light began to remove the template from the coating. At 20 μm, there was a larger change than that observed at 10 μm as the higher concentration allowed more of the TMPyP molecules to rebind with the TiO_2/TMPyP film.

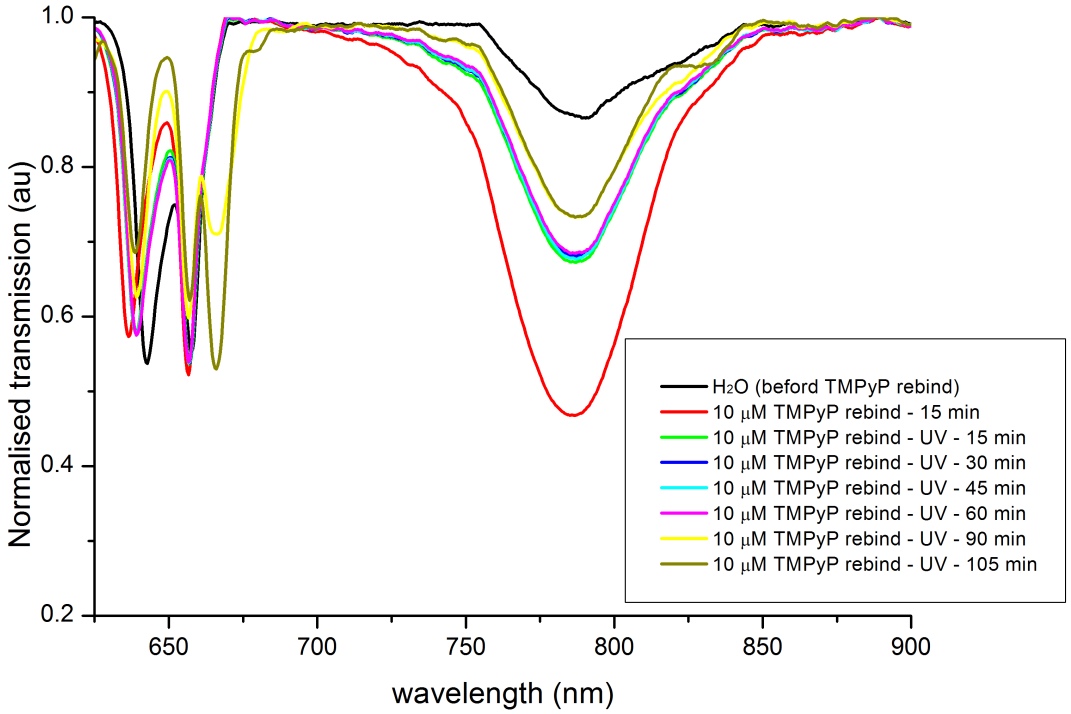

Figure 5.15: Transmission spectra of the 96 μm LPG after the rebinding of TMPyP (10 μM) to TiO_2/TMPyP film with and without UV light.

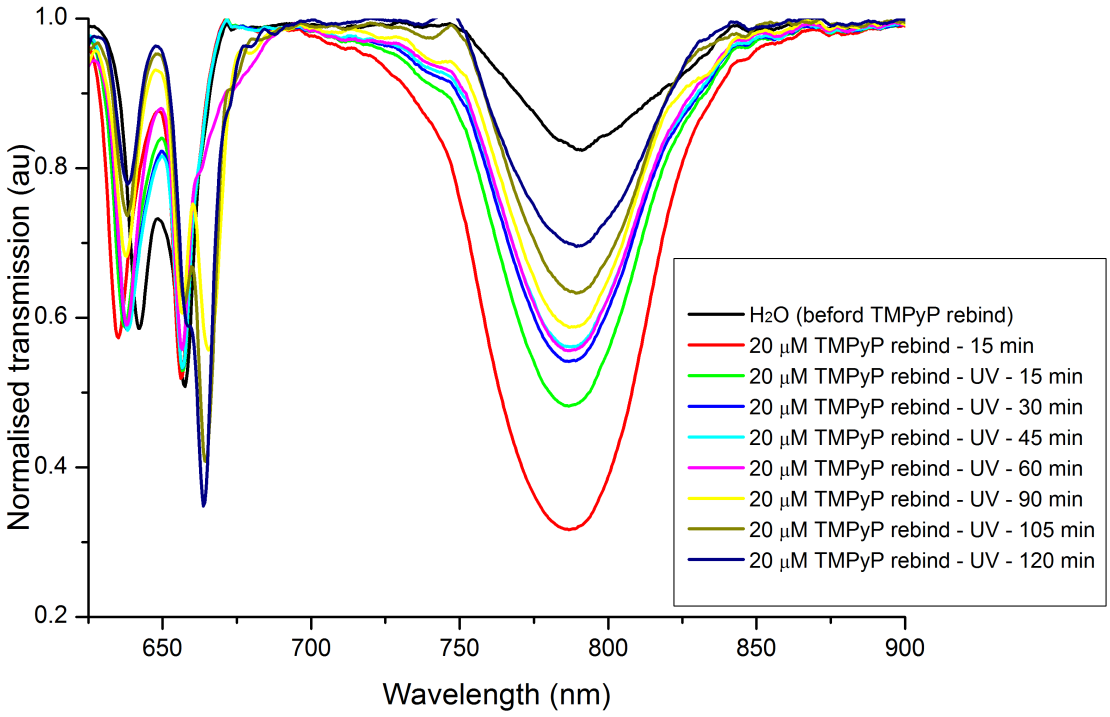

Figure 5.16: Transmission spectra of the 96 μm LPG after the rebinding of TMPyP (20 μM) to TiO_2/TMPyP film with and without UV light.

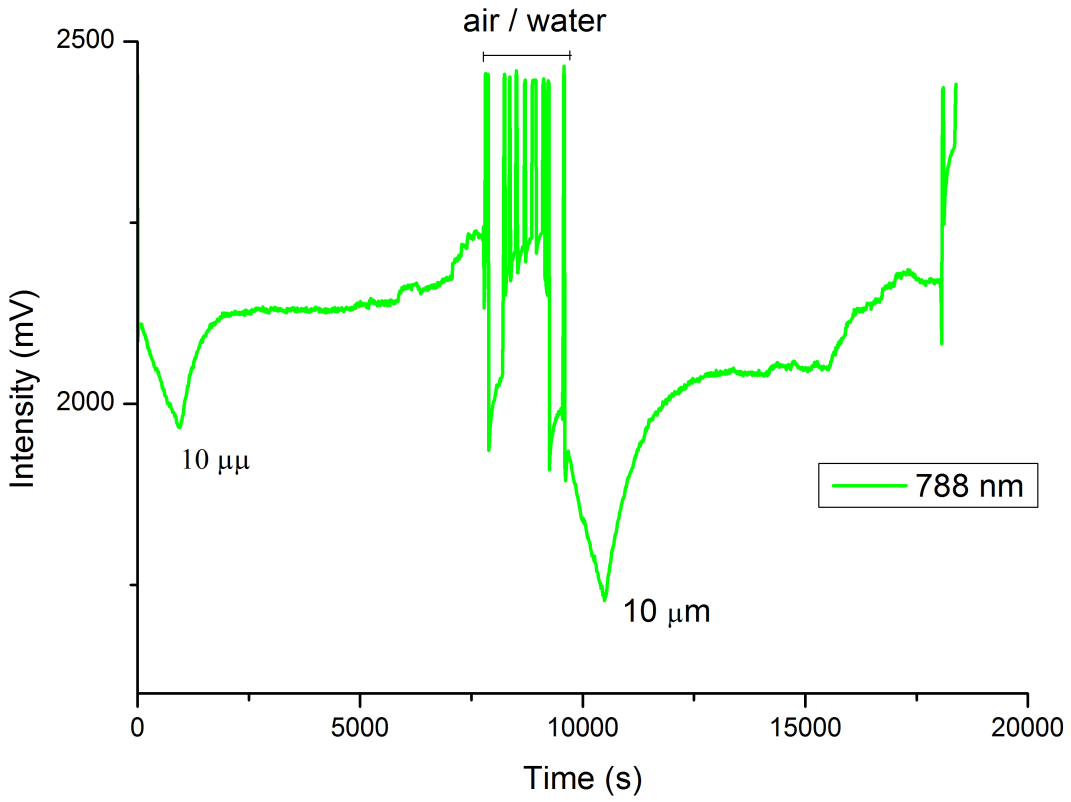

Figure 5.17: Change of the TiO_2/TMPyP film under UV light measured at 788 nm for 10 μM and 20 μM concentrations of TMPyP. The section labelled air/water was the time of interchange between the different concentrations of TMPyP.

5.4 Summary and conclusion

Liquid phase deposition was used to create a nanoscale coating on the cladding of an optical fibre containing an LPG. The coating was prepared by incorporating a TMPyP porphyrin template into a TiO_2 matrix by means of electrostatic interaction. The TiO_2 film was formed by a chemical reaction between the H_3BO_3 and $(NH_4)_2TiF_6$ in an aqueous solution. After the LPG was coated with the TiO_2/TMPyP, the template was removed. By exploiting the LPGs intrinsic sensitivity to refractive index changes of the nanoscale coating, the binding behaviours of different porphyrins were examined. It was found that the transmission spectrum of the coated LPG exhibited a higher sensitivity to the target TMPyP compound that had been used as the template than it did to other, structurally similar porphyrins, showing high selectivity. This shows potential for the development of species specific chemical sensors with the ability to distinguish between compounds with similar chemical behaviour but different molecular shape. Due to the photocatalytic properties of the TiO_2 film, ultraviolet light was successfully used as an alternative means of breaking down (instead of HCl) and therefore removing the template compound from the coating.

References

[1] C S Cheung, S M Topliss, S W James, and Tatam R P. Response of fibre optic long period gratings operating near the phase matching turning point to the deposition of nanostructured coatings. *Journal of the Optical Society of America B Optical Physics*, 25(6):897–902, 2008.

[2] I Del Villar, M Achaerandio, Matías I R, and F J Arregui. Deposition of overlays by electrostatic self-assembly in long-period fiber gratings. *Optics Letters*, 30(7):720–722, 2005.

[3] N D Rees, S W James, R P Tatam, and G J Ashwell. Optical fiber long-period gratings with langmuirblodgett thin-film overlay. *Optics Letters*, 27(9):686–688, 2002.

[4] G J Ashwell, P D Jackson, G Jeffries, Gentle I R, and C H L Kennard. Controlling the structure of transparent Langmuir-Blodgett films for nonlinear optical applications. *Journal of Materials Chemistry*, 6(2):137–141, 1996.

[5] G W Smith, M F Daniel, J W Barton, and Ratcliffe N. Pyroelectric activity in non-centrosymmetric Langmuir-Blodgett multilayer films. *Thin Solid Films*, 132(1-4):125–134, 1985.

[6] R K Iler. Multilayers of colloidal particles. *Journal of Colloid and Interface Science*, 21(6):569–594, 1966.

[7] G Decher, J D Hong, and Schmitt J. Buildup of ultrathin multilayer films by a self-assembly process: lll. consecutively alternating adsorption of anionic and cationic polyelectrolytes on charged surfaces. *Thin Solid Films*, 210-211(2):831–835, 1992.

[8] Y Zhao, F Pang, Y Dong, J Wen, S Chen, and T Wang. Refractive index sensitivity enhancement of optical fiber cladding mode by depositing nanofilm via ALD technology. *Optics Express*, 21(22):26136–26143, 2013.

[9] A Cusano, P Pilla, L Contessa, A Iadicicco, S Campopiano, A Cutolo, M Giordano, and G Guerra. High-sensitivity optical chemosensor based on coated long-period gratings for sub-ppm chemical detection in water. *Applied Physics Letters*, 87(23):234105 – 234105–3, 2005.

[10] M Tatemichi, M Sakamoto, M Mizuhata, S Deki, and T Takeuchi. Protein-templated organic/inorganic hybrid materials prepared by liquid-phase deposition. *Journal of American Chemical Society*, 129(35):10906–10910, 2007.

[11] J P Viricelle, A Pauly, L Mazet, J Brunet, M Bouvet, C Varenne, and C Pijolat. Selectivity improvement of semi-conducting gas sensors by selective filter for atmospheric pollutants detection. *Materials Science and Engineering: C*, 26(2-3):186–195, 2006.

[12] S M Topliss, S W James, F Davis, S P J Higson, and R P Tatam. Optical fibre long period grating based selective vapour sensing of volatile organic compounds. *Sensors and Actuators B: Chemical*, 143(2):629–634, 2010.

[13] S Korposh, F Davis, S W James, T Wang, Lee S-W, S Higson, and R P Tatam. Detection of volatile organic compounds (VOCs) using an optical fibre long period grating with a calixarene anchored mesoporous thin film. *Proceedings of the SPIE, 5th European Workshop on Optical Fibre Sensors*, 8794(87941I-1-87941I-4):784–792, 2013.

[14] J Saunders, M A Dreher, J A Barnes, C M Crudden, R S Brown, H-P Loock, and D-X Xu. Detection of volatile organic compounds with functionalized long-period gratings and micro-ring resonators. *Proceedings of the IEEE, ICO International Conference on Information Photonics*, pages 1–2, 2011.

[15] S Korposh, S W James, S W Lee, S Topliss, S C Cheung, W J Batty, and R P Tatam. Fiber optic long period grating sensors with a nanoassembled mesoporous film of sio_2 nanoparticles. *Optics Express*, 18(12):13227–13238, 2010.

[16] J Corres, I R Matias, I Villar, and F J Arregui. Design of ph sensors in long-period fiber gratings using polymeric nanocoatings. *IEEE sensors journal*, 7(3):463, 2007.

[17] D H Yang, N Takahara, S W Lee, and T Kunitake. Fabrication of glucose-sensitive TiO_2 ultrathin films by molecular imprinting and selective detection of monosaccharides. *Sensors and Actuators B*, 130(1):379–385, 2008.

[18] F H Dickey. The preparation of specific adsorbents. *Proceedings of the National Academy of Sciences*, 35(5):227–229, 1949.

[19] L Pauling. A theory of the structure and process of formation of antibodies. *Journal of the American Chemical Society*, 62(10):2643–2657, 1940.

[20] E L Holthoff and F V Bright. Molecularly imprinted xerogels as platforms for sensing. *Accounts of Chemical Research*, 40(9):756–767, 2007.

[21] M J Ju, D H Yang, S W Lee, T Kunitake, K Hayashi, and K Toko. Fabrication of TiO_2/γ-CD films for nitro aromatic compounds and its sensing application via cyclic surface-polarization impedence (cSPI) spectroscopy. *Sensors and Actuators B*, 123(1):359–367, 2007.

[22] S W Lee, D H Yang, and T Kunitake. Regioselective imprinting of anthracenecarboxylic acids onto TiO_2 gel ultrathin films: an approach to thin film sensor. *Sensors and Actuators B*, 104(1):35–42, 2005.

[23] T Kunitake and S W Lee. Molecular imprinting in ultrathin titania gel films via surface sol-gel process. *Analytica Chimica Acta*, 504(1):1–6, 2004.

[24] M Komiyama, T Takeuchi, T Mukawa, and H Asanuma. *Molecular Imprinting*. WILEY-VCH, 2003.

[25] S W Lee, I Ichinose, and T Kunitake. Molecular imprinting of azobenzene carboxylic acid on a TiO_2 ultrathin film by the surface sol-gel process. *Langmuir*, 14(10):2857–2863, 1998.

[26] G M Murray, A L Jenkins, A Bzhelyansky, and O M Uy. Molecularly imprinted polymers for selective sequestering and sensing of ions. *John Hopkins APL Technical Digest*, 18(4):464–472, 1997.

[27] N Mizutani, Yang D H, R Selyanchyn, S Korposh, S W Lee, and T Kunitake. Remarkable enantioselectivity of molecularly imprinted tio_2 nano-thin films. *Analytica Chimica Acta*, 694(1-2):142–150, 2011.

[28] M Hashizume and T Kunitake. Preparationg of self-supporting ultrathin films of titania by spin coating. *Langmuir*, 19(24):10173–10178, 2003.

[29] T P Niesen and M R Guire. Review: deposition of ceramic thin films at low temperatures from aqueous solutions. *Journal of Electroceramics*, 6(3):169–207, 2001.

[30] A Mujahid, P A Lieberzeit, and F L Dickert. Chemical sensors based on molecularly imprinted sol-gel materials. *Materials*, 3(4):2196–2217, 2010.

[31] G Williams, B Seger, and P V Kamat. TiO_2-graphene nanocomposites. UV-assisted photocatalytic reduction of graphene oxide. *ACS Nano*, 2(7):1487–1491, 2008.

[32] S D Richardson, A D Jr Thruston, T W Collette, K S Patterson, B W Jr Lykins, and J C Ireland. Identification of TiO_2/UV disinfection byproducts in drinking water. *Environmentla Science & Technology*, 30(11):1137–1139, 1996.

[33] R Thiruvenkatachari, S Vigneswaran, and I S Moon. A review on UV/TiO_2 photocatalytic oxidation process. *Korean Journal of Chemical Engineering*, 25(1):64–72, 2008.

[34] M F M James and R J Hift. Porphyrias. *British Journal of Anaesthesia*, 85(1):143–153, 2000.

[35] Y Masuda and K Koumoto. Advances in nanointegration methodologies: patterning, positioning, and self assembly. In R Asthana M Singh, T Ohji and S Mathur, editors, *Ceramic Integration and Joining Technologies. From Macro to Nanoscale*, pages 523–574. 2011.

Chapter 6

A chirped long period grating sensor for monitoring flow direction and cure of a resin

6.1 Introduction

6.2 Resin Infusion and Flow

Composite materials are being increasingly used as structural materials for applications such as aerospace, automotive and marine, as they are lightweight, yet very strong when compared to traditional materials, such as aluminium, often used for the same purpose [1]. Straightforward and cost effective ways of monitoring the development process (resin infusion and cure monitoring) and damage assessment are being explored, particularly for in-situ and real time measurements. An attractive avenue is offered by a variety of optical fibre sensors [1, 2, 3, 4]. Optical fibre sensors offer advantages over conventional sensors used in composite material processing. These advantages include (but are not limited to): their small dimensions (diameter is typically 40 μm - 125 μm), their immunity to electro-magnetic interference and their multiplexing capabilities (many sensors can be located at different spatial locations along a single length of fibre), high signal-to-noise ratio as the signal is wavelength encoded and they can be used in harsh or volatile environments. They can also be monitored in real time and in-situ.

The fibre optic sensors can be embedded into the composite material, and due to their small dimensions they are less likely to compromise the integrity of the structure and studies have shown that the durability of the material can remain

unaffected [1]. This is highly dependent on the orientation of the optical fibre with respect to the fibres of the composite material. The monitoring of infusion, i.e. the presence of resin and the degree of cure of resin, is currently carried out empirically as commercially available sensors (for example, dielectric sensors) are not conducive for embedding into composites during the manufacturing process. These sensors can be used to monitor the manufacturing stages, such as when resin is being infused into the preform as a means of bonding together components. The low permeability material of the preform is resistant to resin flow which can lead to inconsistencies as the resin is not uniformly spread throughout the material [3]. When this occurs, the structural integrity becomes affected as resin voids become defect sites. In many cases it is not possible to physically see the flow, due to for example most materials being non-transparent/translucent or have a complex shape, so alternative methods have to be used to monitor the process.

The use of optical fibre sensing technologies aimed at addressing this monitoring problem has been investigate, exploiting devices such as standard LPGs and tilted fibre Bragg gratings (TFBGs) embedded within the material to act as refractometers [2, 5]. As light is coupled from the core mode of the LPG to the cladding mode, these devices are sensitive to changes in surrounding refractive index. As the resin flows over the grating, the change of refractive index causes a concomitant change in the transmission spectrum [2]. Etched fibre sensors, where the cladding of the fibre has been partially or completely removed so the evanescent wave of the core can interact with the surrounding medium, have also been used for measuring resin flow [1, 3, 6]. By multiplexing gratings such as FBGs onto the same section of fibre, it is possible to differentiate between several different parameters which provides an indication of the degree of cure of a resin. These parameters include strain, temperature [4] and refractive index. Reflections of light propagating in the fibre core from a cleaved fibre end have also been used to monitor resin infusion and degree of cure via the changes in refractive index of the resin. This is known as a Fresnel refractometer [7].The optical fibre sensors previously used for monitoring resin infusion are able to spatially detect when resin has reached the fibre. However, they have not been able to easily determine the direction of flow. The concept of a directional flow sensor was introduced by Buggy et al. [7] where they immersed a chirped long period grating in a refractive index oil causing a change in the shape of attenuation band of the LPG's transmission spectrum. The shape of the band was dependent on whether the shorter periods or longer periods of the LPG were covered.

The following experiment describes the use of a continuously chirped LPG to test its capability to determine the direction of flow of refractive index oils and of a UV-cured epoxy resin as well as the ability to monitor the cure of said resin.

6.3 Experiment

A continuously chirped long period grating (CCLPG) with an effective length of 35 mm and periodicity ranging linearly over its length from 400 μm to 420 μm was fabricated in a single mode fibre with a cut off wavelength of 627 nm (Fibercore PS750) using the point-by-point method described in chapter 3. This chirp rate was chosen so that the attenuation bands in the transmission spectrum would be broadened but not spectrally overlap with each other. The length of the LPG was chosen as it provided a transmission spectrum with reasonably high enough attenuation for this experiment yet allowed the LPG to be handled easily for instance when manoeuvring it during different aspects of the experiments. The LPG was monitored by coupling light from a tungsten-halogen light source to a high resolution CCD spectrometer (Ocean Optics HR4000).

Figure 6.1 shows a 400 μm - 420 μm period CCLPG transmission spectrum along with individual 400 μm and 420 μm uniform period LPGs. The attenuation bands of the CCLPG appear positioned in between the bands of the two uniform period LPGs. The extreme wavelength bounds of the CCLPG bands are coincident with the wavelengths of the attenuation bands of two uniform period LPGs, as expected. The comparison can be seen where the individual attenuation bands have a relatively narrow bandwidth with a uniform period LPG, whereas the bands of the CCLPG have a much larger bandwidth and decrease in attenuation. This is because the wavelengths that are coupled to vary as a function of the position along the CCLPG. Figure 6.2 shows a simplified representation of the spectrum of a chirped LPG. A chirped LPG can be said to be a composition of multiple uniform period LPGs spaced closely together.

Oil and resin flow

Cargille refractive index oils with indices of 1.4166 $\pm$ 0.0012 and 1.5302 $\pm$ 0.0012 (calculated using the Cauchy equations for a wavelength of 950 nm, the centre of the LP_{07} attenuation band [8]) were used to determine the response of the grating to refractive indices lower (former) and greater (latter) than that of the cladding of the optical fibre. The refractive index of 1.4166 is also close to the refractive

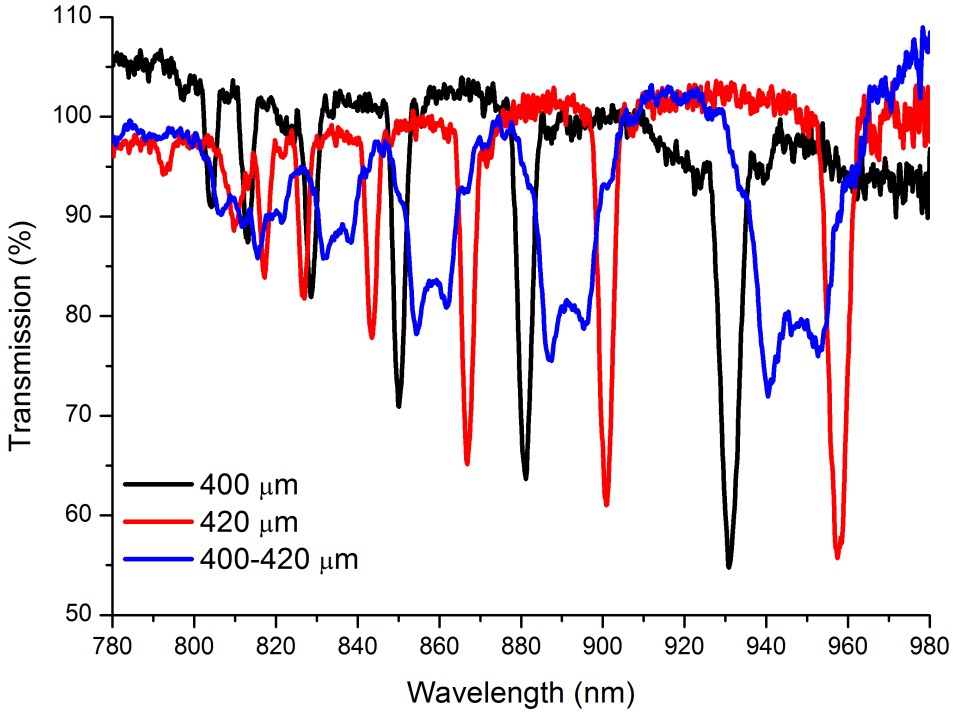

Figure 6.1: Transmission spectra of uniform period LPGs with a period of 400 μm and 420 μm (black and red lines, respectively) and a CCLPG with a period of 400 μm - 420 μm (blue line). All had a length of 35 mm and were written on Fibrecore PS750 fibre with a cutoff wavelength of 627 nm.

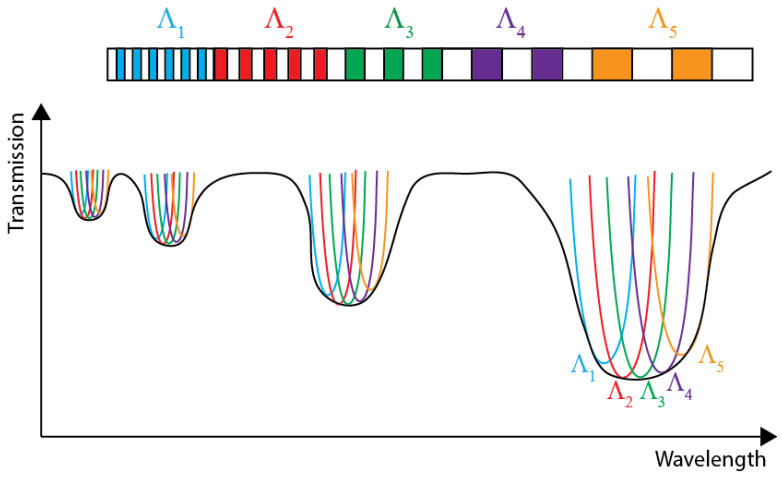

Figure 6.2: Simplified representation of the transmission spectrum of a chirped LPG (step chirped). The black line represents the bands of the chirped LPG that are comprised of individual uniform period LPGs (coloured lines). Λ_i represents the periods of the individual constituent LPGs.

index of the UV cured epoxy resin used in this experiment and 1.5302 is similar to the typical refractive indices of resins often used in composite material fabrication employed by the aerospace industry.

The CCLPG was secured along the inside a long, thin plastic channel. This was then positioned at an incline of $1.2 \pm 0.1\ ^{o}$, relative to the table surface, to allow the oil to flow slowly over the grating in one direction. 200 μl of oil was pipetted into the channel at the highest point (see figure 6.3). The incline of the channel was then reversed so the oil would flow in the opposite direction relative to the chirp of the grating. The directional flow experiments were repeated using a UV cured epoxy resin which had an uncured refractive index of 1.4230, specified at 589 nm (Epotek OG-134) [9]. For the resin directional flow experiments a step chirped long period grating (SCLPG) with the same parameters was also fabricated and used. However, instead of a continuous linear chirp, the discrete step change in each period from one group of periods to another was 2 μm. A 2 μm step chirp was chosen to ensure the change in periods would allow the grating to be different from a CCLPG yet be small enough such that there were still broadened attenuation bands. If the step chirp is too large, the corresponding attenuation bands produced from the different periods will not overlap and there will be no broadened attenuation bands. The SCLPG was added to the same channel to compare the response of both gratings.

Epoxy resin curing

The CCLPG and SCLPG were also used to monitor the resin as it went through the curing process. The resin was held in a small Teflon cell and the CCLPG and SCLPG were placed within the liquid resin. The ends were glued in order to keep the LPGs taut within the resin. To measure the change in refractive index during cure and determine any correlation between the sensors, optical fibre Fresnel based refractometers were also placed inside the resin to provide independent measurements. The Fresnel refractometer provided localised measurements that could be calibrated easily. The Fresnel refractometer worked by taking the ratio of reflected light from the cleaved end of an optical fibre immersed in the resin, referenced to the reflection from a cleaved fibre end in air as shown in figure 6.4.

Figure 6.5 shows the wavelength response relating to changing surrounding refractive index of the attenuation band corresponding to the LP_{07} mode of a 400μm period LPG. A 7^{th} order polynomial was used to fit a curve and generate a transfer function relating the wavelength shift to the surrounding refractive index. The

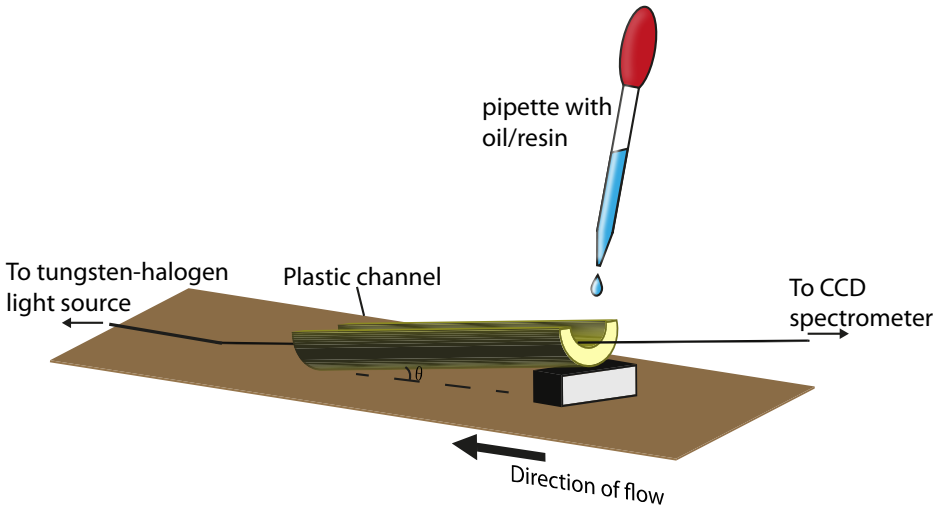

Figure 6.3: Experimental configuration for the directional flow experiment. The plastic channel was inclined at an angle θ, and the oil or resin was added at the highest point of the channel and slowly flowed over the chirped LPG. The transmission spectrum was monitored by coupling the light from a broadband light source to a CCD spectrometer.

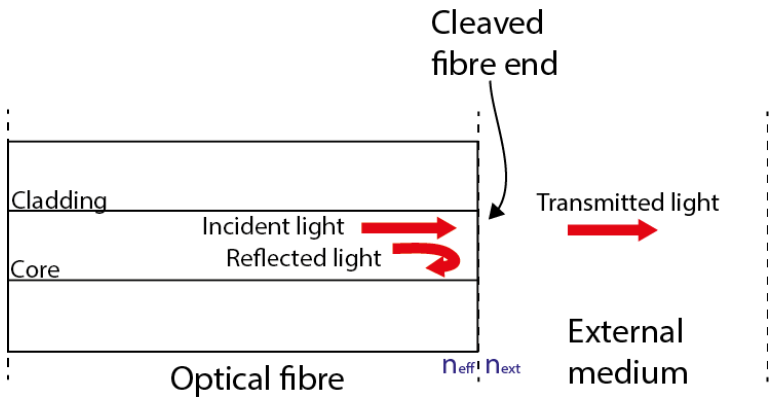

Figure 6.4: Illustration showing the principle of a Fresnel refractometer. Light reflected from the sensor tip is referenced against light reflected from a reference tip in air.

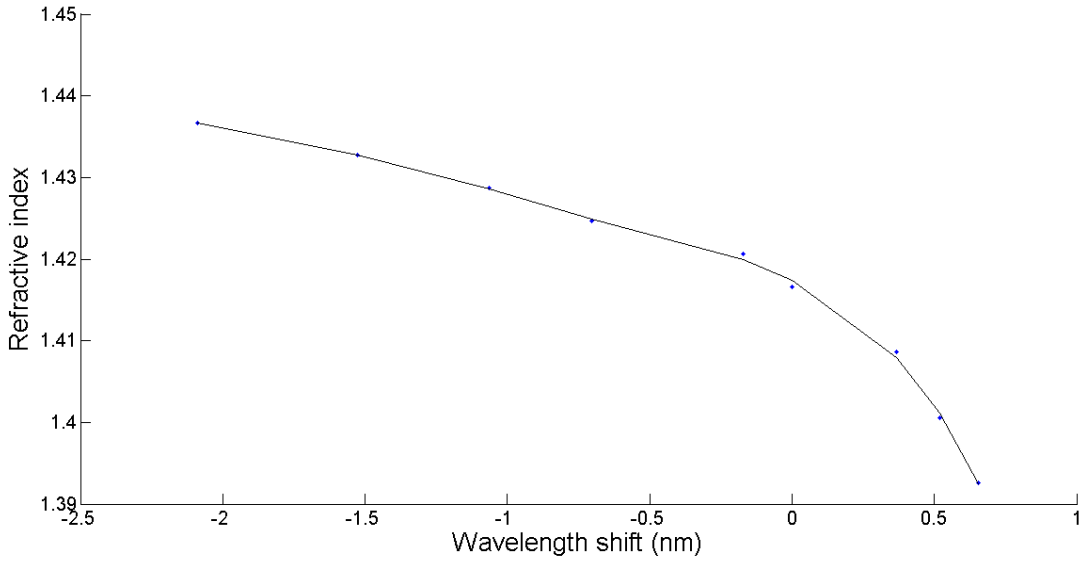

Figure 6.5: LP_{07} mode of an LPG response to surrounding refractive index. The data points were best fitted with a 7^{th} order polynomial to generate a function relating the wavelength shift to the surrounding refractive index.

transfer function is used later to transform the wavelength shifts measured during resin cure into refractive index.

Figure 6.6 shows the experimental set up for monitoring the curing of the UV-cured resin. A superluminescent diode (SLD) (Covega 1005) with a bandwidth of 100 nm centred at 1550 nm, and a output power of 15 mW was intensity modulated at a frequency of 1 kHz and the output was coupled into a network of 3dB directional couplers. By using an SLD, the short coherence length avoids unwanted interference noise due to a shorter path length. The modulation frequency was chosen as it was sufficiently high to overcome unwanted signals that may arise from the fibre system, for example, reflections or scattering at connections. One arm of the coupler directed the laser output through to measure the reflection from the resin/fibre interface, where the reflected signal was monitored by a photodiode detector, pd1. The other output was used to provide a reference by measuring the reflections at the air/fibre interface. This signal was monitored using the photodiode detector, pd2. The outputs of the photo detectors (New Focus, Model 2011) were monitored using electronic card lock-in amplifiers (National Instruments NI PXI-4462). A uniform period LPG of period 400 μm was also placed in the resin for comparison purposes with the CCLPG and SCLPG. This LPG was monitored by viewing the transmission spectrum on an Ocean Optics CCD spectrometer (S2000). A UV lamp which was

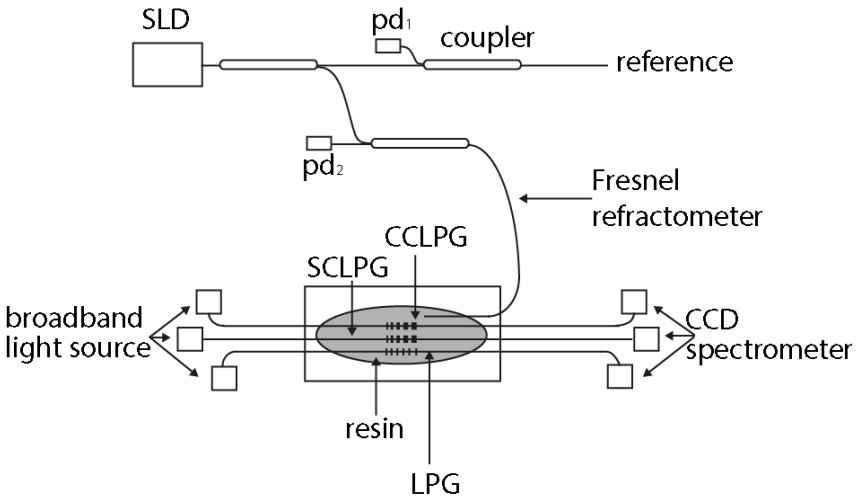

Figure 6.6: Experimental configuration for monitoring the cure of a resin. A CCLPG, SCLPG, LPG and Fresnel refractometer were used to monitor the cure of the resin. The CCLPG, SCLPG and LPG were observed by coupling light from a broadband light source to a CCD spectrometer. The refractometer readings were monitored using a modulated superluminescent diode (SLD) and a series of couplers and photodiode detectors, pd_1 and pd_2

operated at the wavelength of 365 nm (Superlite-UV Lumatec) was placed above the resin and the resin was left to cure for 65 minutes. Measurements were recorded every 30 seconds during the cure process. The temperature was measured using a thermocouple placed in the resin, close to the gratings, with readings taken every 30 seconds.

6.4 Results and Discussion

6.4.1 Oil and resin flow

The following figures, figure 6.7 to fig:flowresincclpg shows the evolution of the attenuation band corresponding to the LP_{07} cladding mode of the continuously chirped long period grating. The change in the shape of the band was evident when oil with a refractive index of 1.5302 (higher than that of the cladding) flowed over the CCLPG in the direction of firstly increasing and secondly decreasing chirp period. Figure 6.7 (a) shows the flow of oil in the direction of increasing chirp period (400 μm - 420 μm). The 0% line shows the attenuation band in its original state, where no oil was present. The 50% line shows the change in the shape of the band after oil had flowed over 50% of the grating length. The lower wavelength region

of the spectral attenuation band diminished, as the high index oil covered grating periods corresponding to this particular section of the grating, causing a decrease in the coupling efficiency.

The oil was also flowed over the CCLPG in the decreasing chirp period direction (420 μm - 400 μm). Figure 6.7 (b) shows the attenuation band coupling to the LP_{07} cladding mode at 0%, 50% and 100% coverage of the grating length. At 50% coverage , the profile of the band changed such that at higher wavelengths it became reduced as the efficiency of the coupled modes decreased. At 100%, the propagating cladding modes were no longer supported by the cladding and oil interface. Instead, the resonance corresponded to leaky mode coupling from Fresnel reflections at the interface of the cladding and the oil [10, 11]. The wavelength of the attenuation band does not change, however there is a reduction in the minimum transmission of the band which corresponds to refractive indices greater that the refractive index of the fibre cladding.

Figure 6.8 shows how the CCLPG is affected when oil with a refractive index of 1.4166 (lower than cladding) was flowed in the increasing and decreasing chirp period directions. When the refractive index of the external surroundings is lower than that of the fibre cladding, total internal reflection (TIR) is the dominant effect responsible for guiding the coupled cladding mode. With the flow in the direction of increasing chirp period, the lower wavelengths of the attenuation band became less prominent. When the grating length had been 100% covered, the attenuation band returned to its original profile/shape with a shift to a lower wavelength corresponding to the change in the refractive index from the oil (index is lower than that of the cladding). For flow in the decreasing chirp period direction, the opposite effect was evident. The shape changes of the band started after a greater grating length coverage than for the first flow direction (2% for increasing period direction and 6% for decreasing period direction) due to the nature of the structure of a CCLPG, that there is a greater number of periods nearer the 400 μm side of the grating than the 420 μm side.

The effect of the resin of refractive index 1.423 on the LP_{07} cladding mode of the grating showed a trend consistent with that of the oil of refractive index 1.4166. As the resin was flowed over the grating in opposing directions, the shape profile of the attenuation band changed dependent on the direction of the flow (see figure 6.9).

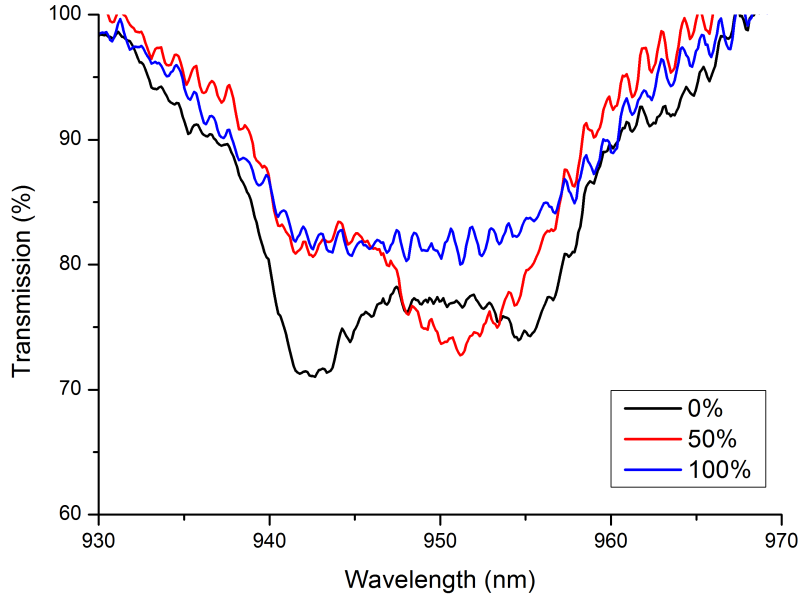

(a)

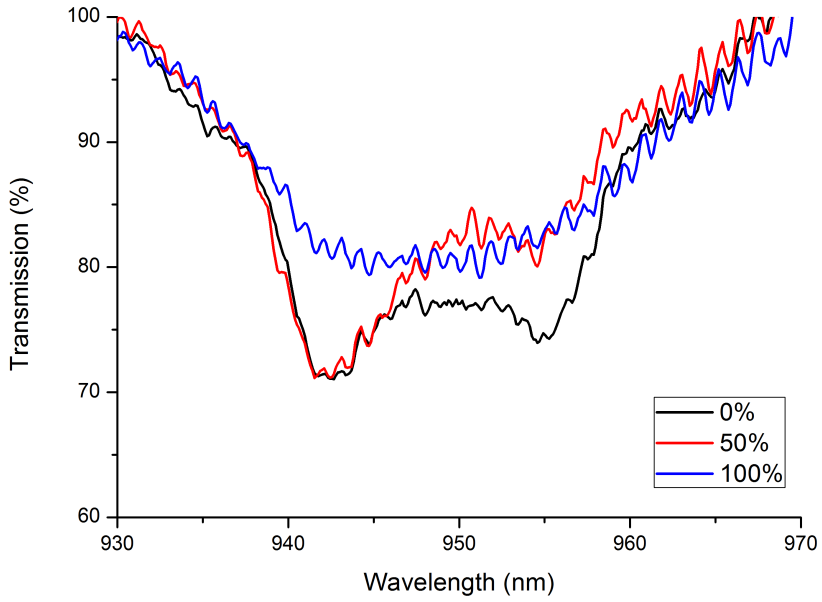

(b)

Figure 6.7: The change in the profile of the attenuation band at the LP_{07} mode of the CCLPG as the oil with RI 1.5302 was flowed in the (a) 400 μm - 420 μm period direction and (b) 400 μm - 420 μm period direction. 0% is when no part of the grating has been covered. 50% is where half of the grating length has been covered and 100% is where the entire grating is covered.

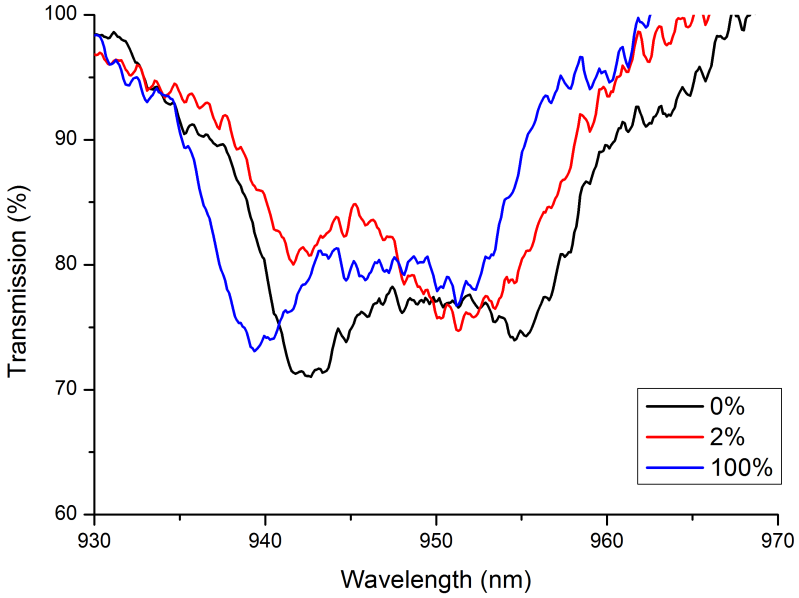

(a)

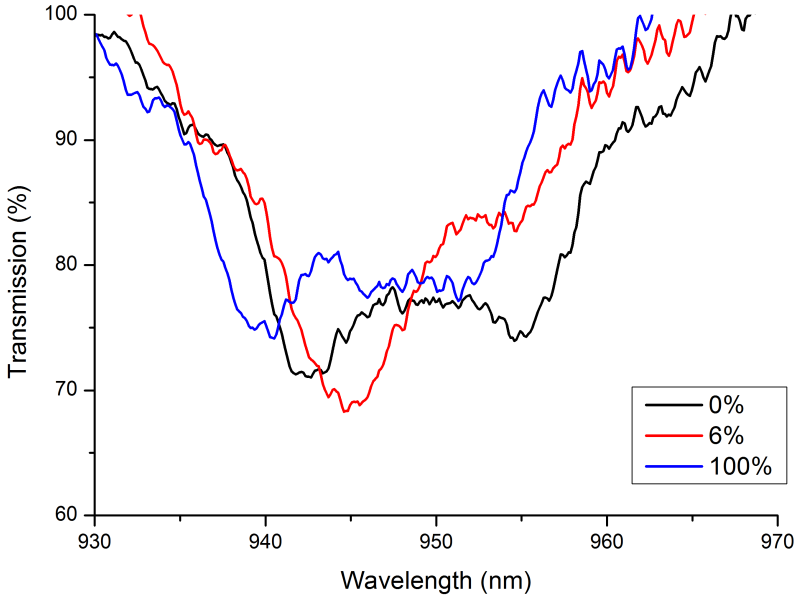

(b)

Figure 6.8: The change in the profile of the attenuation band at the LP_{07} mode of the CCLPG as the oil with RI 1.4166 was flowed in the (a) 400 μm - 420 μm period direction and (b) 420 μm - 400 μm period direction. (a) 2% and (b) 6% are the lengths of grating covered where the band profile shape changes due to flow direction and 100% is where the entire grating is covered.

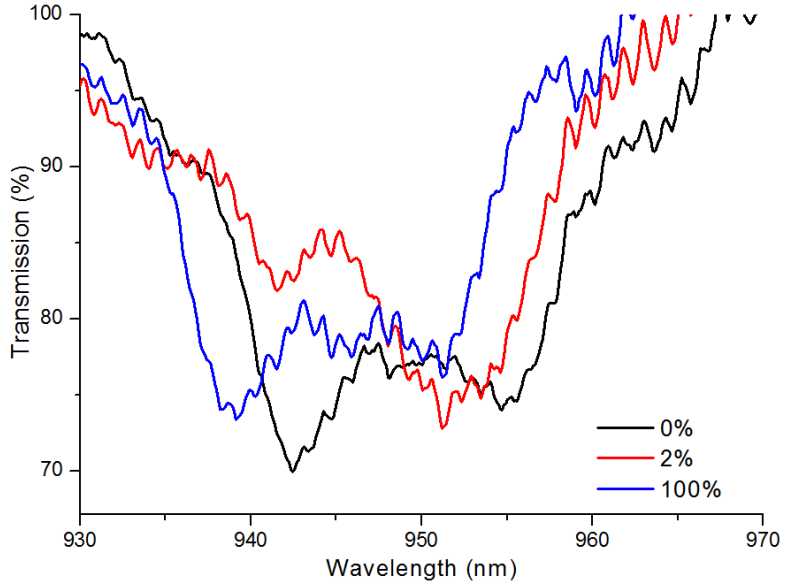

(a)

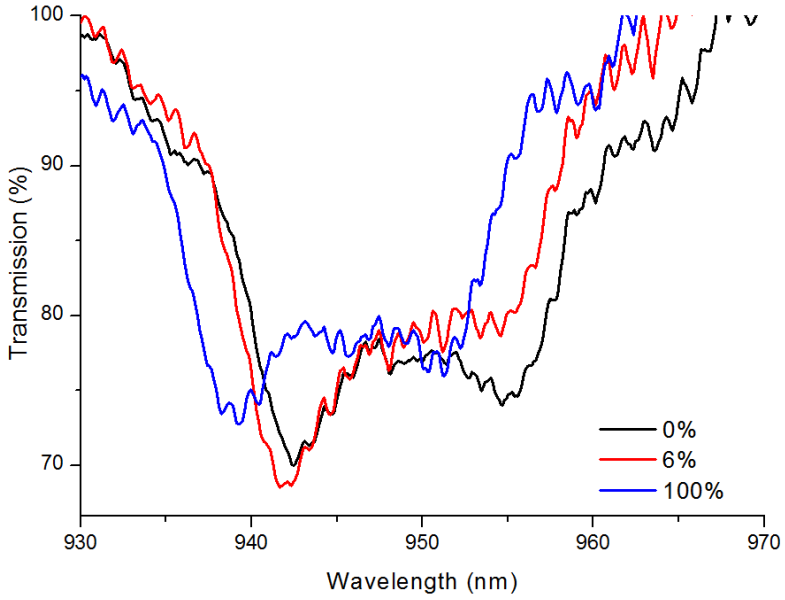

(b)

Figure 6.9: The change in the profile of the attenuation band at the LP_{07} mode of the CCLPG as the resin was flowed in the (a) 400 μm - 420 μm period direction and (b) 420 μm - 400 μm period direction. (a) 2% and (b) 6% are the lengths of grating covered where the band profile/shape changes due to flow direction and 100% is where the entire grating is covered.

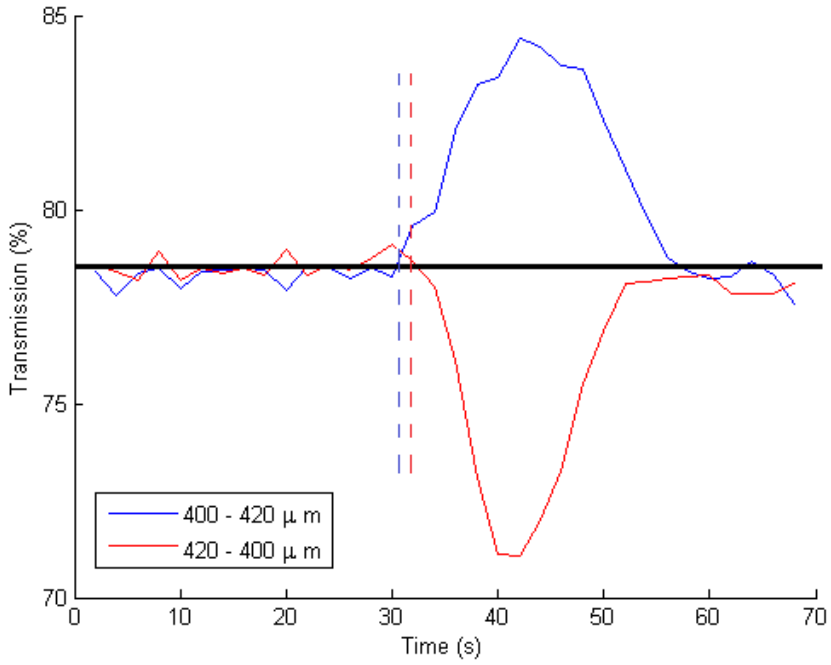

Figure 6.10: Evolution of the CCLPG transmission spectrum over time as resin it flowed over the length of the grating in the increasing and decreasing chirp period directions. The blue line represents resin flow in the 400 μm - 420 μm period direction and the red line represents flow in the 420 μm - 400 μm period direction. The horizontal and vertical lines act to give a rough guide to indicate the change in the shape of the attenuation band with flow.

To compare the capabilities of the SCLPG and CCLPG, they were both held in the same channel at the same time and the resin was flowed through the channel. The two LPGs were able to detect the arrival of the resin under near identical conditions. Figures 6.10 and 6.11 show the transmission of the LP_{07} mode of the CCLPG and SCLPG over time, as resin flowed across the length of the grating. As can be seen, depending on the direction of the resin (increasing or decreasing chirp period direction), the two curves displace in opposing directions. The figures also confirm that in the increasing chirp period direction, the attenuation band reacts quicker to the introduction of resin than in the decreasing chirp period direction (though this is less obvious for the CCLPG). In the direction of decreasing period, the resin has to cover a larger distance before enough periods of similar length can impact a change in the transmission spectrum. In the case of flow from the smaller period direction, an appreciable number of periods are covered in a shorter spatial distance and a change in the spectrum will be see earlier. This also explains the time lapse between the onset of resin flow and change in spatial profile experienced in the 420 μm - 400 μm period direction, as the resin has to cover a relatively larger grating distance. In the opposite direction, the detection is relatively instantaneous; the resin front reaches the grating after 30 $\pm$ 1 s, and a change is detected almost instantly.

The detection provided (transmission spectrum profile change) by the SCLPG follows the same trend as that of the CCLPG but as it lacks the intermediate periods provided by the CCLPG, which can be said to be equivalent to a loss of resolution. In the direction of the decreasing period direction, a longer time is taken before a spectral change is seen. The actual spectral change is over a shorter period of time due to the reduced number of different sized periods. Though the resin completely covers the two gratings after 23 $\pm$ 1 s, only the spectral profile of the CCLPG changes for the entire duration with the time reduced for the SCLPG.

6.4.2 Resin cure

Figure 6.12 shows the change in temperature during the cure process. The thermocouple showed that there was a 2 ^{o}C decrease in temperature of the resin after an initial rise of about 0.5 ^{o}C. This rise in temperature can be attributed to the exothermic reaction that occurred shortly after the UV lamp was turned on.

Figures 6.13, 6.14 and 6.15 shows the wavelength shift of the attenuation band corre-

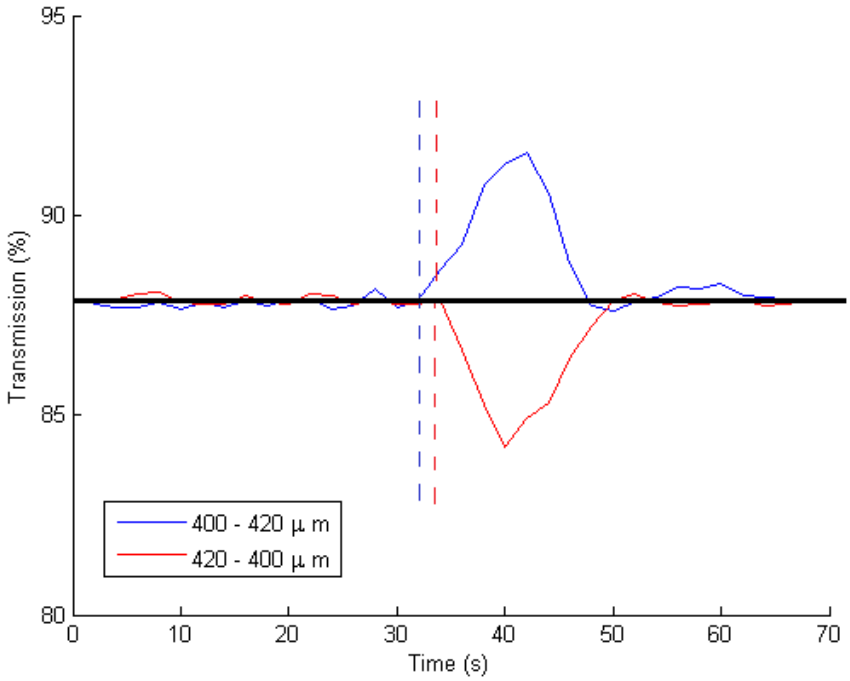

Figure 6.11: Evolution of the SCLPG transmission spectrum over time as resin it flowed over the length of the grating in the increasing and decreasing chirp period directions. The blue line represents resin flow in the 400 μm - 420 μm period direction and the red line represents flow in the 420 μm - 400 μm period direction. The horizontal and vertical lines act to give a rough guide to indicate the change in the shape of the attenuation band with flow.

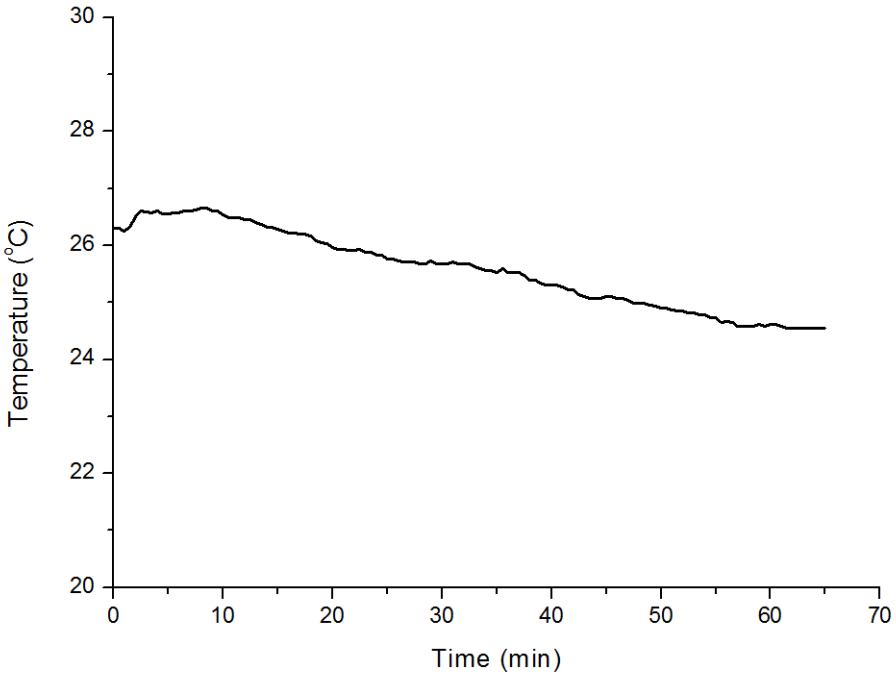

Figure 6.12: Temperature of the epoxy resin as measured by a thermocouple during the cure process.

sponding to the LP_{07} mode of the CCLPG, SCLPG and uniform period LPG as the resin was being cured. The final shifts in wavelength corresponding to the change in refractive index for the CCLPG and SCLPG were comparable at -1.1 ± 0.1 nm and -1.1 ± 0.1 nm respectively. The band of the uniform period LPG shifted by -0.6 ± 0.1 nm. This shift may be due to the LPG being spatially displaced from the other two gratings and it did not get exposed to the same UV flux level. This was confirmed by a second Fresnel refractometer placed at a similar spatial position. It also showed a diminished response as the degree of cure was less.

The measured wavelength shifts are converted to changes in refractive index with the aid of the calibration curve of figure 6.5. The responses of the fibre gratings to the changes in the refractive index were compared with the refractive indices measured by the Fresnel refractometer in the same experiment. There was a good linear correlation of 96% between the wavelength shifts of the CCLPG and the change in refractive index measured with the Fresnel refractometer. The linear correlation obtained for the SCLPG and LPG were 91% and 97%, respectively. The LPG had a slightly higher correlation due to the narrower bandwidth of the attenuation bands which could give a higher resolution. The difference in refractive indices for the long period gratings and the Fresnel refractometer are due to the measurements being

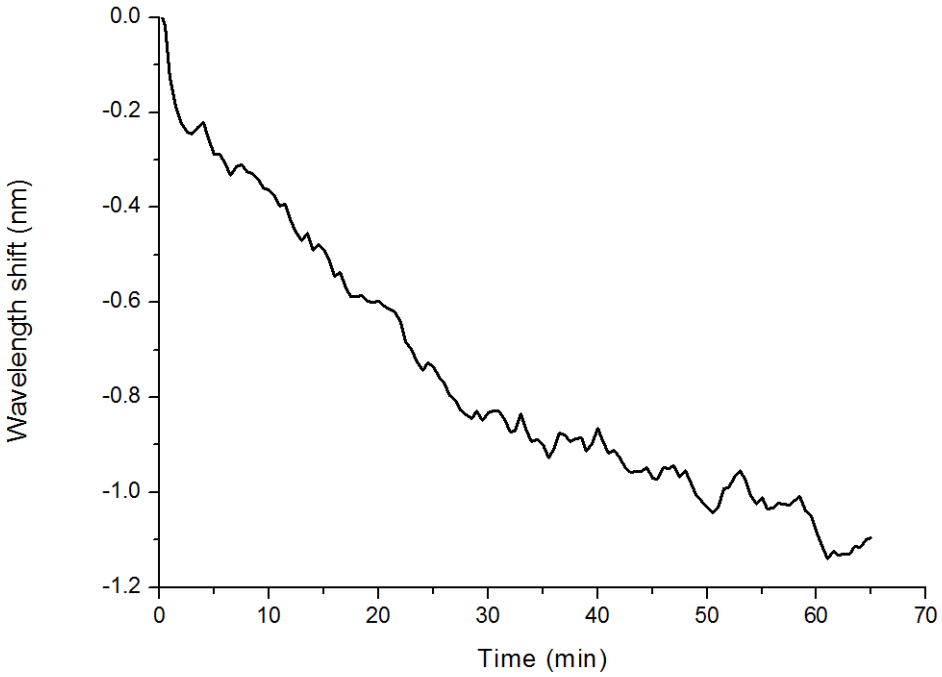

Figure 6.13: Wavelength shift of the LP_{07} mode of the continuously chirped long period grating with ranging from period 400 μm - 420 μm, measured during the curing of the epoxy resin over 65 minutes.

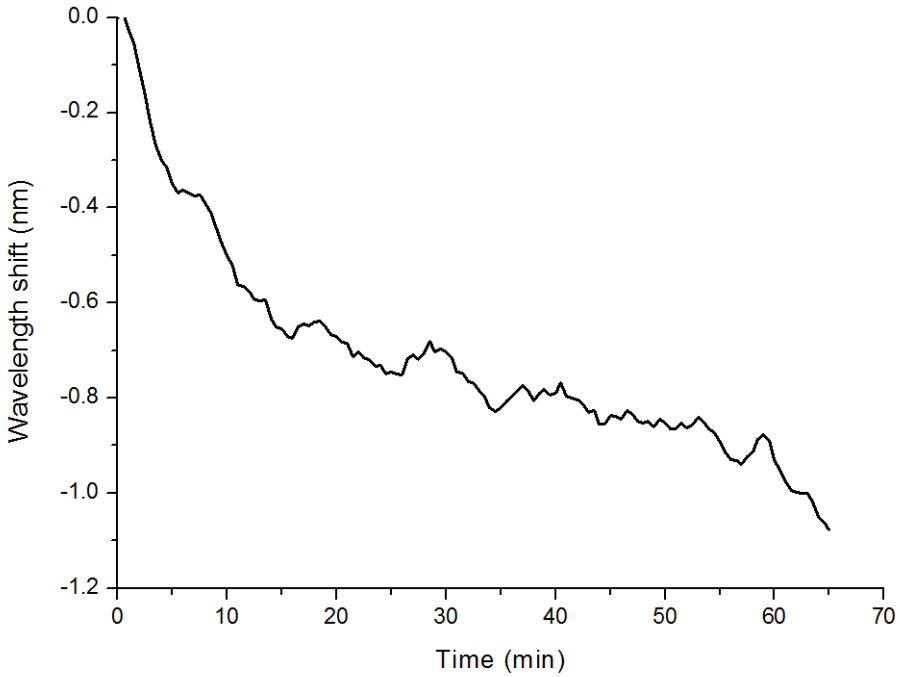

Figure 6.14: Wavelength shift of the LP_{07} mode of the step chirped long period grating with a period 400 μm - 420 μm during epoxy resin cure over 65 minutes.

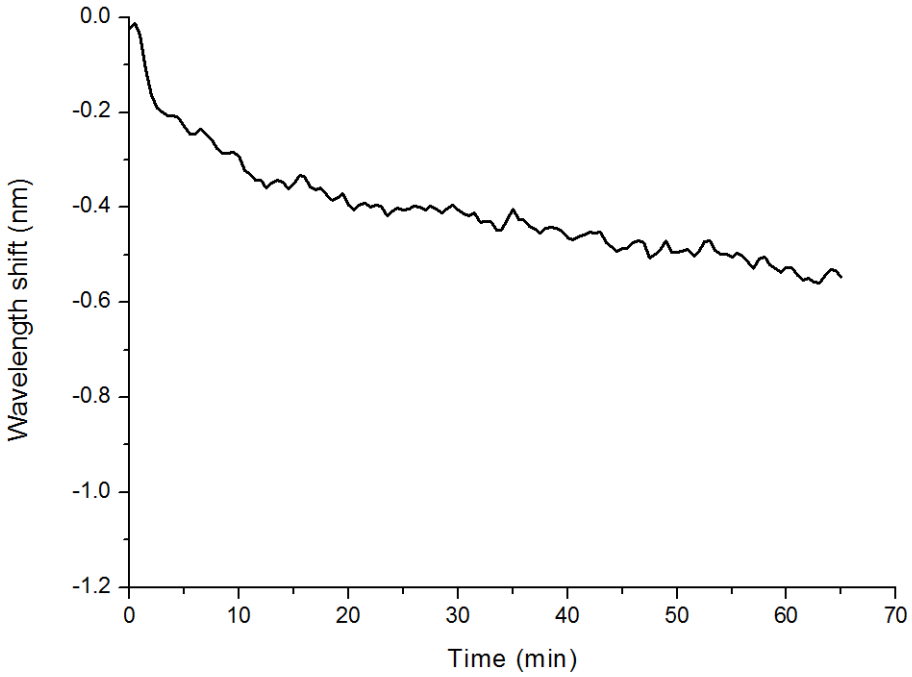

Figure 6.15: Wavelength shift of the LP_{07} mode of the long period grating with period ranging from 400 μm during epoxy resin cure over 65 minutes.

taken at different wavelengths. The wavelengths of the bands of the gratings were around the 950 nm region whereas (as mentioned in section 6.3 Epoxy resin curing) the source for the refractometer had a wavelength of 1550 nm. These measurements indicate that sensitivity was not compromised when using the CCLPG and SCLPG to monitor the cure process of a resin.

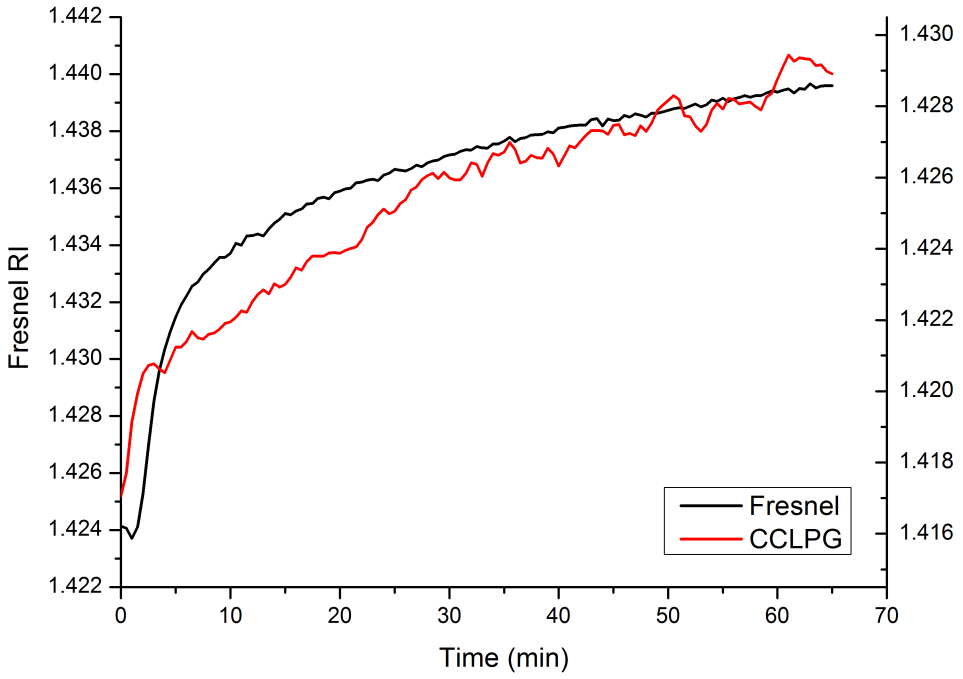

(a)

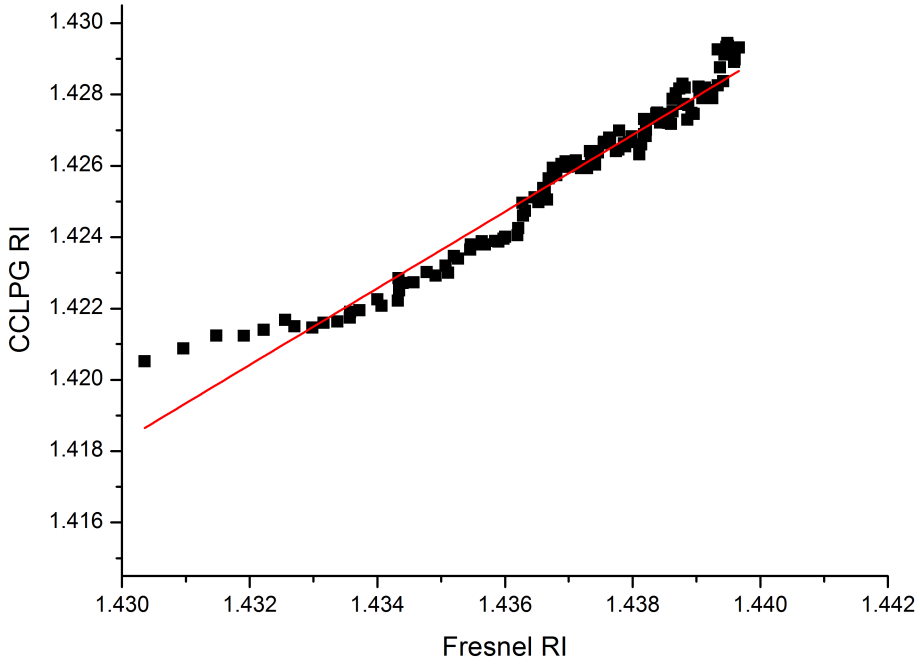

(b)

Figure 6.16: Correlation of refractive index change of the Fresnel refractometer and CCLPG with a period 400 μm - 420 μm obtained during epoxy resin cure. (a) shows the change in refractive index for the CCLPG (red curve) and Fresnel refractometer (black curve) and (b) shows the plot of CCLPG refractive index against refractive index measured using a Fresnel refractometer. A linear fit (solid red line) was added to show a correlation coefficient of 96%.

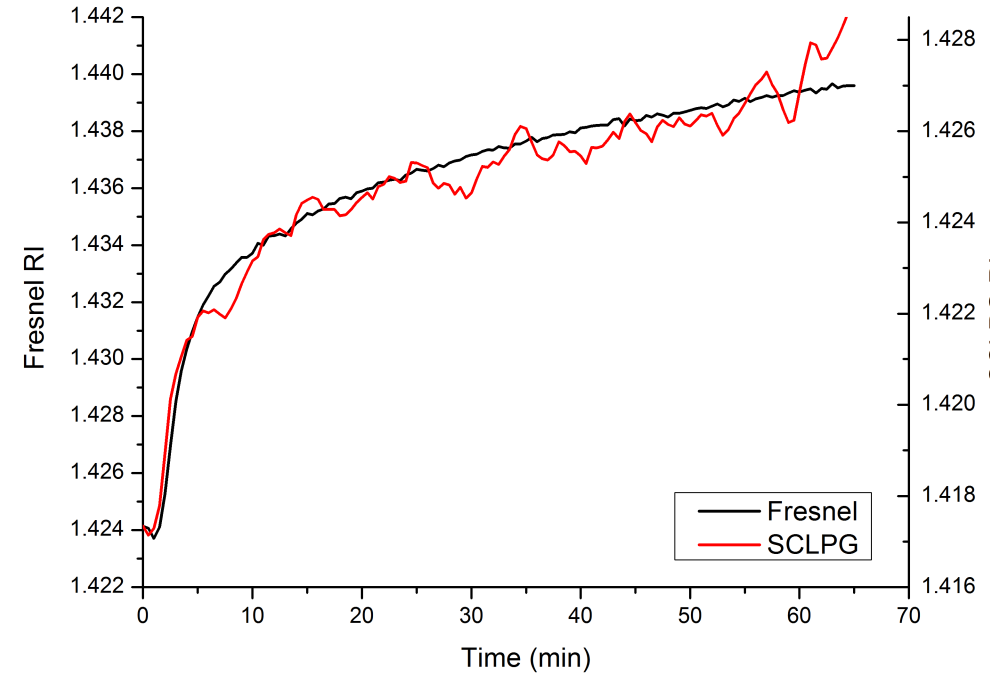

(a)

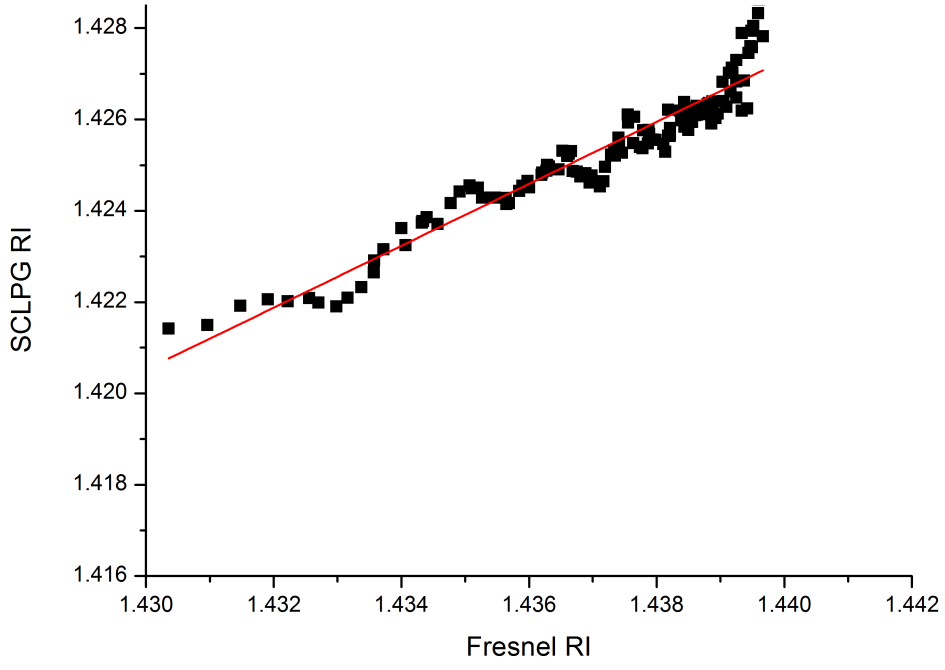

(b)

Figure 6.17: Correlation of refractive index change of the Fresnel refractometer and SCLPG with a period 400 μm to 420 μm obtained during epoxy resin cure. (a) shows the change in refractive index for the SCLPG (red curve) and refractometer (black curve) and (b) shows the plot of SCLPG refractive index against refractive index measured using a Fresnel refractometer. A linear fit (solid red line) was added to show a correlation coefficient of 91%.

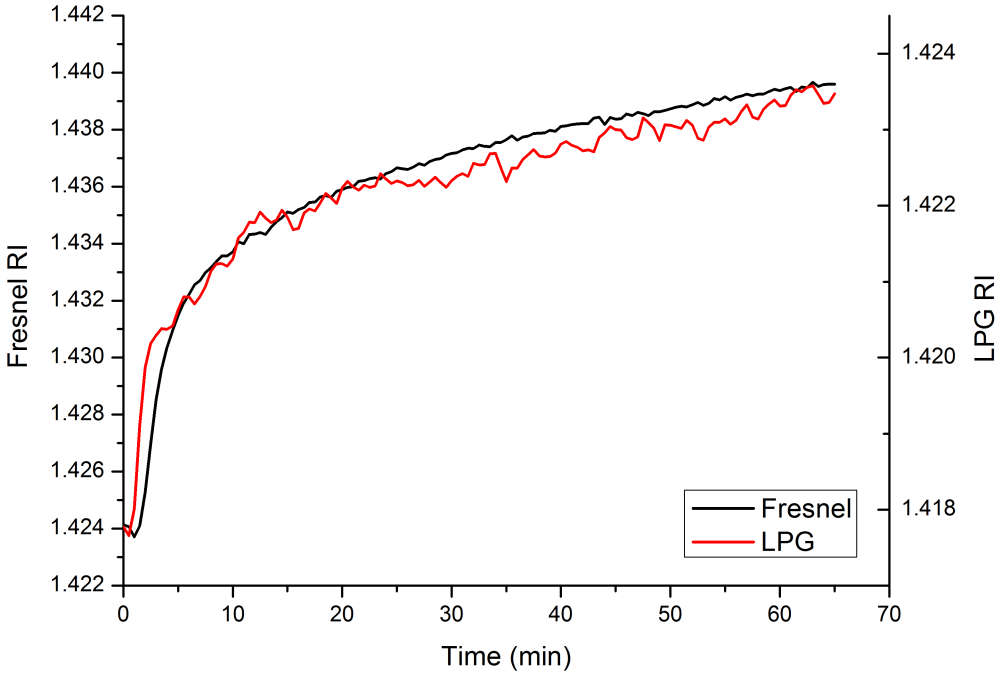

(a)

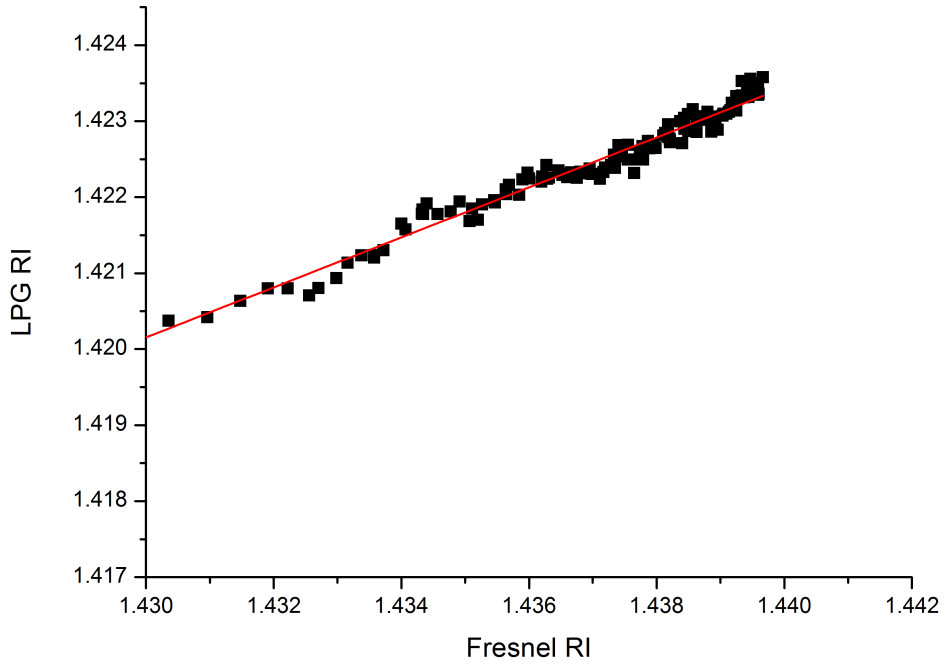

(b)

Figure 6.18: Correlation of refractive index change of the Fresnel refractometer and LPG with a period 400 μm during epoxy resin cure. (a) shows the change in refractive index for the LPG (red curve) and refractometer (black curve) and (b) shows the plot of LPG refractive index against refractive index measured using a Fresnel refractometer. A linear fit (solid red line) was added to show a correlation coefficient of 97%.

6.5 Summary and conclusion

A continuously chirped long period grating was demonstrated as a directional flow sensor using oils of refractive index lower and greater than that of the fibre cladding and using a UV-cured epoxy resin. The change in the shape of the attenuation band profile was shown to be dependent on the direction of flow of the oil and resin with respect to grating orientation. When the resin or oil was flowed in the increasing chirp direction, the band appeared to move toward the longer wavelengths. In the decreasing chirp direction, the opposite was seen and the band moved to the left (shorter wavelengths), having more prominence at a lower wavelength. For directional flow, the CCLPG was shown to be more responsive than the SCLPG. This implies that the CCLPG would make a more sensitive directional flow sensor when compared to a SCLPG.

The CCLPG and SCLPG were used for monitoring resin cure and the sensitivity of the attenuation bands were compared with the sensitivity of a uniform period LPG. The experiment demonstrated that the sensitivity can be said to not be affected when using a CCLPG or SCLPG during the cure process. The change in refractive index during cure also correlated well with the results from the Fresnel refractometer, with correlation coefficients of 96% for the CCLPG and 91% for the LPG.

References

[1] C Keulen, B Rocha, M Yildiz, and A Suleman. Embedded fiber optic sensors for monitoring processing, quality and structural health of resin transfer molded components. *Journal of Physics: Conference Series*, 305(1):1–9, 2011.

[2] S J Buggy, E Chehura, S W James, and R P Tatam. Optical fibre grating refractometers for resin cure monitoring. *Journal of Optics A: Pure and Applied Optics*, 9(6):S60–S71, 2007.

[3] C Keulen, M Yildiz, and A Suleman. Multiplexed FBG and etched fiber sensors for process and health monitoring of 2-&-3-D RTM components. *Journal of Reinforced Plastics and Composites*, 30(12):1055–1064, 2011.

[4] S Triollet, L Robert, E Marin, and Y Ouerdane. Liquid resin infusion process monitoring with embedded superimposed long period and short period Bragg grating sensor. *EPJ Web of Conferences*, 6(34003):1–9, 2010.

[5] E Chehura, R Jarzebinka, E F Reia Da Costa, A A Skordos, S W James, I K Partridge, and R P Tatam. Multiplexed fibre optic sensors for monitoring resin infusion, flow, and cure in composite material processing. *Proceedings of the SPIE*, 8693:F1–F7, 2013.

[6] N Gupta and R Sundaram. Fiber optic sensors for monitoring flow in vacuum enhanced resin infusion technology (VERITy) process. *Composites: Part A*, 40(8):1065–1070, 2009.

[7] S J Buggy, S W James, and R P Tatam. A long period grating based directional flow sensor. *Proceedings of the SPIE*, 7004:70045P–1–70045P–4, 2008.

[8] Cargille Ltd. Cauchy equations data sheet.

[9] Epoxy Technology Inc. EPO−TEK® OG134 technical data sheet. accessed [13/12/2012].

[10] H J Patrick, A D Kersey, and F Bucholtz. Analysis of the response of long period fiber gratings to external index of refraction. *Journal of Lightwave Technology*, 16(9):1606–1612, 1998.

[11] D B Stegall and T Erdogan. Leaky cladding mode propagation in long-period fiber grating devices. *IEEE Photonics Technology Letters*, 11(3):343–345, 1999.

Chapter 7

Summary and future research

7.1 Thesis summary and conclusion

The study of long period grating sensors through design, fabrication and sensing application was presented in this thesis.

A versatile point-by-point long period grating fabrication set up was developed from an existing system. This system allowed the fabrication of repeatable LPGs at PMTP, where the transmission spectra are sensitive to small changes in the environment. To assist in the process for creating repeatable gratings, a number of factors were taken into account. For instance, a passive temperature environment was introduced, computer controlled stages with high precision were programmed and optics for use with high-power laser systems were used. The system also presented the capability for writing different configurations of LPGs.

Experiments have been carried out to evaluate the practical characteristics of the spectrum of a long period grating (LPG) when subjected to a range of measurands, namely temperature, tensile strain, and surrounding refractive index. The results showed that the LPG written at the phase matching turning was shown to have the high sensitivity to all measurands. Both the uniform period LPG and chirped LPG showed a relatively low sensitivities to axial strain, 0.81 $\pm$ 0.03 pm$(\mu\epsilon)^{-1}$ and 0.95 $\pm$ 0.06 pm$(\mu\epsilon)^{-1}$ respectively, compared to temperature (-174 $\pm$ 2.3 and -193 $\pm$ 4.9 pm$(^{\circ}C)^{-1}$, respectively). When comparing the change in wavelength due to the surrounding refractive index, the shift in the wavelength of the attenuations was much greater with the LPG at the PMTP than LPG with a long uniform period and the continuously chirped LPG. With the surrounding refractive index of 1.445 $\pm$ 0.0012 the maximum shifts were 203 $\pm$ 2.1 nm, 14.89 $\pm$ 0.4 nm and

12.04 ± 0.2 nm respectively.

In the fabrication of optical fibre gratings, the optical fibre is sometimes hydrogen loaded to enhance its photosensitivity and improve the fabrication process. The diffusion of hydrogen out of the fibre after grating fabrication can have a significant influence of the properties of the modes of the optical fibre and thus on the transmission spectrum of the fibre grating device. The influence of the this effect on the performance of the sensors, and the means for controlling it, are examined. When a 400 μm period long period grating was left over the period of 5 days, the wavelength of the largest shifted attenuation band changed by a total of 52 nm. By annealling, it was possible to rapidly remove some hydrogen from the optical fibre to prolong the stability of the attenuation bands of the transmission spectrum.

There is considerable interest in the development of optical fibre based chemical sensors. The current trends in this area involve the deposition of a functional nanoscale coating onto the surface of the optical fibre. Chemically induced changes in the optical characteristics of the coating can influence the properties of modes propagating i0n the optical fibre, which can be observed by monitoring the transmission spectrum of the fibre device. Appropriate choice of coating material can offer analyte-specific operation. Chapter 5 showed that it is possible to create a species specific chemical sensor using a molecularly imprinted coating. The sensor experienced greatest sensitivity when exposed to the original over other chemicals with a similar chemical structure.

Chapter 6 showed the successful demonstration of using a CCLPG as a directional flow sensor and for epoxy resin cure monitoring. When compared to that of a SCLPG, the CCLPG showed a larger response when used to detect the directional flow of a resin. The LPG, CCLPG and SCLPG were used for monitoring resin cure and the change in refractive index also correlated well with the results from the Fresnel refractometer. with correlation coefficients of 97%, 96% and 91%, respectively.

7.2 Future research

The output of the research and the work carried out in this thesis reveals a number of the concepts studied which could gain from further study. This section serves to outline the potential areas of future research to build on the work of this thesis.

A natural extension of this work would be to design, fabricate and test different configurations of LPGs in other types of optical fibre such as photonic crystal fibre. This would create novel sensors with new characteristics and possibly new sensing capabilities. Photonic crystal fibre architecture has air holes running down the cladding structure and the fibres also exist in endlessly single mode construction. Due to the air holes, the fibre possesses low thermal sensitivity while having a low Young's modulus and hence high strain sensitivity. The air holes may also be infused with other materials to modify the fibre properties [1] and thus enhance sensitivity to measurements when LPGs are fabricated in the fibre.

Another avenue could be to write a particular LPG configuration or a combination of LPGs inside a tapered fibre. For instance, writing a LPG at phase matching turning point inside of a tapered fibre would potentially increase the sensitivity of the sensor.Phase matching turning point LPG sensors have been proven to have the highest sensitivity to environmental changes [2, 3] and by tapering a fibre, the tail of the core electric field (evanescent field) is exposed more such that it spreads out of the fibre into the medium surrounding it. This makes a tapered optical fibre on its own a useful sensor and gives it the ability to sense different environmental parameters. Further enhancement in sensitivity can therefore be achieved by combining an LPG sensor configuration and a tapered optical fibre sensor. Yoon et al. demonstrated an LPG inscribed in a tapered fibre and found improved strain sensitivity [4].

It was reported in chapter 5 that when attempting to rebind the template with the TiO_2/TMPyP film, the attenuation of the LPG transmission spectrum did not return to its original position. This may be due to the potential surface damage caused by HCl when used as a means of removing the template from the coating. Further investigations on the effects of HCl, such as relating to prolonged or repeated exposure should be considered. UV irradiation is a possible alternative avenue to explore as a means of removing the template from the composite film without causing surface damage. This molecular imprinting technique for species-specific analysis could also be applied to different configurations of LPGs, with their capabilities compared and analysed. Again, this may include an LPG sensor configuration (e.g. LPGs at the PMTP) fabricated in a tapered fibre. As this work only investigated the capabilities of the sensor using certain porphyrins, a continuation would be to look at different materials making it possible to differentiate between compounds with similar chemical behaviours but different geometric shape. A molecularly imprinted thin film on an LPG could be used to look into using transparent compounds as

templates. The coating could aid in providing visual confirmation of the presence of the compound.

Further investigations into the work involving the chirped LPGs as flow sensors. The CCLPG sensor was tested in an epoxy resin and was shown to respond well, being able to determine the direction of flow, as described in chapter 6. The next step could be to embed the chirped long period gratings into complex structures made from composite material. This would allow them to be tested as real time and in-situ directional flow and cure sensors when carrying out the cure and infusion process of resin. When monitoring the flow of a resin on large components it is likely that multiple LPGs would be required, making it advantageous to multiplex these sensors. Introducing the use of optical switches will reduce the number of components (for example light sources and spectrometers) required while at the same time benefiting from the use of the same light source and spectrometer performance/conditions over all the sensors. The flow rate of resin during infusion is considerably slow when compared to the switching rates of commercial optical switches which are typically in excess of 5 kHz. A large number of LPG sensors can therefore be multiplexed without compromising the sampling rate. Figure 7.1 shows the setup that could be used. CCLPGs could also be used to detect the rate of flow of a resin front as the length of the grating is predetermined before fabrication which means the time taken for an entire grating to be covered by the resin could be recorded during the infusion process.

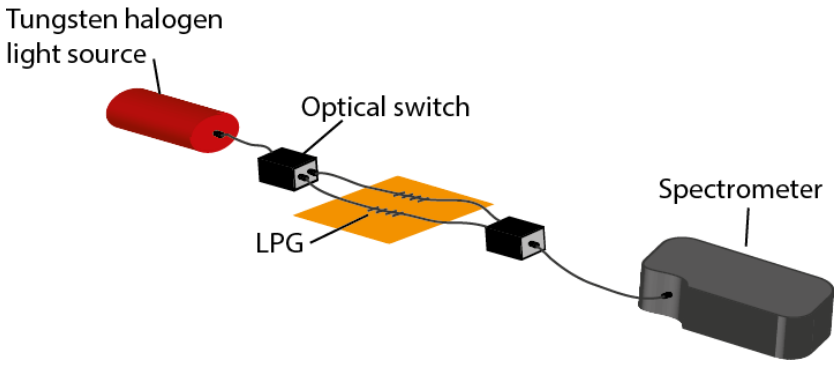

Figure 7.1: A potential setup for interrogating more than one LPG sensor using one spectrometer and light source. A 1 x N switch can be used for N number of LPGs in separate optical fibres.

The fabrication of long period gratings was shown to be highly susceptible to the surrounding environment (chapter 3), especially temperature. The temperature of the system was only passively controlled. A possible way to improve the stability of

the fabrication process would be to encase the system such that it would be possible to actively monitor, control and change the temperature of the chamber as required. The output power of the laser system was also shown to vary during fabrication of LPGs. Typically the laser output power, in the steady state, varied by approximately 8% over 5 hours. A computer controlled variable attenuator, external to the laser system, could be included in the fabrication set up. By monitoring a reference laser beam power with a power meter with a fast response time, the variable attenuator will be actively controlled in a PID loop to maintain the power throughout the fabrication process.

References

[1] X Yang and Wang L. Silver nanocrystals modied microstructured polymer optical bres for chemical and optical sensing. *Optics Communications*, 280:368–373, 2007.

[2] C S Cheung, S M Topliss, S W James, and Tatam R P. Response of fibre optic long period gratings operating near the phase matching turning point to the deposition of nanostructured coatings. *Journal of the Optical Society of America B Optical Physics*, 25(6):897–902, 2008.

[3] X Shu, T Allsop, B Gwandu, and Bennion I Zhang, L. High-temperature sensitivity of long-period gratings in BGe codoped fiber. *IEEE Photonics Technology Letters*, 13(8):818–820, 2001.

[4] M S Yoon, H J Kim, and Y G Han. Long-period fiber grating inscribed in a tapered fiber. *Proceedings of BGPP*, BTu1C:1–2, 2012.

List of publications

Peer-reviewed journals

1. T Wang, S Korposh, R Wong, R Tatam, and S W Lee. A novel ammonia gas sensor using a nanoassembled polyelectrolyte thin film on fiber-optic long-period gratings. *Chemistry Letters*, 41(10):1297-1299, 2012.

2. M Partridge, R Wong, M Collins, S James, F Davis, R Tatam, and S Higson. Modifying monolayer behaviour by incorporating subphase additives and improving Langmuir Blodgett thin film deposition on optical fibres. *Materials Chemistry and Physics*, 144(1-2):179-185, 2014

3. M Partridge, R Wong, S W James, F Davis, S Higson, R P Tatam. Long period grating based toluene sensor for use with water contamination. *Sensors & Actuators: B. Chemical*, submitted Feb 2014

4. R Y N Wong, E Chehura, S E Staines, S W James, and R P Tatam. Fabrication of fiber optic long period gratings operating at the phase matching turning point using a UV laser. *Applied Optics*, In press May 2014

Conferences

1. R Y N Wong, E Chehura, S W James, and R P Tatam. A chirped long-period grating sensor for monitoring flow direction and cure of a resin. *Proceedings of the SPIE*, 8693:86930E-1-86930E-8, 2013. SPIE Smart Structures/NDE Conference, San Diego, United States (March 2013)

2. S Korposh, R Wong, S James, and R Tatam. Temperature and thermo-optic coefficient measurements using optical fibre long period gratings operating at phase matching turning point. *Proceedings of the SPIE*, 8794:87942N-1-86930E-4, 2013. 5^{th} European Workshop on Optical Fibre Sensors, Krakow, Poland (EWOFS May 2013)

Appendix A

LabView program used in computer controlled fabrication system